The Influence of Fuel Properties on Threshold Combustion in Aviation Gas Turbine Engines

Thesis presented for the degree

Doctor of Philosophy

in the Department Mechanical Engineering University of Cape Town

Author: Victor Burger

Supervisor: Professor Andrew Yates

February 2017

Abstract

This body of work investigated the influence of alternative jet fuel properties on aviation gas turbine performance at threshold combustor operating conditions. It focused on altitude blowout performance and was in part motivated by results that were encountered during an aviation industry evaluation of synthetic kerosene that complied with the Jet A-1 specification, but differed from the fuel that was used as a reference in terms of some significant properties. As a consequence the relative impact of physical properties and reaction chemistry properties were of primary interest in this study.

The thesis considered the potential to blend a range of different alternative jet fuel formulations which exhibited independent variations in properties relating to evaporation and reaction behaviour whilst still conforming to legislated physical fuel specifications. It further explored the potential for said variations having a detectable and significant influence on the simulated high altitude extinction behaviour in a representative aviation gas turbine combustor. Based on the findings, appropriate metrics were suggested for scientifically quantifying the appropriate properties and conclusions were drawn about the potential impact of alternative jet fuel properties on blowout performance.

These subjects were addressed primarily through the theoretical analyses of targeted experimental programmes. The experimental design adopted a novel approach of formulating eight test fuels to reflect real-world alternative fuel compositions while still enabling a targeted evaluation of the influences of both physical and chemical reaction properties. A detailed characterisation was performed of the test fuels' physical and reaction properties. The extinction and spray behaviours of the fuels were then evaluated in a laboratory scale combustor featuring dual-swirl geometry and a single prefilming airblast atomiser. The various experimental data sets were interpreted within the context of a theoretical model analysis. In doing so the relative performance of alternative jet fuel formulations under laboratory burner conditions were translated to predict relative real world altitude performance. This approach was validated against aforementioned industry evaluation results and demonstrated to be consistent.

A technically defensible explanation was provided for the previously unexplored anomalous altitude extinction results that were observed during the industry evaluation of synthetic jet fuel. A conclusive case was made for the extinction limit differences having been caused by the relative differences in chemical ignition delays of the fuels.

The probability of volatility (distillation profile) and fuel physical properties playing a significant role in the impaired altitude performance was discredited. Evaporation-controlled combustion efficiency was, however, shown to become a significant factor at low air mass flow rates or when the fuel evaporation is compromised.

The influence of flame speed and chemical ignition delays were investigated. Laminar flame speed was shown not to correlate with LBO, discrediting its use as a proxy for reaction rate. The study showed a correlation between the lean blowout behaviour of jet fuels and the ignition delays associated with their derived cetane numbers. Additionally, there was substantive support indicating that an even stronger correlation could be obtained by operating the IQT™ device that is used to measure these delays at an elevated temperature.

The thesis makes a contribution towards the development of both technical understanding and practical tools for evaluating the potential operating limits of alternative jet fuel formulations.

Acknowledgements

I wish to thank the following people:

- Professor Andy Yates, for his indispensable guidance, encouragement and support.
- Dr Carl Viljoen for playing a key role in initiating the collaboration with German Aerospace Centre (DLR) and for trying his best to educate a mechanical engineer in the dark art of chemistry.
- Dr Mariam Ajam and Dr Rina van der Westhuizen for their assistance with the fuel matrix characterisation.
- Sasol Energy Technology, headed by Paul Morgan, for the support and funding of this project.
- The DLR Institute of Combustion Technology, headed Prof. Dr Manfred Aigner, and especially Dr Thomas Mosbach for hosting me in Stuttgart.
- Dr Clemens Naumann for the shock tube ignition delay characterisation of the test fuels.
- Dr William O'Loughlin and Jasper Grohmann, for their assistance during the model-combustor test measurements.
- My parents for their love, support, and patiently explaining organic chemistry and gas chromatography to me.

This thesis is dedicated to my wife, Zelda, for her love, support, and patience without which I would not have been able to conclude this work.

Contents

List of Figures

List of Tables

Acronyms

AFT	(p 38)	adiabatic flame temperature
ALR	(p 18)	air/liquid mass ratio
AVTUR	(p 3)	aviation turbine fuel – reference Jet A-1
CJF	(p 49)	crude-derived Jet A-1
CJF/D	(p 49)	crude-derived Jet A-1 + 50% n-dodecane
DCN	(p 27)	derived cetane number
DEF STAN	(p 2)	UK defence standard
DLR	(p 51)	German Aerospace Centre
FAR	(p 50)	fuel/air mass ratio
FID	(p 50)	flame ionisation detector
FSJF	(p 2)	fully synthetic jet fuel
FT	(p 48)	Fischer-Tropsch
GC	(p 50)	gas chromatography
GCxGC	(p 50)	two-dimensional gas chromatography
GTL	(p 26)	gas to liquids
HCPP	(p 49)	hydrogenated cat-poly petrol
HTSK	(p 49)	synthetic paraffinic kerosene (SPK)
HN	(p 49)	heavy naphtha refinery stream
ICAO	(p 14)	International Civil Aviation Organisation
ISA	(p 14)	international standard atmosphere
IQT™	(p 30)	ignition quality tester (manufactured by AET, Canada)
LBO	(p 1)	lean blowout
LFS	(p 25)	laminar flame speed
LTHR	(p 30)	low temperature heat release
LTSK	(p 49)	experimental GTL kerosene
MSL	(p 14)	mean sea level
NTC	(p 59)	negative temperature coefficient
OEM	(p 2)	original equipment manufacturer
PDA	(p 50)	phase Doppler anemometry
PIV	(p 53)	particle image velocimetry
SFSAK	(p 3)	Sasol fully synthetic aviation kerosene (see SJF1)
SJF1	(p 49)	FSJF employed during certification process
SJF2	(p 49)	commercial FSJF
SJF2+	(p 49)	commercial FSJF + 1.5% HCPP

SMD	(p18)	Sauter mean diameter
SPK	(p 26)	synthetic paraffinic kerosene
TOF-MS	(p 50)	time–of–flight mass spectrometry

Nomenclature

A_f	flame area, [m^2]
A_{ref}	combustor reference area, [m^2]
B	constant (eq. 2.7)
d	dynamic head, [m]
dy_F	dimensionless fuel disappearance fraction
d_q	quench distance, [m]
D	instantaneous droplet diameter, characteristic diameter (eq. 4.6) [m]
Da	Damköhler number
D_0	starting droplet diameter, [m]
D_P	prefilmer diameter, [m]
D_{ref}	width of combustor casing, [m]
D_{32}	Sauter mean diameter, [m]
f_c	fraction of airflow involved in combustion
G_y	axial momentum flux
G_θ	angular momentum flux
h	height above sea level, [km]
H	lower specific energy of fuel, [J/kg]
i	reaction order exponent
j	reaction order exponent
K	proportionality constant
K_θ	modified proportionality constant
K'_{CJF}	reaction-controlled proportionality constant for reference fuel CJF
K''_{CJF}	evaporation-controlled proportionality constant for reference fuel CJF
l	mixing length, [m]
m	mass of fuel droplet, [kg]
m_0	starting droplet mass, [kg]
$\dot{m}$	rate of fuel evaporation / mass change rate, [kg/s]
$\dot{m}_f$	rate of fuel evaporation per unit surface area, [kg/m^2s]
n	number of droplets
$\dot{N}$	molar air flow rate, [moles/s]

P pressure, [Pa]

ΔP_L combustor liner pressure differential, [Pa]

q fuel/air mass ratio

q_{ref} reference dynamic pressure, [Pa]

R gas constant / characteristic radial distance (eq. 5.1)

Re drop Reynolds number

R_u universal gas constant

S_a annular geometric swirl number

S_c centre geometric swirl number

S_L laminar flame speed, [m/s]

S_t small scale turbulent flame speed, [m/s]

S_T large scale turbulent flame speed, [m/s]

t time, [s]

t_e droplet lifetime, [s]

Δt_r residence time of air in combustor, [s]

T temperature, [K]

ΔT temperature rise due to combustion, [K]

$\bar{u}$ rms component of fluctuating velocity, [m/s]

U velocity, [m/s]

U_j turbulent jet velocity, [m/s]

U_{ref} combustor reference velocity, [m/s]

V volume, [m^3]

v velocity, [m/s]

x_F fuel mole fraction

x_O oxygen mole fraction

x_S stoichiometric fuel mole fraction

Y_F overall fuel fraction consumed

α thermal diffusivity

ϵ turbulent exchange coefficient

ϕ equivalence ratio

λ evaporation constant, [m^2/s]

λ_{eff} effective evaporation constant, [m^2/s]

ν kinematic viscosity, [m^2/s]

μ dynamic viscosity, [kg/m.s]

η_c combustion efficiency

η_e combustion efficiency (evaporation-controlled)
η_m combustion efficiency (mixing-controlled)
η_θ combustion efficiency (reaction-controlled)
τ delay
τ_c constant delay offset
τ_e evaporation timescale
τ_m mixing timescale
τ_{res} residence timescale
τ_θ reaction timescale
ρ density, [kg/m^3]
σ surface tension, [kg/s^2]

Subscripts

ave average value
A air
c combustion zone value
F fuel
L liquid
ov overall value
(rel) relative to reference value
sl sea level
0 initial value
3 combustor inlet value

1 Introduction

Gas turbines dominate aviation propulsion and while they have traditionally always been considered to be omnivorous fuel consumers, the demands of modern aviation has resulted in a much more constrained fuel tolerance. Aviation gas turbines need to operate over a wide range of ambient conditions while attaining ever increasing efficiency and emission targets. In order to satisfy these demands jet fuel is subjected to performance-based specifications which have traditionally allowed any combination of hydrocarbons that satisfied the required performance, provided that they were petroleum-derived. Significant performance properties include energy content, smoke point, thermal stability, lubricity, volatility, non-corrosivity and cleanliness. Since the 1940s the specifications have focused predominantly on distillation, volatility, freeze point, thermal stability and volume yield [1, 2]. In addition, handling and safety requirements constrain a number of fuel properties. The consequence is that modern-day aviation fuel is controlled by very explicit specifications that evolved out of a global industry consensus approach. Environmental and energy security considerations have stimulated interest in alternatives to petroleum-derived jet fuel which in turn resulted in an industry-wide review of the complete list of jet-fuel specifications. Sasol played a key role in this process as the world's first producer of approved and certified semi-synthetic and fully-synthetic jet fuels [3].

It is noteworthy that no direct or indirect fuel autoignition specifications are applied to jet fuel, presumably due to the argument that under normal combustion conditions chemical reaction timescales are negligible relative to spray vaporization time scales [4]. The combustion performance of practical aircraft combustors is known to be influenced more by physical processes of heat transfer, mass transfer, thermodynamics, gas dynamics and fluid dynamics than by chemical processes. While chemical reaction rates are acknowledged as being of great importance, they are largely disregarded in high temperature flames due to being considered to be relatively rapid and not rate controlling. Emphasis is placed on large scale mixing and the interdiffusion of fuel and air as the rate controlling steps. Chemical processes are, however, known to be of particular importance for the formation of pollutant emissions and for the lean light-off and lean blowout (LBO or weak extinction) limits at high flight altitudes [5].

Literature acknowledges the importance of chemical reaction timescales in the combustion of well atomised fuels at low pressures and lean equivalence ratios as well as under threshold combustion conditions such as encountered during altitude blowout

and relight. Increased interest in alternative aviation fuel formulations, and the related opportunity to influence chemical reaction rates to a greater degree than traditionally possible in the case of petroleum-derived jet fuel, has prompted examination of the influence of physical and chemical fuel properties on gas turbine combustion behaviour. A number of studies have reported ignition and extinction behaviour being influenced by fuel formulation to varying degrees although it is difficult to separate the influence of fuel formulation on chemical reaction and fuel evaporation and mixing. These studies employed experimental setups ranging from laboratory scale combustors to full scale gas turbines and test fuels ranging from single component fuels to full boiling range jet fuel formulations. Findings ranged from reports of appreciable differences to relative insensitivity to fuel formulation [6, 7, 8, 9, 10, 11].

The potential impact of fuel formulation on threshold combustion was also highlighted by altitude blowout results that were encountered during the evaluation of synthetic kerosene (Sasol fully synthetic jet fuel or FSJF) as a Jet A-1 aviation turbine fuel under DEF STAN 91-91 [12, 13].

1.1 Thesis structure

The thesis commences with a summary of the altitude blowout experience that emerged during the FSJF certification process. This is followed by a chapter entailing a preliminary theoretical assessment of combustion efficiency and its impact on the flight envelope. The context of the FSJF results and the theoretical assessment provide the foundation for the formulation of three thesis hypotheses and the project plan to address these. A review of relevant literature follows in order to provide context and background. Based on the guidance provided by the preliminary theory and literature, a more detailed and focused theoretical assessment is presented. The experimental design that was formulated to address the hypotheses is presented next. The experimental results follow as does a subsequent analysis and discussion chapter aimed at interpreting the results in terms of the hypotheses. Finally some concluding remarks and recommendations are presented.

1.2 FSJF certification: Altitude extinction findings

During the FSJF certification process, Southwest Research Institute (SwRI) assessed the results from detailed laboratory testing and submitted the findings to the engine original equipment manufacturers (OEMs), the British MOD Aviation Fuels Committee, the Aviation Fuels Group of the Coordinating Research Council, and the ASTM J1

Aviation Fuels Subcommittee. Following the evaluation of the fuel properties and characteristics, as detailed in a comprehensive report by Moses and Wilson [12], the OEMs requested engine and combustor tests to confirm no adverse effects on engine performance and operation. This resulted in a series of test programs being conducted and or monitored by the OEMs focusing on engine performance, endurance, emissions, atomisation, ignition and relight, and lean blowout. Moses compiled a report detailing the results and interpretation of the various engine test programmes, which was instrumental in the eventual approval of FSJF under DEF STAN 91-91 [13]. The findings from these test reports contained the following aspects which related specifically to altitude ignition and extinction.

Rolls-Royce plc. was entrusted with conducting a combustor rig-based evaluation of ground ambient cold day relight and extinction performance. The test program was executed at Smiths Ltd's high altitude facility in Burnley, UK. A full annular combustion test system representative of a modern aero gas turbine was used in a configuration equipped with airblast fuel spray nozzles. A reference test fuel (AVTUR) was evaluated alongside the FSJF, which was referred to in the report as "Sasol Fully Synthetic Aviation Kerosene" or SFSAK. Ignition, stability (extinction limit) and blowout tests were conducted at several altitude pressures to map the likely operating envelope. A detailed summary of the test methodology is contained in the full test report [14]. Both the reference AVTUR and SFSAK were mapped over a range of operating conditions with ignition, extinction, and blowout loops being compared at the same conditions (e.g. same time to ignition and number of sectors lit/extinguished). The ignition and extinction performance was translated to an altitude-Mach number realm by applying typical windmilling performance to calculate altitude and Mach numbers for each combustor pressure and air mass flow combination. Results from more than 200 test points are presented in Figure 1.1 (from the test report) which includes three data sets: one ground ambient cold day case and two altitude cases. Although the ground ambient cold day results are not a windmilling relight condition, it was included in order to present all the data on a single graph.

The figure reflects the blowout extinction and ignition conditions for SFSAK and AVTUR. Some differences between the fuels were noted in the high altitude, high sub-sonic Mach number region. The most distinct differences were recorded in the relative blowout extinction performance of the two fuels. The lean and rich extinction boundaries of the two fuels were close, but differences increased towards the blowout point with an almost 6% difference in relative air flow at first sector blowout and more

than 10% difference in final sector blowout. The SFSAK blowout points occurred at lower combustor mass flows than those recorded by the AVTUR fuel. This translated into the significant difference in blowout extinction points of the two fuels in the higher altitude and Mach number regime of the windmilling envelope shown in Figure 1.1.

Only marginal ignition boundary differences were recorded and were considered to be within the test method accuracy of 0.005 Fuel-to-Air ratio. The SFSAK toe ignition point occurred at a 2.5% lower air mass flow than for AVTUR.

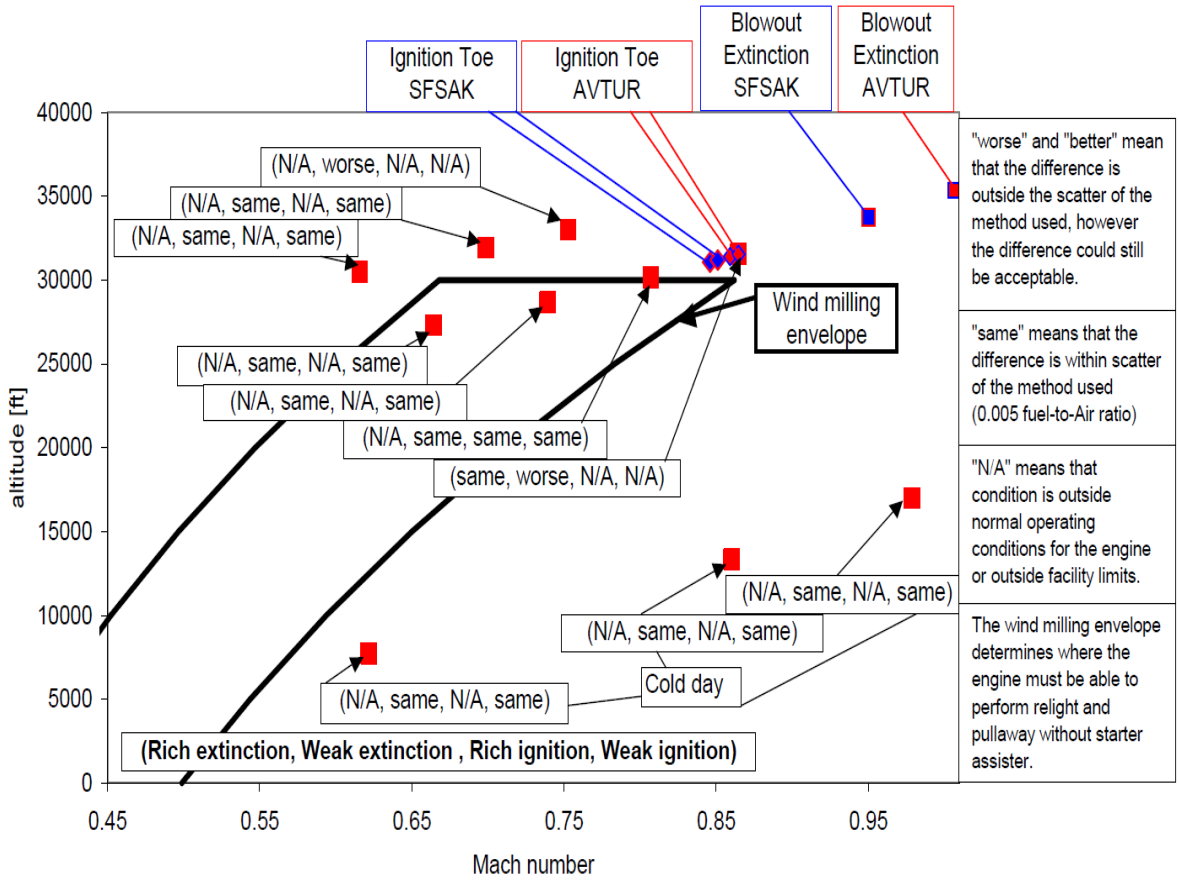

Point with lower air mass flow than Toe point; Ignition Toe point for AVTUR; Ignition Toe point for SFSAK; Blowout point for AVTUR; Blowout point for SFSAK

Figure 1.1: Mach number carpet - Relative performance of AVTUR and SFSAK (from original Rolls-Royce report [14])

The report focused on differences in boiling point distribution between the two fuels (Figure 1.2) and identified it as a potential cause for the blowout differences. It was, however, acknowledged that “the possibility of a chemical issue could not be ruled out.” In light of these results the OEMs recommended further lean blowout tests at lower

altitude conditions that are more relevant to descent where throttle manoeuvres are expected to be more likely to cause lean combustion.

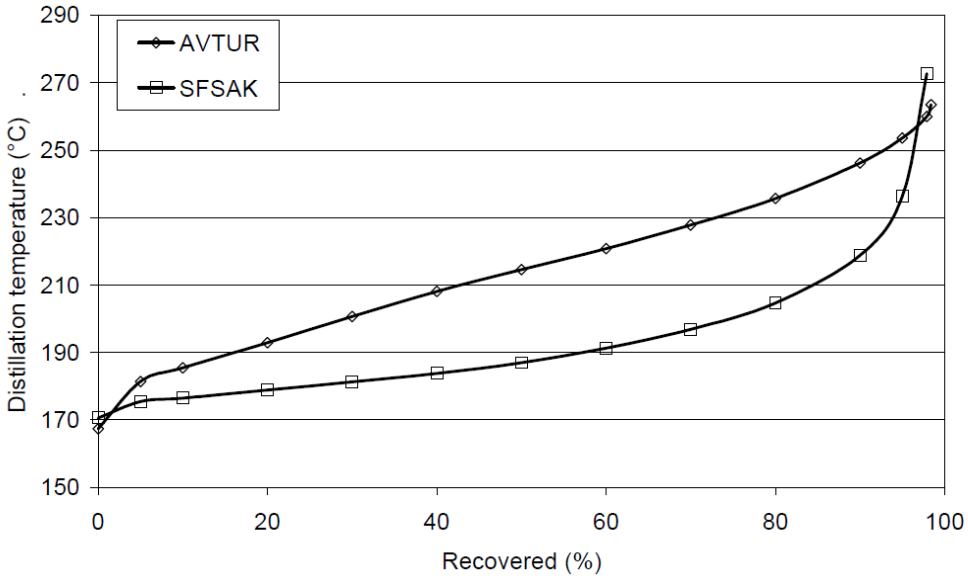

Figure 1.2: ASTM D86 distillation curves for AVTUR and SFSAK test fuels (from original Rolls-Royce report [14])

In response to the issue raised by Rolls-Royce, Honeywell Aerospace conducted low-temperature atomisation (at -40°C) and lean blowout tests. The atomisation of the FSJF was reported to be as good as or better than the Jet A reference fuel for both airblast and pressure type fuel atomisers. This was ascribed to the lower specific gravity and viscosity of FSJF and it was concluded that FSJF would provide well-defined spray distribution and droplet size for reliable cold starting [15]

Lean stability or lean blowout testing was conducted at representative flight and ground deceleration conditions from sea level up to an altitude of 25000 ft. A full scale reverse-flow annular combustor rig with dual-orifice fuel atomisers was employed. Three fuels were evaluated, the FSJF test fuel, Jet A (ASTM D 1655), and weathered JP-5 (MIL-DTL-5624) which had some volatile components removed and therefore exhibited a flat distillation profile similar to the FSJF . Blowout points were obtained by reducing fuel flow after stable combustion had been established. Further detail of the test facility and measurement procedure is contained in the report.

The results as shown in Figure 1.3 were reported “relative” to those obtained by the Jet A reference and the authors of the report concluded that lean stability at sea level was very similar for the three fuels. A “limited fuel effect” was noted at the higher

simulated altitude (25000 ft.) test point were the FSJF results fell between those recorded by JP-5 and the Jet A reference. The relative differences were considered to be small and ordered according to the front-end boiling point distribution of the three fuels. The distillation curves of the three fuels are presented in Figure 1.4. The JP-5 exhibited a similarly flat distillation profile to that of the FSJF, but while it had the same flash point the overall distillation was shifted to higher boiling points and the front-end volatility ranking is apparent. Honeywell concluded that the blowout performance differences that were reported by Rolls-Royce were not due to chemistry and that FSJF recorded no adverse effect on combustor lean stability characteristics. The differences at higher altitude conditions were ascribed to boiling point distribution; volatility and flash point in particular.

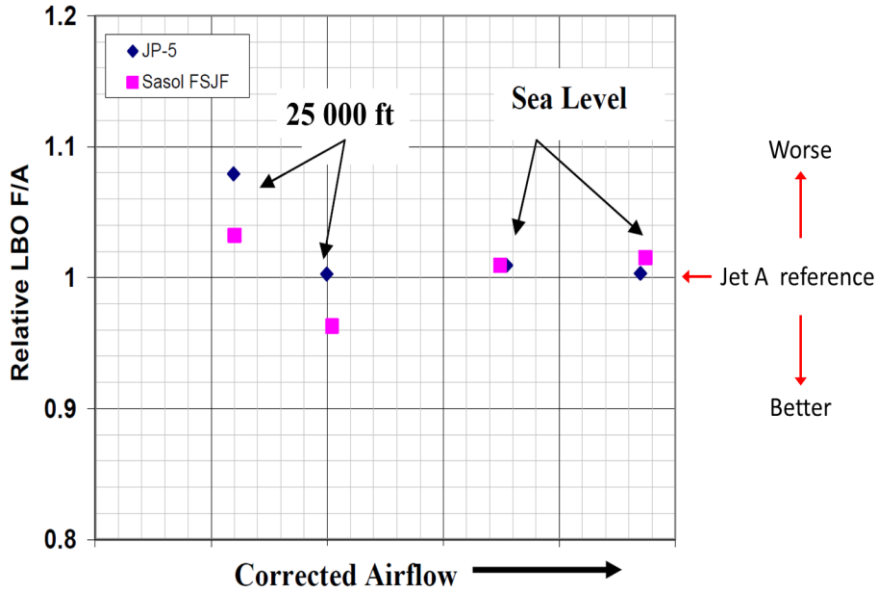

Figure 1.3: Lean blowout performance of JP-5 and FSJF relative to Jet A reference fuel (from original Honeywell Aerospace report [15])

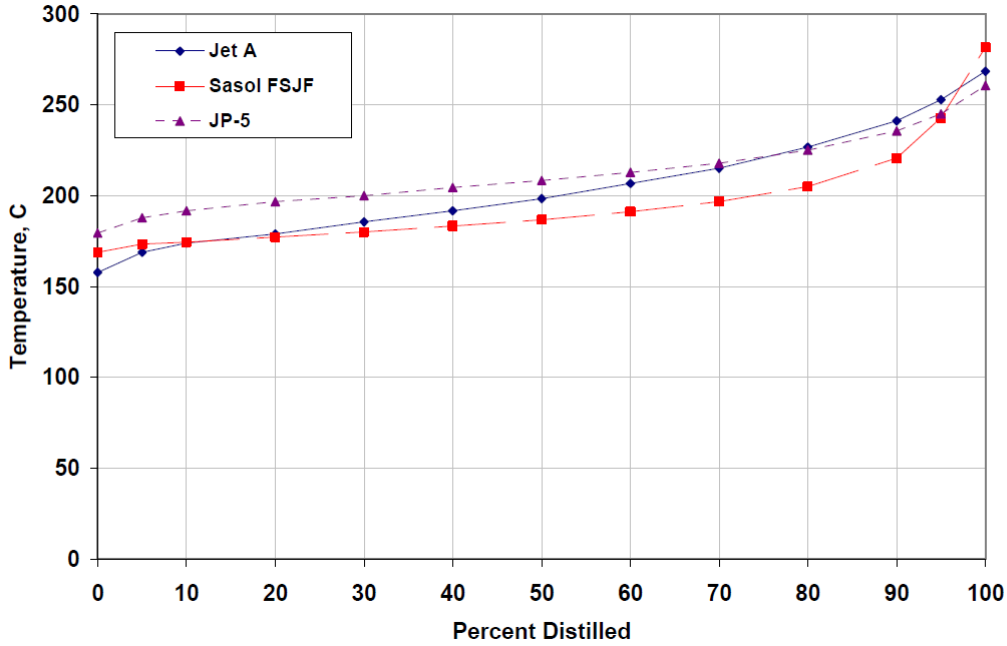

Figure 1.4: Distillation curves for Jet A, FSJF, and JP-5 test fuels (from original Honeywell Aerospace report [15])

While the two studies by Honeywell and Rolls-Royce provided the industry with sufficient confidence to certify FSJF (with the specified minimum distillation gradient), the results suggested that the relative influences of physical and chemical properties on altitude ignition and extinction had not been addressed fully. In order to explore this subject further it is necessary to first consider the theoretical constraints that apply to combustion efficiency over the altitude-velocity operating envelope.

2 Preliminary Theoretical Assessment and Project Plan

In order to formulate a project hypothesis, it was necessary to subject the results from the Rolls-Royce and Honeywell Aerospace evaluations to a preliminary theoretical root-cause analysis. Aviation safety authorities such as the Federal Aviation Administration and the European Aviation Safety Agency require the submission and validation of so-called flight envelopes that define the ignition and extinction boundaries of combustion in an aviation gas turbine. These flight envelopes are essentially the result of the interplay between atmospheric conditions, hardware design and operation, and combustion efficiency. In the following section simplified theoretical treatments of combustion efficiency and flight envelopes are employed to examine the potential for different fuel properties to influence flight envelope boundaries.

2.1 Combustion efficiency

Gas turbine combustors need to burn stably over a wide range of operating conditions while maintaining overall combustion efficiencies in excess of 99 percent in order to meet emissions regulations. Aviation gas turbines furthermore need to ignite readily after an inflight flameout and attain primary zone combustion efficiencies of 75 to 80 percent as they accelerate back up to normal operation. Lower combustion efficiency levels could result in rich extinction due to over fuelling in order to overcome the narrow stability limits at altitude while higher levels could result in an unnecessarily large combustor [16]. A well-established model for relating combustion efficiency to combustor operating conditions and dimensions is based on the total time required for combustion being equal to the sum of the times required for fuel evaporation, mixing of the reactants (fuel vapour, air and combustion products) and the chemical reaction. The time available for combustion is inversely proportional to the airflow rate, which means that the combustion efficiency can be expressed as follows.

$$\eta_c = f\left((airflow\ rate)^{-1}\left(\frac{1}{evaporation\ rate} + \frac{1}{mixing\ rate} + \frac{1}{chemical\ reaction\ rate}\right)^{-1}\right) \quad [2.1]$$

It is understood that under normal conditions the maximum heat release rate is governed by either evaporation, mixing or chemical reaction rates, but under transient conditions between either of these regimes the overall combustion efficiency could be influenced by two of the three concurrently.

2.1.1 Evaporation-controlled system

In a system where the mixing and reaction rates are sufficiently fast for the fuel evaporation to be the rate-controlling step, the fuel is assumed to instantly mix and burn with the surrounding air as soon as it evaporates. Under such conditions the evaluation of evaporation and droplet lifetime is of interest since it determines the residence time required for combustion to occur. An expanded treatment including all relevant derivation is included in Appendix A.

The evaporation of a spherical droplet is accepted to consist of an unsteady state or heat-up period during which the droplet temperature increases with time until the drop attains its wet-bulb temperature. This transient period is followed by relatively steady-state evaporation during which the droplet diameter, D, changes according to the so-called "D^2 law of droplet evaporation" that was first formulated by Godsave [17]. Typical assumptions include: that the droplet is spherical, that the fuel is a pure single boiling point liquid and that radiant heat transfer is negligible. The mathematical expression of the law is provided in Equation 2.2 where λ represents the evaporation constant, t the time elapsed and D and D_0 the instantaneous and starting droplet diameters respectively [18].

$$D_o^2 - D^2 = \lambda t \qquad [2.2]$$

Figure 2.1 shows this relationship between D^2 and time as generated by Wood et al. for kerosene and JP-4 droplets [19].The fuel-dependent evaporation constant corresponds to the slope of the linear portion of the graph. During the initial heat-up stage the slope of the graph is very small while the majority of the heat raises the droplet temperature.

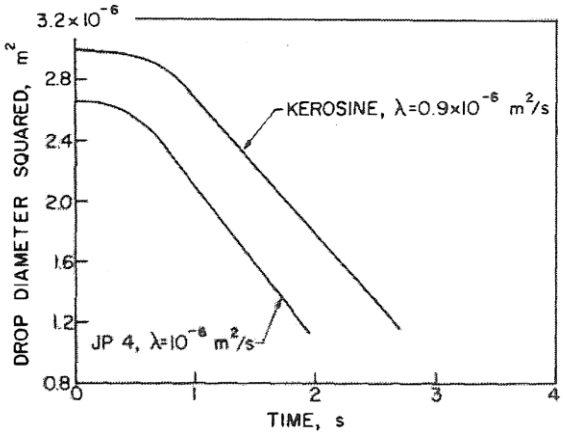

Figure 2.1: Evaporation rate curves for kerosene and JP-4 (from Wood et al. [19])

From Equation 2.2 it follows that the evaporation constant, or slope of the curves in Figure 2.1, are expressed by

$$\lambda = \frac{d}{dt}\,(D^2) \qquad [2.3]$$

As detailed in Appendix A the average fuel spray evaporation rate $\dot{m}_{ave}$, can be expressed in terms of the air density ρ_A, an effective evaporation constant defined by Chin and Lefebvre [20] λ_{eff}, air volume V, fuel/air ratio q, and the initial diameter, D_0.

$$\dot{m}_{ave} = {\rho_A \lambda_{eff} V q}\Big/{D_0^2} \qquad [2.4]$$

This expression for average evaporation rate can be employed in determining the combustion efficiency of a system in which the mixing and reaction rates are sufficiently fast for the fuel evaporation to be the rate-controlling step. The combustion efficiency is therefore governed by the ratio of the rate of fuel evaporation within the combustion zone to the rate of fuel supply.

$$\eta_e = {\dot{m}_{ave}}\Big/{f_c q_c \dot{m}_A} \qquad [2.5]$$

The fraction of the total combustor airflow that takes part in combustion is represented by f_c and the combustion zone fuel/air ratio by q_c. Substituting 2.4 into 2.5 yields:

$$\eta_e = {\rho_A \lambda_{eff} V}\Big/{D_0^2 f_c \dot{m}_A} \qquad [2.6]$$

Equation 2.6 expresses combustion efficiency in terms of the combustor operating conditions (ρ_A , λ_{eff} , $\dot{m}_A$), physical combustor dimensions (V), fuel spray atomiser properties (D_0) and fuel properties (D_0 , λ_{eff}). The equation, however, allows the evaporation efficiency to assume a value greater than 100%. This occurs when the time required for complete evaporation is less than the available time and the fuel within the primary recirculation zone is thus fully vaporised. Under these conditions the combustion efficiency should be assigned a value of 100%. Lefebvre proposes the use of a modified form similar to 2.7 in order to avoid the abrupt discontinuity [21]. The two expressions are compared on the basis of combustion air residence in Figure 2.2. The value of the shape-function constant, B, is typically chosen so that the efficiency derived by 2.6 and 2.7 are coincident at the blowout efficiency of around 80%. It should be noted that 2.7 can over or under predict the base expression 2.6 by up to 15%.

$$\eta_e = 1 - \exp\left(-B\rho_A\lambda_{eff}V \Big/ D_0^2 f_c \dot{m}_A\right) \quad [2.7]$$

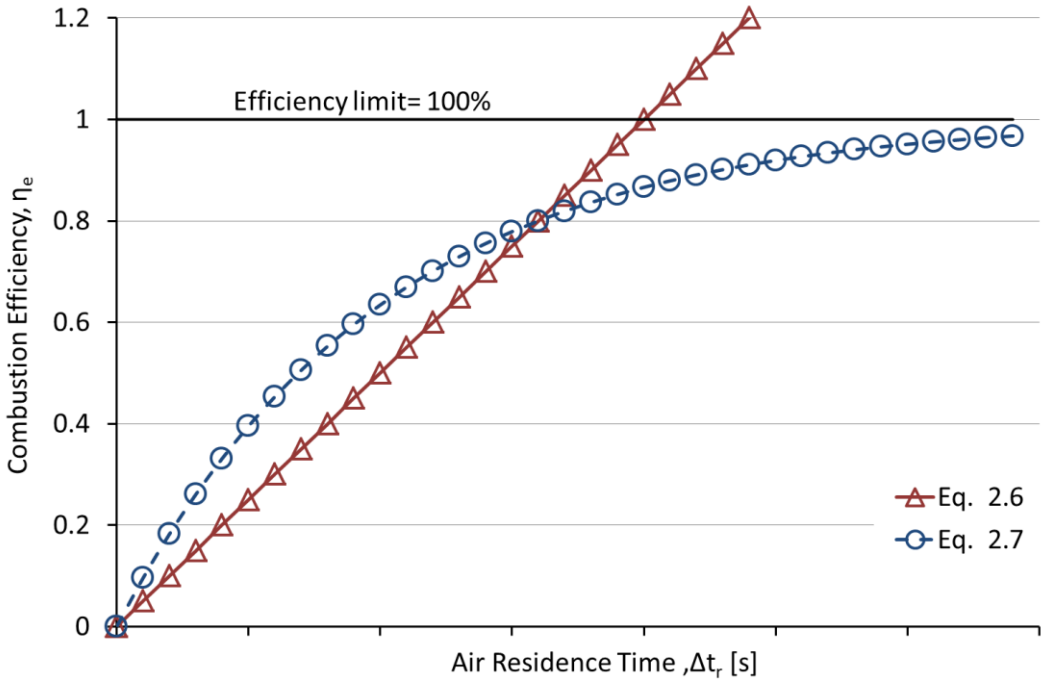

Figure 2.2: Comparison of the direct (eq. 2.6) and exponential (eq. 2.7) expressions for evaporation efficiency

2.1.2 Mixing-controlled system

In his treatment of a system where the fuel evaporation and the chemical reaction kinetics are assumed to be infinitely fast, Lefebvre expressed the combustion efficiency as a function of the mixing and airflow rate [22].

$$\eta_m = f(mixing\ rate/air\ flow\ rate) \quad [2.8]$$

The mixing rate of a turbulent air jet with the gas surrounding it is the product of the eddy diffusivity, the mixing area, and the density gradient between the jet and the surrounding gas. By assuming the eddy diffusivity to be proportional to the product of the mixing length, l, and the turbulent jet velocity, U_j, the mixing rate can be expressed as follows:

$$mixing\ rate = (eddy\ diffusivity)(mixing\ area)(density\ gradient)$$
$$= (lU_j)(l^2)(\rho/l)$$
$$= \rho U_j l^2 \quad [2.9]$$

In a combustor where the turbulent jet velocity is a function of the liner pressure differential, ΔP_L, and density: $U_j \propto (\Delta P_L/\rho_3)^{0.5}$, the mixing rate can be expressed as:

$$mixing\ rate \propto (\rho_3 \Delta P_L)^{0.5} l^2$$
$$\propto (P_3 l^2/T_3^{0.5})(\Delta P_L/P_3)^{0.5} \quad [2.10]$$

Substituting the mixing rate expression into 2.8 and assuming the mixing length to be proportional to the combustor size, A_{ref}, the combustion efficiency in a mixing-controlled system can be expressed as [22]:

$$\eta_m = f\left((P_3 A_{ref}/\dot{m}_A T_3^{0.5})(\Delta P_L/P_3)^{0.5}\right) \quad [2.11]$$

2.1.3 Reaction-controlled system

There are several theoretical approaches which attempt to characterise combustion efficiency in a system where chemical kinetics are considered to be rate-controlling and evaporation and mixing rates are assumed to both be infinitely fast [23, 24, 25]. These will be examined in greater detail later, but for this preliminary assessment the commonly used well-stirred reactor provides an adequate representation.

The well-stirred reactor approximates the combustion zone as a perfectly stirred reactor into which air and fuel flows at a constant rate and the reactants are mixed instantaneously with all material in the reactor. Combustion products are assumed to leave the reactor at a constant rate with temperature and compositional properties identical to that of the reactor or zone. In Lefebvre's treatment the governing reaction rate equation (2.12) is presented without explanation [26] as is the case in his referenced source of this equation, Longwell et al. [27].

$$\eta_c \phi \dot{m}_A = C_{cf} V T^{0.5}\, e^{(-E/RT)} \rho^n x_F^m x_O^{n-m} \quad 2.12]$$

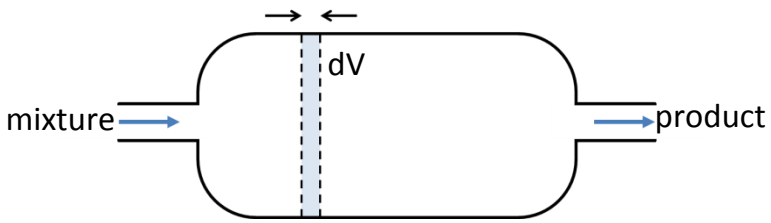

Figure 2.3: The well-stirred reactor concept

A full derivation has, however, been presented by Strehlow [28] based on the theoretical reactor volume depicted in Figure 2.3. The fuel supply in moles per second is given by $Fuel\ Supply = \phi x_s \dot{N}$, where ϕ is the molar equivalence ratio, x_s is the stoichiometric fuel mole fraction and $\dot{N}$ is the air flow rate in moles per second. Assuming a steady flow of premixed reactants into an unstirred reactor, the fuel in volume element dV is consumed at a rate -$\frac{d}{dt}[F]dV$ where the fuel concentration, $[F]$, is the number of fuel moles per unit volume. A dimensionless fuel disappearance fraction, dy_F, can be defined as follows.

$$dy_F = \frac{Local\ fuel\ consumption\ rate}{Overall\ fuel\ supply\ rate} = \frac{-\frac{d}{dt}[F]dV}{\phi x_s \dot{N}}$$

$$\therefore \frac{d}{dt}[F]dV = -\phi x_s \dot{N} dy_F \qquad [2.13]$$

The differential equation can be solved by grouping the variables and integrating over the reactor volume as well as the fuel consumption profile.

$$\int_V \frac{dV}{\phi x_s \dot{N}} = -\int_0^{Y_F} \frac{dy_F}{\frac{d}{dt}[F]} \qquad [2.14]$$

where the limit, Y_F, is the overall fuel fraction consumed. The integral on the right is difficult to evaluate due to the reaction rate, $\frac{d}{dt}[F]$, being a function of both concentration and time. By assuming the reactor to be well-stirred containing a homogeneous mixture of reactants and products, $\frac{d}{dt}[F]$ is assumed to be constant which means that the integration yields:

$$\frac{V}{\phi x_s \dot{N}} = -\frac{Y_F}{\frac{d}{dt}[F]} \qquad [2.15]$$

$$\therefore \frac{x_s \dot{N}}{V} = -\frac{1}{\phi Y_F}\frac{d}{dt}[F] \qquad [2.16]$$

The reaction rate can be expressed in terms of the fuel and oxidiser concentrations and an Arrhenius temperature dependence.

Note: Strehlow uses n and m as reaction order coefficients, while Lefebvre uses m and n-m notation. The fuel and oxidiser reaction order coefficients i and j are therefore used here to avoid confusion.

$$\frac{d}{dt}[F] \propto -[F]^i\,[O]^j e^{-E/RT} \qquad [2.17]$$

The initial concentrations of fuel and oxidiser in a constant-volume adiabatic system may be written as $[F] = x_F \frac{P_O}{R_u T_O}$ and $[O] = x_O \frac{P_O}{R_u T_O}$.

With $\dot{N} \propto \dot{m}_A$ and $Y_F \equiv \eta_c = \eta_\theta$, Equation 2.17 into 2.16 results in:

$$\eta_\theta \phi \dot{m}_A \propto V e^{-E/RT} \rho^{i+j} x_F^i x_O^j \qquad [2.18]$$

Strehlow omitted a pre-exponential temperature dependence from the Arrhenius expression which Laidler and Lefebvre included, resulting in the $T^{0.5}$ discrepancy between equations 2.12 and 2.18. This is revisited in Chapter 4.

2.2 Theoretical flight envelope

The operating flight envelope of an aviation gas turbine is shaped by atmospheric conditions, hardware considerations and combustion efficiency limits. Subsonic civil aircraft operate in the troposphere and lower stratosphere up to typical cruise altitudes of approximately 38000 ft. (11.5 km) [29]. Knowledge of the vertical distribution of temperature, pressure, density, viscosity and the speed of sound within the atmosphere is essential for the modelling of flight conditions. The atmosphere, however, does not remain constant at any particular place or time which necessitated the development of a hypothetical approximation known as the standard atmosphere. The International Organisation of Standardisation (ISO) publishes the International Standard Atmosphere, ISA, while a number of authorities such as the International Civil Aviation Organisation (ICAO) and the United States Government publish extensions and subsets of the same atmospheric model. The models assume the air to be at rest (zero turbulence and no wind) and to be free of any moisture or dust. Naturally significant differences are possible between actual atmospheric conditions and the standard atmosphere properties, which are based on average values recorded at a latitude of 45° N. Table 2.1 provides a summary of the mean sea level (MSL) values employed by the ISA.

Table 2.1: International Standard Atmosphere, MSL Conditions [30]

Temperature	T_{sl}	288.15 K
Pressure	P_{sl}	101325 $N.m^{-2}$
Density	ρ_{sl}	1.225 $kg.m^{-3}$
Speed of Sound	a_{sl}	340.294 $m.s^{-1}$
Gravity	g_{sl}	9.80665 $m.s^{-2}$

Temperature, pressure and density decrease with altitude as shown in Figure 2.4. The ISA assumes that temperature falls linearly at a rate of 6.5 K/km in the troposphere below the tropopause (11 km above sea-level). Above 11 km the ISA temperature remains constant at 216.65 K up to an altitude of 20 km. The pressure, altitude relationship is given by Equation 2.19 where h is the height above sea-level in km, M is the molar mass of air and R_u is the universal gas constant. From the ideal gas law density is given by Equation 2.20.

$$P = P_{sl}\left(1 - {}^{6.5h}/_{T_{sl}}\right)^{9.81M/6.5R_u} \quad [2.19]$$

$$\rho = {}^{P}/_{RT} \quad [2.20]$$

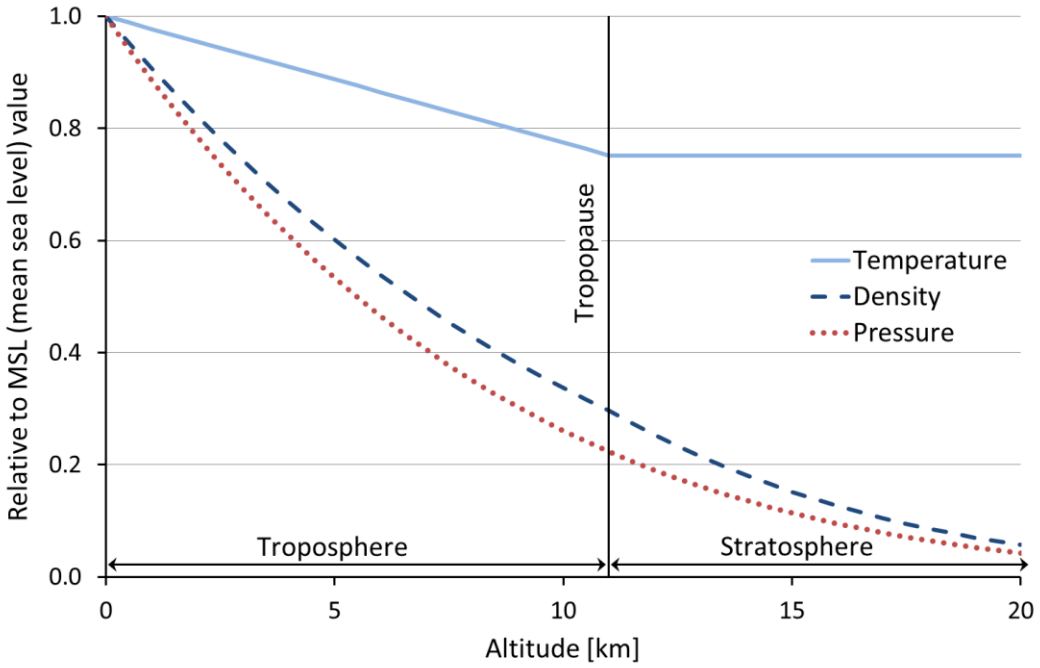

Figure 2.4: Standard atmosphere temperature, pressure and density relative to MSL values

A typical sub-sonic flight altitude-Mach number envelope, also sometimes referred to as a "doghouse plot", is shown in Figure 2.5. Boundary AB is governed by the minimum aircraft speed based on either engine thrust or the minimum stall speed. BC is determined by the operating ceiling of the aircraft and CD is governed by maximum flight Mach number while DE is determined by the maximum engine thrust. The $BCDE$ boundary is of particular interest as far as the differences in altitude blowout and relight behaviour by different fuels are concerned. Although the thermodynamic conditions in the combustor are strongly influenced by the atmospheric temperature and pressure, flight speed also plays a significant role as do design parameters such as bypass ratio, power offtake and exhaust configuration. A simplified approach has been followed to derive combustor temperatures, pressure and mass flow rates corresponding to the flight operating envelope.

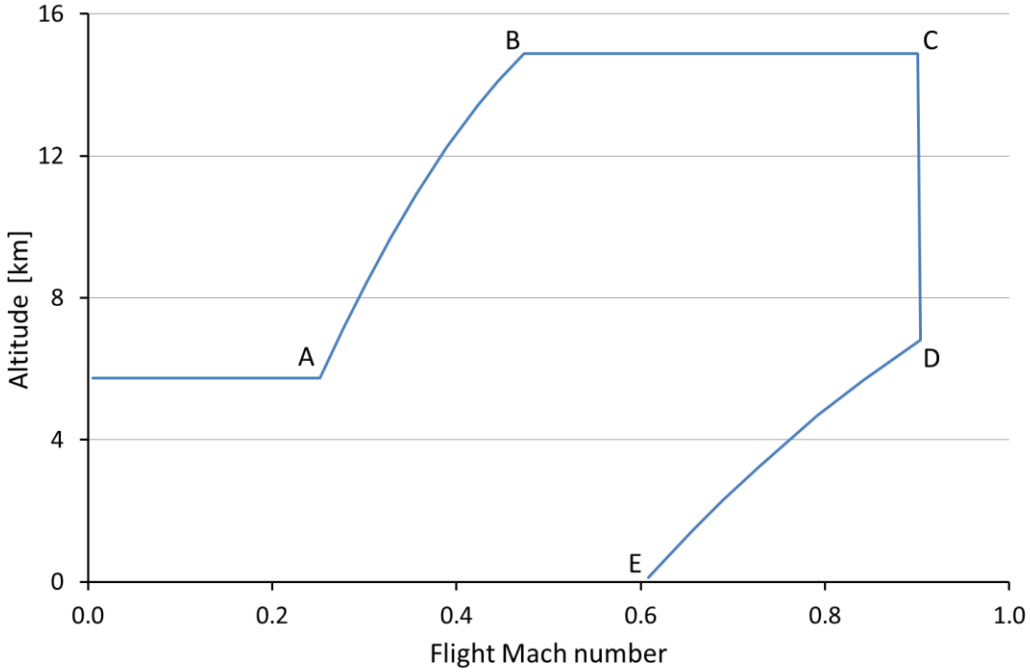

Figure 2.5: Typical idealised sub-sonic flight envelope

Since the greatest disparity between test fuels in the Rolls-Royce evaluation occurred under blowout extinction conditions, this condition was simulated in this preliminary assessment. Conditions prior to in-flight flame-out, or extinction were approximated as follows. Positions 0, 2, and 3 refer to ambient, compressor inlet, and compressor outlet positions respectively. For a given compressor ratio, $r = P_3 / P_0$, the isentropic temperature ratio from the compressor inlet to combustor inlet is given by:

$$\frac{T_{3\text{is}}}{T_2} = r^{(\gamma-1)/\gamma} \quad [2.21]$$

Isentropic compressor efficiencies in modern aircraft gas turbines are typically around 90% [31] and treating the fluid as an ideal gas it can be expressed as

$$\eta_{comp} = \frac{T_{3\text{is}} - T_2}{T_3 - T_2} \quad [2.22]$$

The actual temperature ratio over the compressor is thus given by

$$\frac{T_3}{T_2} = 1 + \frac{r^{(\gamma-1)/\gamma} - 1}{\eta_{comp}} \quad [2.23]$$

The stagnation pressure can be calculated via the isentropic relationship

$$P_0 = P\left(1 + \frac{\gamma-1}{2}M^2\right)^{\gamma/(\gamma-1)} \quad [2.24]$$

2.2.1 Combustion efficiency influences

Boundary $BCDE$ in Figure 2.5 can be impacted by combustion efficiency and therefore fuel influences on combustion efficiency can potentially also delimit the envelope boundary. This potential impact was investigated by applying the modelled evaporation-mixing- and reaction-controlled efficiency expressions to the idealised altitude, Mach number model. Physical hardware parameters and proportionality constants were arbitrarily chosen to illustrate potential envelope limits. The mixing-controlled efficiency as defined in Equation 2.11 is insensitive to flight conditions and does not impact boundary $BCDE$. This is revisited in Chapter 4.

Equation 2.6 was employed to model the evaporation-controlled efficiency over the operating altitude temperature, pressure, and air mass flow range.

$$\eta_e = {\rho_A \lambda_{eff} V}\Big/{D_0^2 f_c \dot{m}_A} \quad [2.6]$$

Combustion efficiencies of at least 75 to 80% are required to sustain combustion and prevent flameout [16]. A combustion efficiency limit of 75% was therefore used to calculate the corresponding maximum flight Mach numbers. Chin and Lefebvre [20] presented plots of effective evaporation constants versus boiling point for various values of droplet size and velocity at three pressures and three ambient temperatures. They acknowledged that while a single fuel property cannot fully describe evaporation characteristics of any given fuel, average boiling point has the benefit of being directly

related to vapour pressure and fuel volatility. Using these three plots, Equation 2.25 was derived empirically for calculating the effective evaporation constant. The omission of droplet size and velocity was deemed to be an acceptable simplification for an initial investigation. The fuel boiling point was treated as constant for a single fuel model and is revisited in Section 7.3 for the evaluation of multiple fuels with variable boiling point temperatures.

$$\lambda_{eff} \propto P^{0.09}\, T^{1.8} \qquad [2.25]$$

The majority gas turbines employ prefilming airblast atomisers combined with strong swirling flow to ensure fine atomisation and dispersion of droplets throughout the combustion zone. Rizkala and Lefebvre [32] concluded that for fluids such as kerosene with relatively low viscosities the mean droplet size is primarily influenced by surface tension, air velocity and air density while viscosity plays and independent role. They proposed a two-term expression for Sauter mean diameter, SMD, (Equation 2.26) based on analysis of experimental data where the first term is dominated by surface tension and air momentum and the second by liquid viscosity. Lefebvre subsequently presented a modified version (Equation 2.27) with experimentally determined burner-specific constants A and B [33].

$$SMD = 3.33 \times 10^{-3} \frac{(\sigma \rho_L D_P)^{0.5}}{\rho_A U_A}\left(1 + \frac{1}{ALR}\right) + 13.0 \times 10^{-3} \left(\frac{{\mu_L}^2}{\sigma \rho_L}\right)^{0.425} D_P^{0.575} \left(1 + \frac{1}{ALR}\right)^2 \qquad [2.26]$$

$$SMD = A\left(\frac{\sigma}{\rho_A {U_A}^2 D_P}\right)^{0.5}\left(1 + \frac{1}{ALR}\right) + B\left(\frac{{\mu_L}^2}{\sigma \rho_L D_P}\right)^{0.5}\left(1 + \frac{1}{ALR}\right)^2 \qquad [2.27]$$

D_P is the prefilmer diameter, U_A the air velocity, and ALR the air/liquid mass ratio. For low viscosity liquids such as water and kerosene the first term predominates resulting in 2.28.

$$SMD = D_{32} \propto \left(\frac{\sigma}{\rho_A {U_A}^2 D_P}\right)^{0.5}\left(1 + \frac{1}{ALR}\right) \qquad [2.28]$$

With $1 + \frac{1}{ALR} \approx 1 + \frac{\phi}{14.6} \approx 1$ and assuming constant hardware dimensions as well as fuel properties, Equation 2.6 simplifies to:

$$\eta_e \propto P^{1.09} T^{0.8} / \dot{m}_A \qquad [2.29]$$

Applying the atmospheric pressure and temperature values at varying altitude, and setting the blowout threshold evaporative efficiency at a fixed 75%, one obtains the theoretical evaporation-controlled limit curve as is shown in Figure 2.6. Note that the

value of the proportionality constant was arbitrarily chosen for illustration purpose so that the limit contour passed through Mach 0.87 at an altitude of 10 km.

The reaction-controlled combustion efficiency was based on Equation 2.18 and the assumption that for an overall global reaction scheme the fuel and oxygen concentrations could be regarded as referring to the initial concentrations $x_F = \frac{\phi}{\phi+85.7}$ and $x_O = \frac{18}{\phi+85.7}$. With $\phi < 1$ both x_O and the denominator of x_F are nominally constant and can be absorbed into the overall proportionality. Equation 2.18 therefore simplifies to 2.30 and employing exponents of i and j corresponding to the values recommended by Lefebvre [24], the efficiency expression can be further reduced to 2.31. This was employed to produce the theoretical reaction-controlled extinction limit contained in Figure 2.6. Again, the overall proportionally constant was arbitrarily chosen for illustrative purpose only.

$$\eta_\theta \phi \dot{m}_A \propto V e^{-E/RT} \rho^{i+j} \phi^i \quad [2.30]$$

$$\eta_\theta \propto V e^{-E/RT} \rho^{1.75} / \dot{m}_A \quad [2.31]$$

The broken curves parallel to the evaporation and reaction-controlled curves are illustrative of the effect that variations in the proportionally constants have, as would be expected for different fuels with different evaporation and reaction behaviour.

A number of conclusions were drawn from the theoretical treatment and resultant Figure 2.6. The mixing-controlled limit is independent of the air flow and air density (to a first order of magnitude analysis), which discounts it from playing a role in the discrepancy that Rolls-Royce detected at high altitude and high subsonic Mach numbers. This is further reinforced by the fact that fuel properties do not directly influence the parameters contained in the equation governing mixing behaviour (2.11).

The negative gradient of both the evaporation and reaction-controlled limits suggest that either of these aspects could provide a candidate explanation for the fuel-related variance that was detected by Rolls-Royce. The fact that fuel properties could conceivably cause a significant distinction in the manifestation of either of these limiting efficiency boundaries does not contribute to determining the more probable candidate.

The theoretical treatment is supported by the Honeywell Aerospace test results which detected very little distinction between the different test fuels. These tests were

conducted at 25000 ft. (7.62 km) where the flight envelope is not expected to be governed by fuel properties.

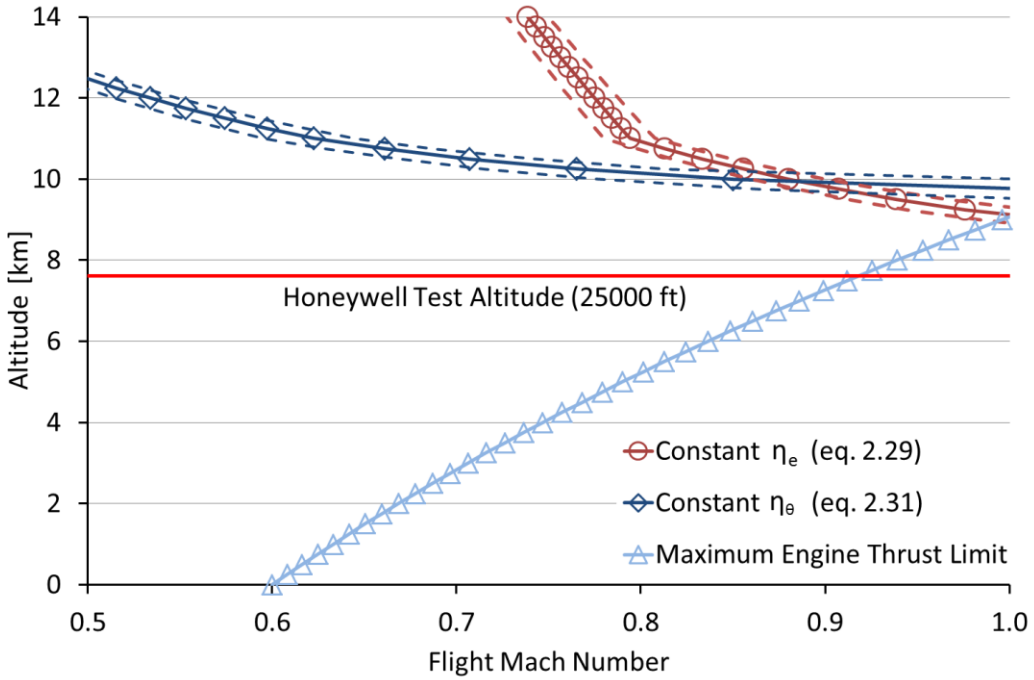

Figure 2.6: Theoretical thrust limit, constant evaporation- and reaction-controlled combustion efficiency traces in the altitude-Mach number domain

Chapter 4 revisits the efficiency limit treatments in terms of fluid-mechanic and chemical timescales to examine their relevance under the different combustor conditions and with different fuels.

2.3 Hypotheses and project plan

The preceding preliminary theoretical treatment identified the root cause of the altitude blowout differences by the Rolls-Royce report as being determined by either the evaporation or the reaction-controlled combustion efficiency but not by mixing efficiency. The following three hypotheses were therefore formulated to define the scope of the thesis:

Hypothesis 1: A range of aviation jet fuels could be blended according to a design-of-experiment strategy to exhibit independent variations in properties relating to evaporation and reaction behaviour whilst still meeting the legislated physical fuel specifications.

Hypothesis 2: The range of variations contemplated in Hypothesis 1 could have a detectable and significant influence on the simulated high altitude extinction behaviour in a representative aviation gas turbine combustor. (Note that this is not a legislated criterion)

Hypothesis 3: The relevant properties described in Hypothesis 1 can be scientifically quantified in an appropriate test apparatus and can be correlated to the high-altitude extinction behaviour described in Hypothesis 2.

The thesis was structured to address these hypotheses primarily through theoretical analyses of targeted experimental programmes. A schematic summary of the thesis structure is presented graphically in Figure 2.7.

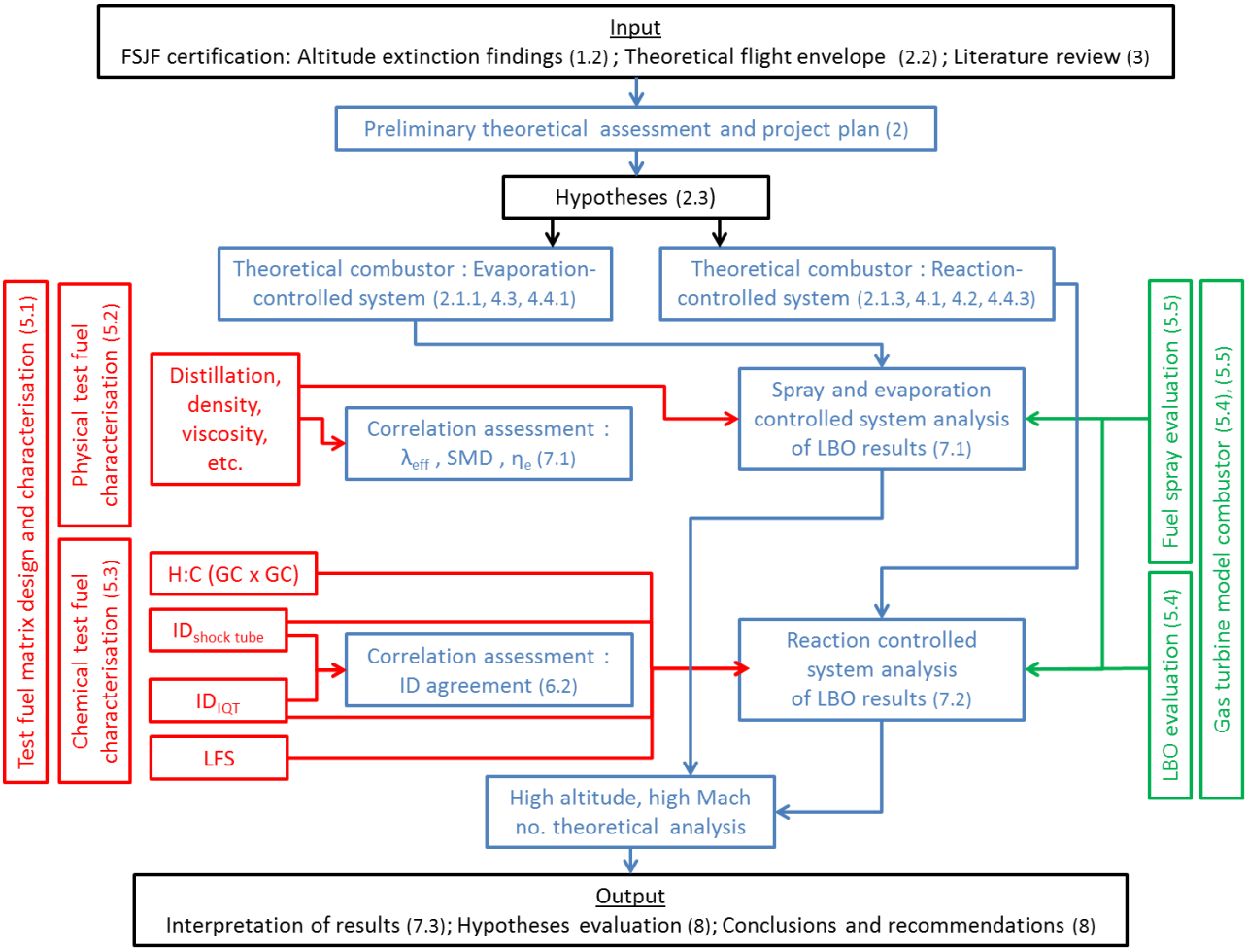

Figure 2.7: Schematic representation of thesis structure with relevant section numbers provided in brackets.

The evaporation and chemical reaction properties of the test fuels were assessed against theoretical models prior to being incorporated in the evaluation of the experimental results. Theoretical models were presented of both evaporation and reaction limited combustion. The theoretical models, fuel properties and results from model-combustor experiments were combined to interrogate evaporation and reaction-controlled extinction behaviour and address hypotheses 1 and 3. By combining these results with a theoretical analysis of higher altitude and Mach number operation, Hypothesis 3 was addressed and an explanation was provided for the results of the FSJF certification tests.

In the following sections a selection of relevant literature is reviewed prior to the theoretical assessment being expanded in support of the experimental design and evaluation of test results.

3 Literature Review

The combustion performance of practical aircraft combustors is known to be primarily influenced more by physical processes of heat transfer, mass transfer, thermodynamics, gas dynamics and fluid dynamics than by chemical processes. While chemical reaction rates are acknowledged as being of great importance they are largely disregarded in high temperature flames due to being considered to be relatively rapid and not rate controlling. Emphasis is placed on large scale mixing and the interdiffusion of fuel and air as the rate controlling steps. Chemical processes are, however, acknowledged to be of particular importance for the formation of pollutant emissions and for the lean light-off and lean blowout (or weak extinction) limits at high flight altitudes [4, 5].

The difficulty in investigating fuel property effects on gas turbine combustion is evident throughout literature. The interrelated nature of various fuel properties precludes the classical experimental research approach of quantifying the effects of varying a single independent parameter while maintaining all others relatively constant. The fact that different hardware designs have been shown to respond differently to fuel property variations is a further confounding factor. One notable example can be found in the response of liner temperature of combustors with either lean or rich primary combustion zones to carbon/hydrogen (C/H) ratio variations. Heat transfer to the liner wall is primarily due to radiation in the case of rich primary zone combustion and is thus governed by flame emissivity, which in turn is influenced by the C/H ratio. In a lean primary combustion zone heat transfer to the liner wall occurs primarily due to forced convection which is relatively insensitive to C/H ratio changes with the gas temperature being dominant [34].

In many instances engine-hardware-oriented studies that focused on investigating the influences of gas turbine fuel properties on combustion analysed the net effect of fuel variations on a specific combustor parameter. In some instances attempts were made to isolate and categorise fuel property effects.

Venkataramani isolated fuel volatility effects from atomisation effects during an investigation of fuel property influences on altitude relight performance [35]. The study focused only on separating the influences of physical fuel properties, while chemical property differences were not investigated. Four test fuels were employed (JP-4, Jet A, Jet A/2040 solvent blend, and Diesel 2) covering a wide range of volatilities. In order to

eliminate fuel specific effects on atomisation, injection equipment was used that maintained equivalent SMD values (50 ± 10 μm) for all test fuels at equal design flow rates. The results revealed, inter alia, that fuel volatility assumed a secondary role in initial (first cup) light-off. Decreased volatility resulted in slightly poorer blowout performance but full-propagation and first cup blowout were found to be independent of fuel volatility. In spite of the previously mentioned acknowledgement that chemical reaction time scales can be significant under threshold conditions such as encountered during altitude relight, the potential influence of the fuels exhibiting different chemical reaction rates was not taken into account. Airblast atomisers were shown to exhibit poorer ignition performance and a stronger volatility dependence than pressure atomisers.

In another investigation aimed at anticipating the combustion performance effects of future fuel formulations, Lefebvre analysed a large body of data from studies conducted by the USAF, Army, Navy and NASA [34]. The matrix of thirteen test fuels included JP-4, JP-8, five blends each of JP-4 and JP-8, as well as a No. 2 diesel which provided three levels of hydrogen content: 12, 13 and 14 percent by mass. The results from the studies were analysed to determine how combustion efficiency, lean blowout limits, ignition performance, liner wall temperature, emissions and pattern factor were influenced by the differences in fuel formulation.

Hydrogen content and/or aromatic content exhibited a significant influence on flame radiance, liner wall temperature and smoke emissions. Physical fuel properties that influenced atomisation quality and evaporation rates were shown to affect lean blowout, ignition, combustion efficiency and CO emissions while liner wall temperature, NO_x and smoke emissions were not influenced by fuel physical properties. Combustion efficiency, lean blowout, ignition and CO and NO_x emissions exhibited a small dependence on fuel chemistry differences. This was attributed to the influence of slight variations in calorific value on combustion temperature. The physical fuel properties had an appreciable effect on pattern factor at low power conditions but this effect decreased to be very small at high power settings where pattern factor effects on vane life are typically most significant. The combustor pattern factor was not influenced by fuel chemistry. It should be noted that in this study the carbon to hydrogen (C/H) ratio was taken as representative of the fuel chemistry differences and no metric

representative of chemical reactivity such as ignition delay or laminar flame speed (LFS), was measured or reported.

Rao and Lefebvre [36] concluded that the presence of sufficient fuel vapour in the ignition zone is the sole determining criterion for ignition of heterogeneous mixtures of fuel droplets in air. Ignition will ensue automatically if sufficient thermal energy is created by the passage of the spark to produce the required amount of fuel vapour. The basis of this argument is the understanding that, over a wide range of operating conditions, the chemical reaction time is very short relative to the time required for producing an adequate amount of fuel vapour in the ignition zone. This is, however, not necessarily the case under threshold conditions where the reaction timescales can be impaired.

Ballal and Lefebvre [37] proposed theoretical models for determining the minimum ignition energy required and the quench distance in liquid fuel sprays. Quench distance is defined as the critical spark-kernel size at which the rate of heat loss at the kernel surface is equal to the rate of heat release throughout the kernel volume, due to the instantaneous combustion of fuel vapour. The kernel must attain this size in order for combustion to propagate unaided and the minimum ignition energy is defined as the amount of energy required from an external source to attain the quenching distance [4].

In a subsequent study the model was extended to include the presence of fuel vapour in the mixture entering the ignition zone and the influence of finite chemical reaction rates, which are known to be significant for well atomised fuels at low pressures and low equivalence ratios [38]. This yielded Equation 3.1 for calculating quenching distance (d_q) for all conditions likely to be encountered in practical combustion systems. A good fit was obtained with experimental data over SMD values ranging from 40 to 150 µm.

$$d_q = \left[\frac{\rho_F {D_{32}}^2}{\rho_A \phi ln(1+B_{st})} + \left(\frac{10\alpha}{S_L}\right)^2\right]^{0.5} \quad [3.1]$$

The first term of the root sum square equation deals with fuel evaporation. Fuel and air densities are represented by ρ_F and ρ_A respectively, Sauter mean diameter by D_{32}, equivalence ratio by ϕ, and the stoichiometric mass transfer number by B_{st}. The second term introduces a measure of a fuel chemistry influence with α representing the thermal diffusivity and S_L the laminar flame speed of the fuel. By dividing the thermal diffusivity by the laminar flame speed, the second term effectively reduces to the

product of the specific heat at constant pressure (C_p), density (ρ) and laminar flame thickness (δ_L). The influence of the chemical reaction rate is thus reflected in terms of the laminar flame thickness. The importance of chemical reaction timescales in the combustion of well atomised fuels at low pressures and lean equivalence ratios as well as under threshold combustion conditions such as encountered during altitude relight and blowout is therefore acknowledged to some degree.

Increased interest in alternative aviation fuel formulations, and the related opportunity to influence chemical reaction rates to a greater degree than traditionally possible in the case of petroleum-derived jet fuel, has prompted investigation into the influence of physical and chemical fuel properties on gas turbine combustion behaviour. A number of recent studies have reported ignition and extinction behaviour being influenced by fuel formulation to varying degrees. These studies employed experimental setups ranging from laboratory scale combustors to full scale gas turbines and test fuels ranging from single component fuels to full boiling range jet fuel formulations. Findings ranged from reports of appreciable differences to relative insensitivity to fuel formulation [6 - 13].

Fyffe et al. conducted an altitude ignition and extinction evaluation of five synthetic paraffinic kerosene (SPK) fuel formulations at the Rolls-Royce plc. sub-atmospheric altitude ignition facility in Derby, UK [8]. A multi-sector representation of an advanced gas turbine combustor and fuel injector was used to evaluate threshold combustion at two test conditions that were considered to be representative of approximate altitude conditions of 25000 to 30000 ft. (7.62 to 9.14 km). The five test fuels were all GTL-derived and were compared against a representative crude-derived Jet A-1. The results were interpreted against three compositional variables that were chosen to define the fuel matrix: carbon number distribution (narrow vs. wide), iso/normal paraffin ratio and total paraffinic content. Unfortunately other fuel properties were not reported which hinders the subsequent critical assessment of the results. Some differences were reported in ignition behaviour but extinction differences were considered to be within the experimental scatter. The study associated low iso/normal paraffin ratios with improved ignition behaviour. This trend is known very well in diesel and gasoline engine fields where the extremities of the respective cetane and octane rating scales are each defined by a normal and iso-paraffinic reference fuel. The results were not subjected to a theoretical assessment and fundamental reasons for the observed behaviour were not

offered but it did support the possibility for fuel formulation differences impacting threshold combustion.

Burger et al. presented results from a lean blowout (LBO) study of 16 different fuel formulations in an in-house developed combustor that was based on the primary zone of an Alison T63. A simplex pressure atomiser nozzle was used in the evaluation. The authors reported blowout limits correlating with volatility and significantly reported a (weak) negative correlation between derived cetane number (DCN) and LBO [7].

A follow-on paper evaluated eight test fuels from the same matrix in a representative aero-engine combustor sector equipped with an airblast atomiser [9]. Significant variability in the results prevented more definitive conclusions being drawn from this study. It is notable that the shape of the extinction limit curves suggests that the tests were conducted in a regime that was primarily influenced by evaporation efficiency. It is significant that under this regime of operation any potential correlation between DCN and LBO was masked. This topic is revisited in more detail under Section 4.3.

Rock et al. reported on an experimental study of lean blowout in a swirl-stabilised combustor equipped with both pressure and airblast atomisers [10]. The study's key motivation was similar to this thesis, to investigate the relative roles of physical properties and chemical kinetic properties on lean blowout behaviour. The test fuel matrix encompassed eight fuels including three crude-derived jet fuels (Jet-A, JP-5, and JP-8) and five formulations that spanned a range of physical and chemical properties. The pressure atomiser blowout tests revealed strong correlations with fuel physical properties, particularly boiling point temperature. Fuels that were less easily atomised and vaporised were harder to blowout. This is in accordance with the concept that delaying atomisation and or vaporisation delays the level of premixing that drives very lean global fuel-air ratios. It creates localised regions of higher fuel-air ratios and elevated flame temperatures which supports combustion. The authors proposed that this behaviour was dependent on the pre-heat temperature being above the fuel flash point and that the reverse behaviour is exhibited when the pre-heat temperature is lower than the flash point which would be in agreement with the work by Burger et al. [7]. It also agrees with the statement by Lefebvre that pressure atomisers typically produce lower fuel/air mixing prior to combustion and have superior blowout performance [39]. With the exception of one fuel, the pressure atomiser results also reported good correlations between blowout and C/H ratio, iso-paraffinic content and

fuel smoke point. The authors ascribed this to a strong co-correlation with the more significant physical parameter T_{90}.

In contrast to the pressure atomiser behaviour, Rock et al. reported no strong correlation between the blowout behaviour recorded with the airblast atomiser and fuel physical properties. The strongest correlation that they recorded was with the iso-paraffinic content of the test fuels which the authors ascribed to being driven by the chemical kinetic properties of the fuel. The authors indicated that no clear correlation was found between the airblast blowout results and cetane number which was supported by substantial scatter in the figures presented. However, closer inspection of the correlation matrix revealed significant negative correlations with LBO for both atomiser options. This was further supported by a strong negative correlation between iso-paraffinic content and cetane numbers. This lacuna within the paper is significant in view of the contradictory observations highlighted in the earlier works. It is especially relevant to the present research initiative and provides a motivation for a careful study of the issue of a possible correlation between the cetane rating of the fuel and LBO.

Grohmann et al. investigated lean blowout differences using the same gas turbine model-combustor that was employed in this thesis [11]. In an attempt to minimise the complexity inherent in multi-component jet fuel, they selected six single-component model fuels to represent normal, branched, cyclic and aromatic hydrocarbons. The paper reported atomisation, vaporisation, chemical kinetic properties and lean blowout results for three of these fuels: n-hexane, n-dodecane and iso-octane. The authors observed that both physical and chemical fuel properties influenced the measured LBO behaviour. Differences in the LBO behaviour of n-hexane and iso-octane were ascribed to chemical kinetic nature of the fuels and in agreement with normal alkanes exhibiting shorter ignition delays than branched alkanes (of the same carbon number). The two fuels exhibited very similar atomisation and vaporisation behaviour.

By comparison n-hexane and n-dodecane revealed comparable chemical kinetic characteristics, but very different atomisation and vaporisation behaviour. At high air pre-heat temperatures the two fuels reported similar LBO results, but at lower pre-heat the larger droplets and lower evaporation rate of n-dodecane was credited with extending LBO limits. The authors proposed a similar explanation to that offered by Rock et al. [10] but interestingly in this instance the atomiser was a prefilming airblast unit.

Bluff-body flames have been studied extensively, but a lack of consensus about the physical and chemical processes that lead to blowout motivated a study by Heulskamp et al. which utilised a large data set of experimental and literature LBO results for bluff-body stabilised flames to develop a correlation for predicting lean blowout [40]. They confirmed a dependence on the Damköhler number with fuel variation playing a significant role. Damköhler number is commonly used in chemical engineering as an expression of the ratio of chemical and fluid-mechanic timescales. Most researchers agree that LBO is governed by it, but there have been different proposals about the definition of the critical timescales. Research such as reported by Shanbhogue et al. advocate the impact of ignition delay while Radhakrishnan et al. and Kariuki et al. presented successful correlations with flame speed which argued that blowout is not governed by ignition timescales [41, 42, 43].

Heulskamp et al. thus endeavoured to provide clarity about critical parameters and their significance to physical and chemical processes. They concluded that pressure, temperature and C/H ratio of the fuel impacted the reactivity of the mixture and contributed to the chemical timescale within the Damköhler number. It was confirmed that blowout was not solely dependent on the fluid mechanic timescales and LFS was discredited as a blowout predictor. Ignition delay was found to be an excellent representation of the chemical timescale in the experimental data set as evidenced by Figure 3.1 where D/U refers to the fluid-mechanic timescale (U is the lip velocity and D is the characteristic diameter of the bluff body).

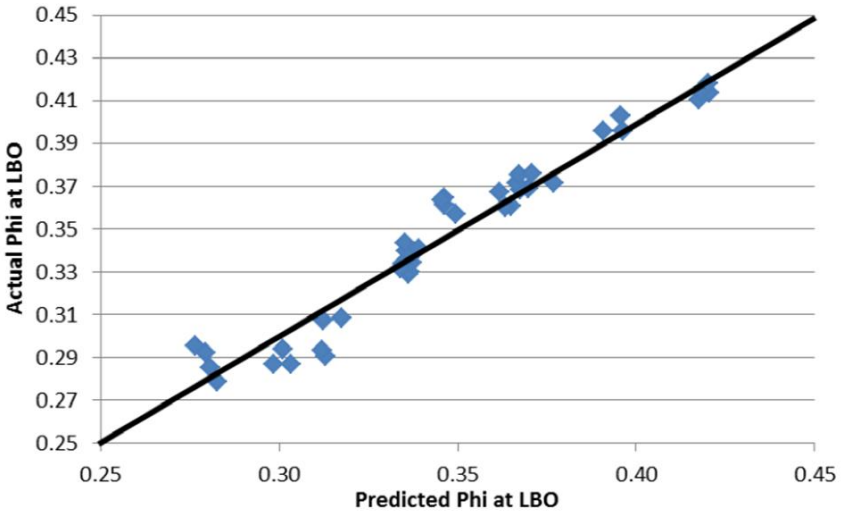

Figure 3.1: Ignition delay dataset correlation results with D/U and IDT as factors (R^2 = 0.918) (from Heulskamp et al. [40])

The authors also advocated the influence of cetane number and C/H ratio on blowout behaviour due to the covariance of these properties with ignition delay. This is in agreement with Colket et al. who reported fuels with higher cetane numbers and higher C/H ratios blowing out at lower equivalence ratios as shown in Figure 3.2 [44].

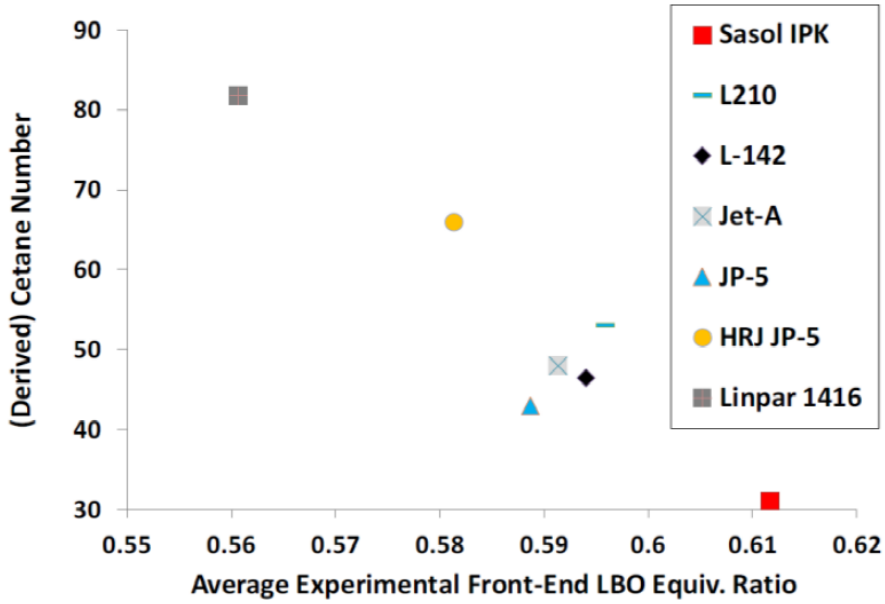

Figure 3.2: Derived cetane number against equivalence ratio at LBO (from Colket et al. [44])

The work by Won et al. [45] also supported the relevance of cetane number to gas turbine combustion and extinction. Their study of the pre-vaporised global combustion behaviour of a selection of petroleum-derived and alternative jet fuels yielded a ‘‘combustion property target (CPT) index” that was developed through regression analysis of results from three experiments. The CPT index was proposed as a fuel screening tool for assessing fully pre-vaporized, kinetically coupled behaviours of potential alternative jet fuel formulations. Derived cetane number (DCN) was included in the analysis as a measure of autoignition propensity. DCN is calculated directly from ignition delay measurements in an ignition quality tester (IQT™) which will be discussed in greater detail under the experimental design in Chapter 5. The resultant CPT index for extinction employed DCN, heat of combustion, and molecular weight and the CPT index for low temperature heat release (LTHR) rate was purely based on DCN. Figure 3.3 reproduces a figure reporting the results of the linear regression of the diffusion flame

extinction at a fixed mass fuel fraction (Y_f = *0.4*). The typical range of JP-8 fuels is demarcated by the dashed rectangle.

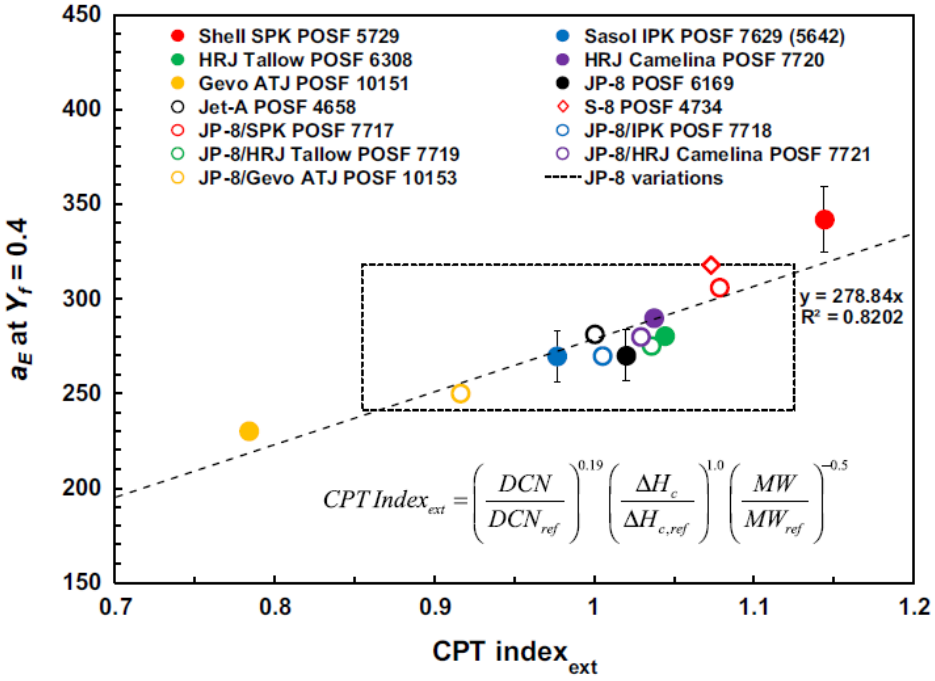

Figure 3.3: CPT index correlation for diffusion flame extinction at Y_f = *0.4* (from Won et al. [45])

Figure 3.4 provides a comparison of DCN and the measured LTHR rate as represented by the maximum H_2O mole fraction in the temperature range between 550 and 700 K.

The authors made the pertinent comment about DCN in the context of LTHR that most of the alternative jet fuels and their blends with petroleum-derived jet fuels were outside of the variability of JP-8. In light of the approval of 50:50 blends of SPK and crude-derived fuel they made the point that low temperature reactivity might not be a critical combustion property for existing gas turbines. However, they highlighted that advanced engine designs are focused on increasing pressure ratios and combustor pressures significantly in order to achieve greater efficiency. Under these conditions low temperature reactivity is expected to play a more significant role under threshold combustion conditions such as LBO and altitude relight.

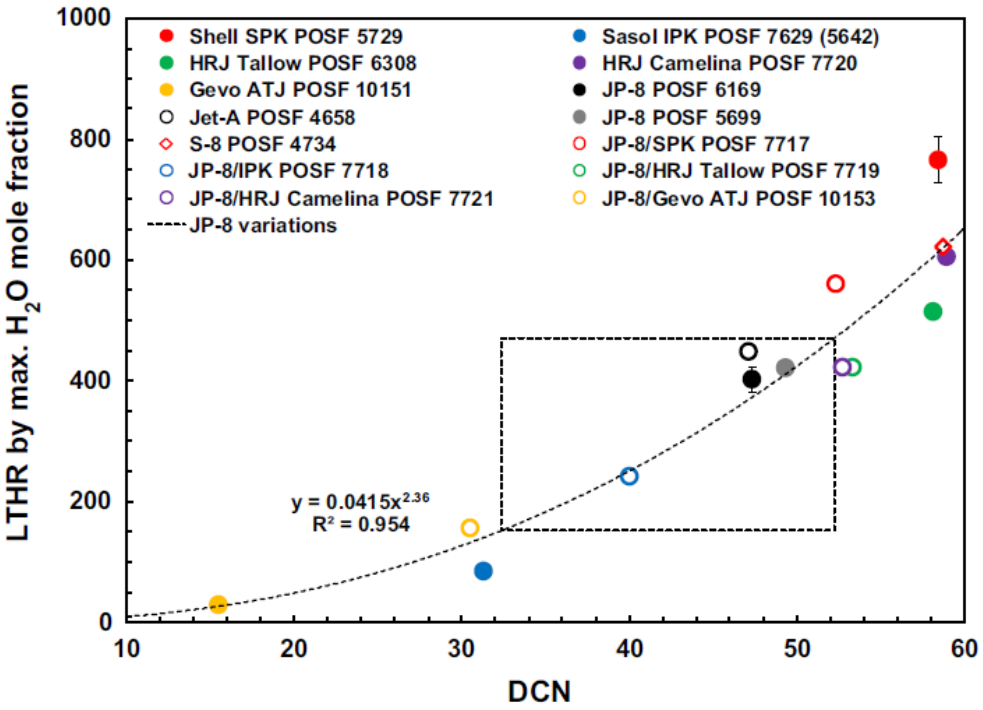

Figure 3.4: Comparison of DCN to measured LTHR (from Won et al. [45])

Evidence from literature clearly supports the importance of considering both physical and chemical fuel properties in the context of threshold combustion and high altitude blowout extinction. There are, however, inconsistencies and omissions in said literature which necessitate further exploration.

One example is the contradicting conclusions regarding the impact of cetane and LFS which require clarification. Associated with this; it has been demonstrated that the comprehensive characterisation of test fuels making use of appropriate metrics is vital. Other areas that have exposed difficulties included the use of test fuel matrices that are both representative of real fuels and also sufficiently differentiated to enable meaningful correlation analyses. The use of technically relevant combustor architecture and injection equipment is another area that has been shown to impact the conclusions drawn by different studies.

A very comprehensive, multi-disciplinary, three-year research initiative known as the National Jet Fuels Combustion Program (NJFCP) is currently in progress in the United States of America. Its aim is to develop an experimental and analytical capability to facilitate OEM's evaluation of fuel physical and chemical properties on engine operability and to streamline the ASTM fuels approval process. Ignition and lean blow-

out and the influence of flight altitude are some of the principal areas of focus for the program. Aspects of the literature cited in this chapter are associated with the first fruits of this program and it is expected that a substantial volume of relevant literature will continue to emerge from this program during 2017 and beyond.

4 Theoretical Assessment

In the following chapter the preliminary theoretical assessment captured in Chapter 2 is expanded. The handling of combustion efficiency in a chemical kinetics driven system is extended. The influence of spray and evaporation on extinction limits is discussed and the significance of the different combustion efficiency definitions is investigated.

4.1 Burning velocity model

It was mentioned that there is more than one approach to defining combustion efficiency in a system where chemical kinetics are considered to be rate-controlling and evaporation and mixing rates are assumed to be infinitely fast [46, 47, 48]. The preliminary theoretical approach in Chapter 2 was based on the well-stirred reactor model. In the following section the alternative burning velocity model is discussed followed by an expansion of the stirred reactor model.

The burning velocity model proposes a combustion zone that is analogous to the flame brush on a Bunsen burner. All the fuel that burns is assumed to burn completely and combustion inefficiency is attributed to some of the mixture passing through the combustion zone without being entrained by the turbulent flame front. The combustion efficiency is then defined as:

$$\eta_\theta = {(heat\ released\ in\ combustion)}\Big/{(heat\ available\ in\ fuel)}$$

$$= {(\rho_g A_f S_T c_p \Delta T}\Big/{(q\dot{m}_A H)} \qquad [4.1]$$

where S_T is the turbulent burning velocity. By definition $c_p\Delta T = qH$ and with the flame area (A_f) assumed to be proportional to the combustor reference area (A_{ref}) 4.1 simplifies to

$$\eta_\theta = {\rho A_f S_T}\Big/{\dot{m}_A} \propto {S_T}\Big/{U_{ref}} \qquad [4.2]$$

In his studies of Bunsen burner flames Damköhler [49] concluded that the effect of turbulence on burning velocity depends on the scale of the turbulence relative to the flame front thickness. He derived the following expression for turbulent burning velocity

where S_t and S_L are the turbulent (small scale) and laminar flame speed respectively, ϵ is the turbulent exchange coefficient, ν the kinematic viscosity, Re the Reynolds number and k a constant:

$$S_t = S_L\sqrt{\frac{\epsilon}{\nu}} = S_L k\sqrt{Re} \quad [4.3]$$

Greenhough and Lefebvre provided a relation between large scale and small scale turbulence by amending Karlovitz's expression for large scale turbulence [23]. The combustion zone is visualised as a region in which small volumina of gas are produced by strong turbulence. These volumina of gas propagate at a burning velocity that is governed by the small scale turbulence and the root mean square value of the fluctuating velocity, $\bar{u}$.

$$S_T = \sqrt{(2S_t\bar{u})} \quad [4.4]$$

Combining 4.3 and 4.4 and substituting into 4.2 yields:

$${\eta_\theta}^2 = {2k\rho^2{A_f}^2 S_L\bar{u}\, Re^{0.5}}\Big/{{\dot{m}_A}^2} \quad [4.5]$$

with Reynolds number defined as:

$$Re = \frac{\mathrm{v}D\rho}{\mu} = \frac{\dot{m}_A D}{A\mu} \quad [4.6]$$

They assumed viscosity to vary little with pressure and thus expressed it as a constant multiplied by a function of temperature

$$\mu = k_1^2\, T^{0.75} \quad [4.7]$$

The fluctuating velocity was expressed in terms of liner pressure loss, ΔP_L, where the fraction of the pressure loss that promotes useful turbulence is denoted by k_2.

$$\bar{u} = \left(\frac{2gk_2\,\Delta P_L}{\rho}\right)^{0.5} \quad [4.8]$$

Further by defining the dynamic head as

$$d = \frac{\rho \mathrm{v}^2}{2g} = \frac{\dot{m}_A}{2g\rho A^2} \quad [4.9]$$

Equation 4.5 becomes

$${\eta_\theta}^2 = \left(\frac{2k}{k_1}\right)\left(\frac{{A_f}^2 D^{0.5}}{A^{1.5}}\right)\left(\frac{\rho^2 S_L^2}{\dot{m}_A T^{0.75}} \times \frac{k_2\Delta P_L}{d}\right)^{0.5} \quad [4.10]$$

They related the laminar flame speed to inlet pressure and temperature in an expression of the form

$$S_L \propto P^{(n-2)/2} f(T) \quad [4.11]$$

where n is the reaction order and $f(T)$ varies with fuel-air ratio and fuel type. This resulted in Lefebvre arriving at Equation 4.12 containing an exponential temperature relationship of empirical origin [24, 25]. The combustor reference area, A_{ref}, was assumed to be proportional to the flame area. D_{ref} is the width of the combustor casing and q_{ref} is the reference dynamic pressure.

$$\eta_\theta = \left[P_3 A_{ref} \left(P_3 D_{ref}\right)^m e^{(T_3/b)} / \dot{m}_A\right] \left[\Delta P_L / q_{ref}\right]^{0.5m} \quad [4.12]$$

There is clearly a disconnect between the left hand side being dimensionless and the right hand side having units of [m/s]. Lefebvre and Halls addressed similar concerns about dimensional inconsistencies by pointing to the introduction of, for example, viscosity expressed as a constant multiplied by temperature. The subsequent omission of the constant introduced dimensions in spite of the formulae essentially being dimensionless. Assigning values of $m = 0.75$ and $b = 300$ resulted in Lefebvre's simplified Equation 4.13.

$$\eta_\theta = f\left[{P_3}^{1.75} D_{ref}^{0.75} e^{(T_3/300)} / \dot{m}_A\right] \quad [4.13]$$

4.2 Stirred Reactor model

The well-stirred reactor model was introduced in Chapter 2 based on a derivation by Strehlow [28] and appeared to be technically more defensible. The derivation yielded Equation 2.18 (repeated here for ease of reference).

$$\eta_\theta \phi \dot{m}_A \propto V e^{-E/RT} \rho^{i+j} x_F^i x_O^j \quad [2.18]$$

The stoichiometric fuel mole fraction, x_s, was "absorbed" into the proportionality relation. Note that, by assuming the reactor contents to be perfectly homogenous it is implied that the chemical reaction between the incoming reactants take place at the temperature and molecular concentrations of the products. Strehlow omitted a pre-exponential temperature dependence from the Arrhenius expression (as explained by Laidler [50]) which Lefebvre included (as $T^{0.5}$) in his equivalent expression:

$$\eta_\theta \phi \dot{m}_A \propto V T^{0.5} e^{-E/RT} \rho^{i+j} x_F^i x_O^j \quad [4.14]$$

The balanced equation for the lean combustion (as would be applicable to LBO) of a kerosene fuel with a representative chemical formula $C_{12}H_{24}$ is as follows:

$$\phi C_{12}H_{24} + 18O_2 + 67.7N_2 = (1-\eta_\theta)\phi C_{12}H_{24} + 12\eta_\theta\phi(CO_2 + H_2O) + 18(1-\eta_\theta\phi)O_2 + 67.7N_2 \quad [4.15]$$

The fuel and oxygen concentrations are therefore given by

$$x_F = \frac{(1-\eta_\theta)\phi}{5\eta_\theta\phi+\phi+85.7} \quad [4.16]$$

and

$$x_O = \frac{18(1-\eta_\theta\phi)}{5\eta_\theta\phi+\phi+85.7} \quad [4.17]$$

Since $\phi < 1$, the denominators in 4.16 and 4.17 can be considered to be nominally constant and absorbed into the proportionality relationship. Substitution into 2.18 yields

$$\eta_\theta\dot{m}_A \propto Ve^{-E/RT}\rho^{i+j}(1-\eta_\theta)^i\phi^{i-1}(1-\eta_\theta\phi)^j$$

$$\therefore \quad \frac{\dot{m}_A}{VP^{i+j}} = K\frac{(1-\eta_\theta)^i\phi^{i-1}(1-\eta_\theta\phi)^j}{T^{i+j}\eta_\theta}e^{-E/RT} \quad [4.18]$$

Note: This expression agrees with Lefebvre's initial reaction-rate theory treatment [51], but when it is recalled three chapters later in the stirred reactor development it is presented as [24]:

$$\eta_\theta = f\left[P_3^2V_ce^{T_3/300}/\dot{m}_A\right] \quad [4.19]$$

No justification is provided for the omitted terms and the change in exponential expression appears fundamentally flawed. It can, however, be shown that over the typical temperature range and with an appropriate adjustment of the proportionality constant $e^{T/300} \cong e^{-400/T}$. The expression $e^{T/b}$ was proposed in chemistry literature during the early 1900s as a chemical reaction rate representation, but it has subsequently been replaced by the Arrhenius formulation, $e^{-E/RT}$, due to it being technically more justifiable which makes Lefebvre's choice to revert to the outmoded form surprising.

Similarly the expression for rich combustion can be derived from the balanced equation:

$$\phi C_{12}H_{24} + 18O_2 + 67.7N_2 = (1-\eta_\theta)\phi C_{12}H_{24} + 12\eta_\theta\phi(CO_2\ or\ CO) + 12\eta_\theta\phi(H_2\ or\ H_2O) + 18(1-\eta_\theta)\phi O_2 + 67.7N_2 \quad [4.20]$$

The fuel and oxygen concentrations are therefore given by

$$x_F = \frac{(1-\eta_\theta)\phi}{5\eta_\theta\phi+\phi+85.7} \quad [4.21]$$

and

$$x_O = \frac{18(1-\eta_\theta)\phi}{5\eta_\theta\phi+\phi+85.7} \quad [4.22]$$

Which for a second-order reaction then yields:

$$\frac{\dot{m}_A}{VP^{i+j}} = K\frac{(1-\eta_\theta)^{i+j}\phi^{i+j-1}}{T^{i+j}\eta_\theta}e^{-E/RT} \quad [4.23]$$

Equations 4.18 and 4.23 provide the relationship between the volumetric flow rate through the combustor and the combustion efficiency (the extent to which combustion was completed during the available residence time) for lean and rich combustion respectively. When plotted for a particular stoichiometric ratio and typical values of E/R and T, the general form (Figure 4.1) compares well with similar figures by Strehlow and Lefebvre.

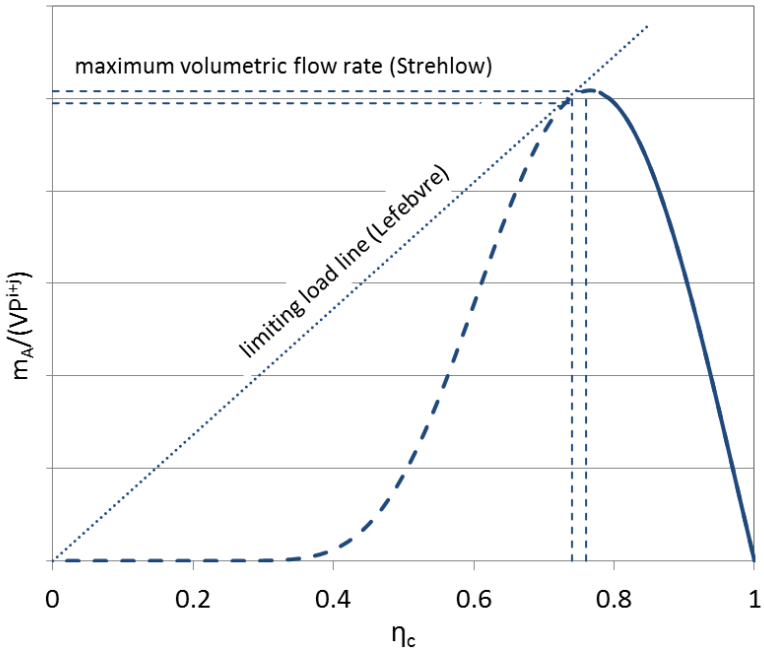

Figure 4.1: Volumetric flow rate vs. efficiency in a typical well-stirred reactor

The right-hand segment of the curve with a negative slope represents stable combustion while the peak represents the maximum flow rate condition beyond which combustion cannot be sustained. The left-hand segment of the curve is not valid since

combustion will always jump to the higher efficiency right-hand side for volumetric flows below the peak value. Lefebvre and Strehlow differ in their definition of the exact blowout point on the diagram. Lefebvre introduces a load line which represents the heat required to raise the reactants to the reaction temperature. At blowout the limiting load line is tangential to the flow rate curve with the point of tangency identifying the associated volumetric flow and combustion efficiency. Strehlow on the other hand maintains that blowout corresponds with the maximum flow rate value. In either case blowout always occurs in a combustion efficiency range of 70% to 90% [26, 52].

Some pure hydrocarbons were modelled over a range of equivalence ratios for which peak values of volumetric flow rates were calculated. The variation in the resultant blowout curves as presented in Figure 4.2, are purely due to the intrinsic differences in adiabatic flame temperature (AFT). The adiabatic flame temperature calculations incorporated CO_2 dissociation and water-gas-shift reactions. In addition to the different flame temperatures, the fuels are also expected to have differences in chemical reaction rates which would result in different proportionality constants (K) in Equations 4.18 and 4.23. The relative behaviour of the fuels in Figure 4.2 is therefore merely illustrative.

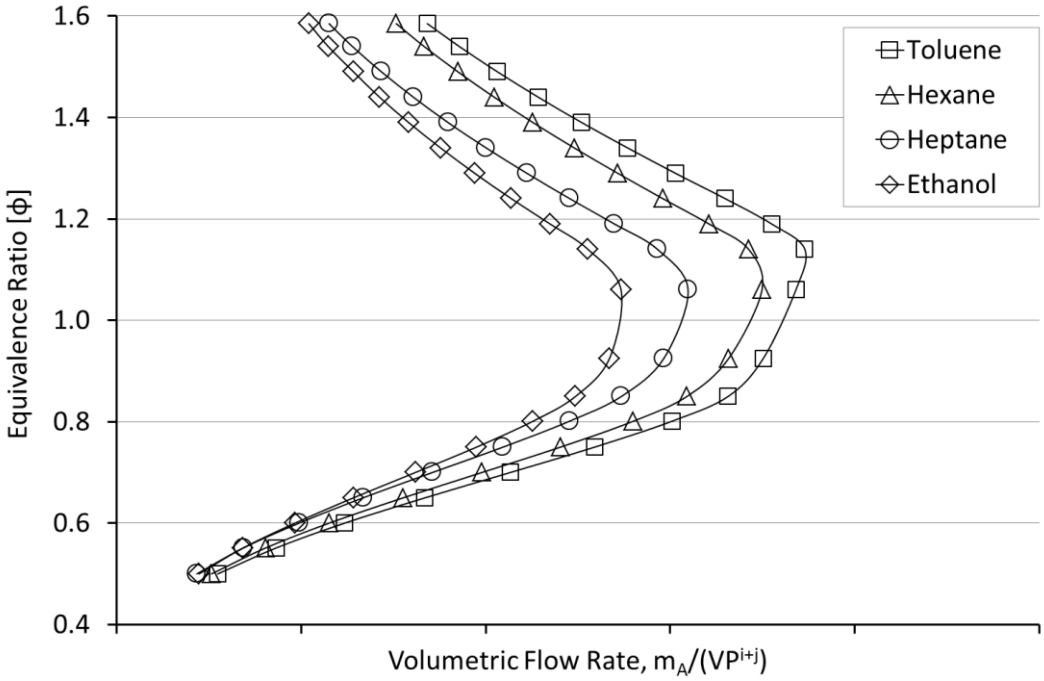

Figure 4.2: Illustrative blowout curves

The relative behaviour of synthetic jet fuel and crude-derived Jet A-1 can be interrogated in a similar fashion. Bester employed surrogate blends of toluene and n-

heptane to calculate AFTs for Jet A-1 and synthetic paraffinic kerosene [53]. The blends were based on matching carbon to hydrogen ratios. Only the initial reactant and final products were evaluated, without considering the intermediate reactions that occur in an actual combustion process. Toluene and n-heptane were used since reliable chemical data for internal energy, enthalpy, and entropy was available (Chemkin). A similar approach was followed here to calculate the AFTs of representative Jet A-1 and fully synthetic jet fuel (FSJF). The carbon to hydrogen ratios were based on two-dimensional gas chromatographic analyses of representative samples of each fuel. Jet A-1 with a hydrogen mass content of 13.9% was simulated by a blend of 24.86% (vol) toluene and 75.14% (vol) n-heptane. A blend of 18.25% (vol) toluene and 81.75% (vol) n-heptane was used to simulate the FSJF with a hydrogen content of 14.48% (mass). Employing these blends, the resultant adiabatic flame temperatures at constant pressure showed a difference between the crude-derived Jet A-1 and FSJF of 3 to 7 Kelvin for typical combustion air-fuel ratios. Although the FSJF would be directionally more sensitive to blowout due to its marginally lower AFT, the difference is too small to have a detectable impact on the altitude blowout envelope.

Fuel-specific differences in ignition delay could, however, have a significant impact on pre-exponential constants (*K*) which in turn could influence relative blowout behaviour. There were various views expressed in Chapter 3 regarding the suitability of DCN as an ignition delay metric for comparing the behaviour of fuels under normal gas turbine combustion conditions and this will also be explored in greater detail later. At this preliminary stage DCN was, however, employed as a convenient proxy for demonstrating the potential influence of different chemical reaction rates. IQT™ measurements could be performed easily for both crude-derived Jet A-1 and FSJF samples. The ignition delays of 4.5 ms and 6.7 ms that were recorded for Jet A-1 and FSJF respectively represents a significant 49% increased delay for FSJF. Relative proportionality constants (*K* values) were proposed based on these relative ignition delays. Figure 4.3 illustrates the resultant cumulative effect of AFT and relative proportionality constant differences for these two fuels. The limiting air mass flow for FSJF is essentially scaled down by 49% which is possibly a simplistic representation since the complex combustion reactions were treated as a single reaction step. In practice the reaction rate is expected to be limited within the chemical reaction pathway by steps which would not necessarily be second order and both fuels may indeed have similar

intermediate reaction steps. However, the fact remains that the calculations were based on real DCN ignition delay differences, highlighting an intrinsic difference in their combustion reaction timescales. It also captures the expected direction of the difference which agrees with some of the results from the FSJF certification process.

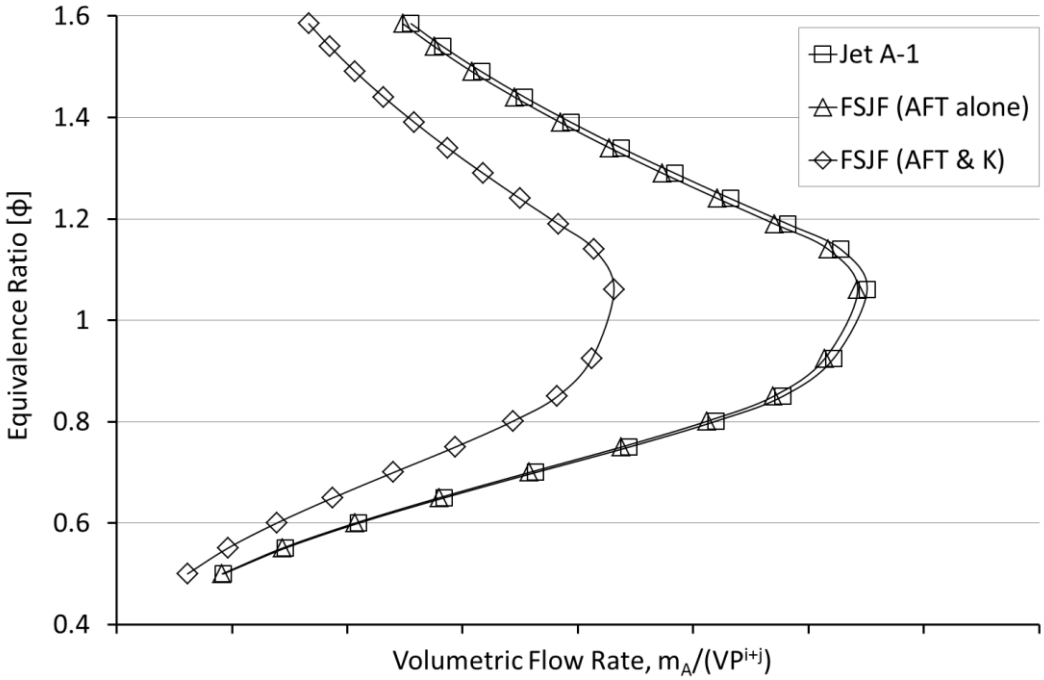

Figure 4.3: Illustrative blowout curves for Jet A-1 and FSJF taking into account AFT alone and the cumulative effect of AFT and proportionality constant differences.

Well-stirred, homogeneous reactors differ significantly from heterogeneous combustors, especially in terms of the local stoichiometry and relevant temperature regimes. The homogeneous character of a stirred reactor, however, makes it particularly amenable to theoretical analysis. Weiss et al. and Strehlow found that the blowout behaviour of fuels in a bluff-body stabilised regime correlated well with the lean blowout behaviour in a spherical stirred reactor. The implication is that the composition in a recirculation zone behind a bluff-body at its lean-limit holding efficiency is related to the composition inside a well-stirred reactor operating at its blowout efficiency [54, 55].

4.3 Evaporation-controlled stability limits

The influence of evaporation can be depicted in a similar manner to the reaction-controlled blowout curves above in order to predict the expected interaction of both

evaporation and reaction limits. Recalling Equation 2.6 the evaporation limited combustion efficiency can be expressed as follows

$$\eta_e = {\rho_A \lambda_{eff} V}\Big/{D_0^2 f_c \dot{m}_A} \quad [2.6]$$

The Sauter mean diameter for prefilming airblast atomisers operating with low viscosity liquids such as kerosene are approximated reliably by Equation 2.28 which simplifies further to Equation 4.24 for a given burner and fuel.

$$SMD \propto \left(\frac{\sigma}{\rho_A {U_A}^2 D_P}\right)^{0.5} \left(1 + \frac{1}{ALR}\right) \quad [2.28]$$

$$SMD \propto \frac{1}{\dot{m}_A}\left(1 + \frac{1}{ALR}\right) \quad [4.24]$$

Substituting 4.24 as the starting diameter into 2.6, ignoring second order effects, and assuming ρ_A and λ_{eff} to be constant for a laboratory burner yields Equation 4.25

$$\eta_e \propto \frac{\dot{m}_A}{\left(1+\frac{1}{ALR}\right)^2} \quad [4.25]$$

By assuming a constant combustion efficiency limit the volumetric flow rate through the combustor reduces to a polynomial function of the equivalence ratio (4.26).

$$\frac{\dot{m}_A}{V P^{i+j}} \propto (1+\phi)^2 \quad [4.26]$$

The effect of both reaction-controlled and evaporation-controlled efficiency limits are illustrated in Figure 4.4. This figure is of particular interest when considering some of the comments contained in the Rolls-Royce test report included as an appendix to the FSJF certification report [13, 14]. The differences in altitude extinction behaviour of the two fuels were explained with the use of an illustrative schematic that is reproduced in Figure 4.5. It was noted that the fuels exhibited negligible differences at the lean and rich extremities of the stability boundaries, but notable differences near the toe of the curve. In light of the preceding theoretical treatment, the effect of (fuel-related) differences in evaporation are not expected to be revealed at the toe of the blowout curve. In fact with increasing volume flow through the combustor, the evaporation limits are expected to widen and become less of a constraint. The evaporation is only expected to constrain the toe region where the reaction boundary is relatively impaired. Evaporation is therefore not expected to cause a difference in the relative shape of the

toe. This would argue against a connection existing between the differences that were observed in the blowout limits and evaporation-related fuel properties.

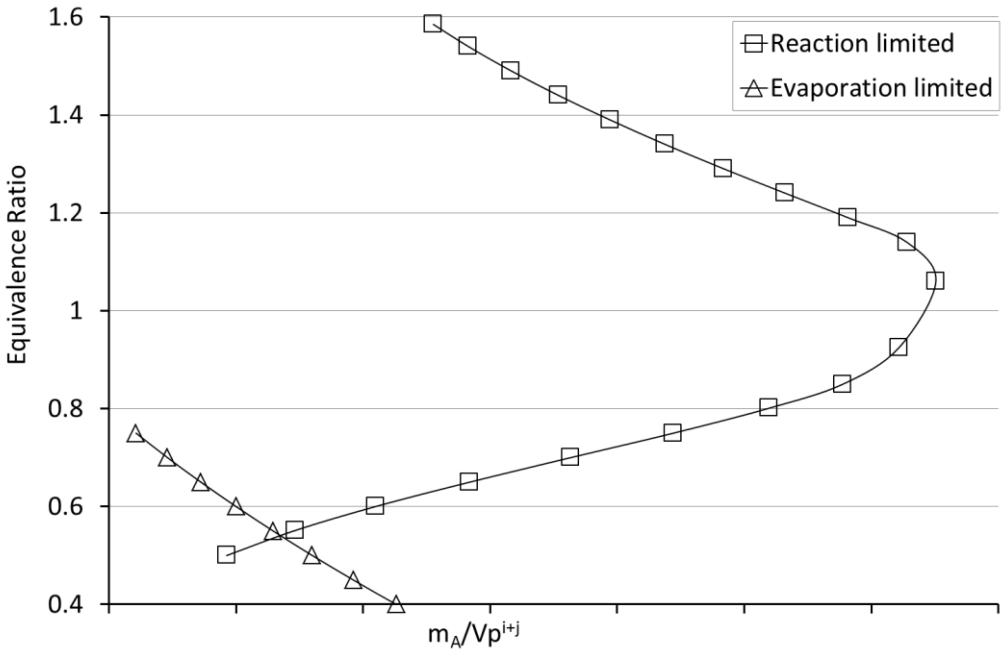

Figure 4.4: Illustrative reaction and evaporation limited extinction blowout curves

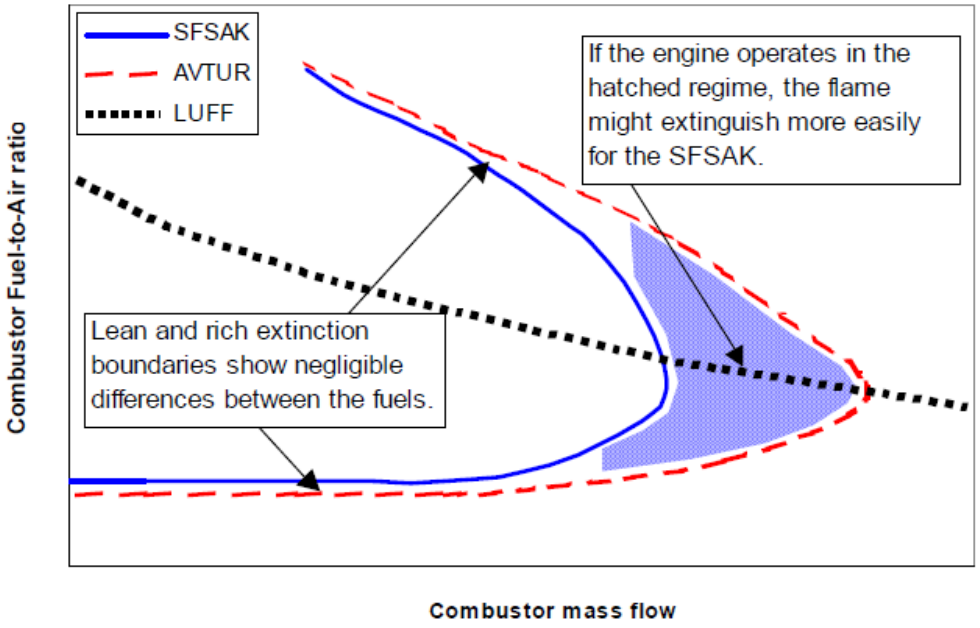

Figure 4.5: Extinction performance for simulated wind milling operating condition, schematic representation of the result. (LUFF = Fuelling line) (from Rolls-Royce report [14])

4.4 Combustion Efficiencies

Evaporation-, mixing-, and reaction-controlled efficiencies can also be considered in terms of fluid-mechanic and chemical timescales to gain insight into their relevance under the different combustor conditions and how they potentially impact combustion limits. The usefulness of representing combustion efficiency in this way will be seen later in Chapter 7.

4.4.1 Evaporation-controlled efficiency

Equation 2.6 was used to express the evaporation-controlled combustion efficiency in terms of the combustor operating conditions (ρ_A , λ_{eff} , $\dot{m}_A$), physical combustor dimensions (V), fuel spray characteristics (D_0) and fuel properties (D_0 , λ_{eff}). Rearranging Equation 2.6, the evaporation-controlled combustion efficiency can be expressed as Equation 4.27.

$$\eta_e \propto \left(\frac{\rho_A V}{\dot{m}_A}\right)\left(\frac{\lambda_{eff}}{D_0^2}\right) \qquad [4.27]$$

The first term on the right hand side of the equation is equivalent to the residence time of the air in the combustion chamber, τ_{res} and, as discussed in Appendix A, the second term is the inverse of the droplet lifetime or evaporation delay time, τ_e. The expression therefore represents the logical argument that the combustion efficiency amounts to the ratio of the air residence time in the combustor to the droplet evaporation time.

$$\eta_e = \frac{Air\ residence\ time}{Droplet\ evaporation\ time} = \frac{\tau_{res}}{\tau_e} \qquad [4.28]$$

It is possible to illustrate the blowout limit of a given fuel (and at a chosen combustion efficiency limit) by expressing both the air residence time and evaporation time in terms of air mass flow rate. In a laboratory model-combustor operated at constant pressure and temperature, the fluid-mechanic timescale, or air residence time, becomes a function of the inverse of the air mass flow rate. Recalling Equation 2.28 for SMDs and assuming constant hardware dimensions, fuel properties, the relative velocity and associated effective evaporation constant of finely atomised droplets being relatively insensitive to the air mass flow rate [20, 56], and with $1 + \frac{1}{ALR} \approx 1$ the droplet evaporation can be approximated as:

$$\tau_e = \left(\frac{D_0^2}{\lambda_{eff}}\right) \propto \left(\frac{1}{\dot{m}_A{}^2}\right) \qquad [4.29]$$

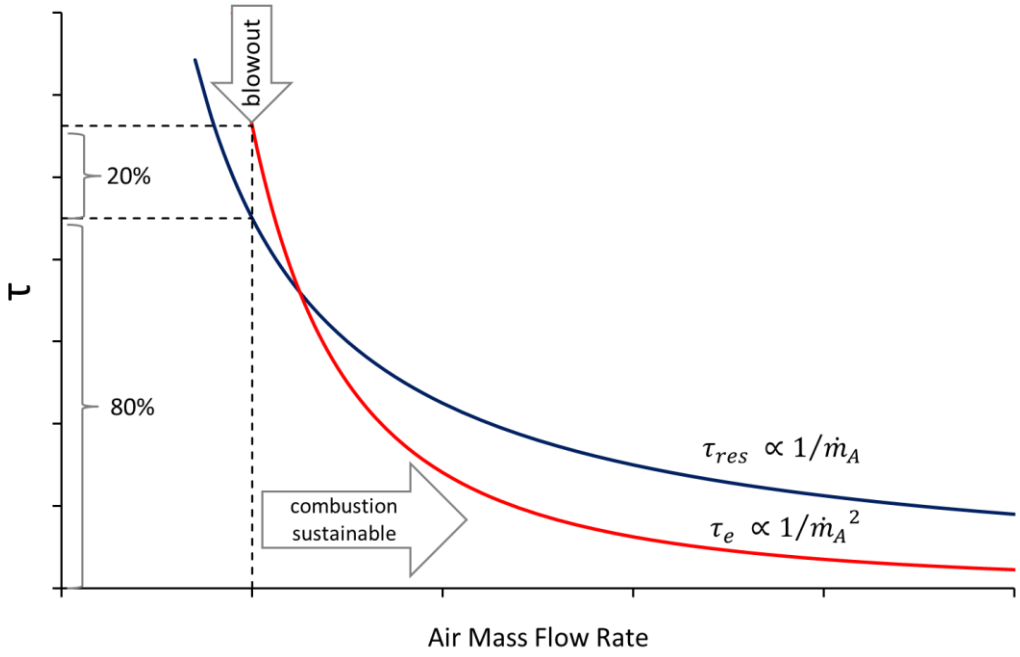

Figure 4.6: Illustrative timescales in an evaporation limited system with fixed inlet pressure and temperature

Figure 4.6 represents an evaporation-controlled system where the limiting combustion efficiency has been assumed to be at 80%. Combustion can be sustained as long as the residence time is greater than 80% of the evaporation delay. This would dictate a minimum air mass flow rate at which blowout occurs and below which combustion is impossible. At any airflow rates above the blowout point the air residence time would be sufficient for the evaporation efficiency to be greater than 80% and evaporation would not play a limiting role. This confirms the conclusion from Section 4.3 and Figure 4.4 that evaporation limits are expected to constrain combustion at lower air mass flow rates. Fuel-related differences in properties that effect evaporation would be relevant under these conditions, but play a much less important role at higher mass flow rates.

4.4.2 Mixing-controlled efficiency

The combustion efficiency in a mixing-controlled system was expressed by Equation 2.11.

$$\eta_m = f\left(\left(P_3 A_{ref}/\dot{m}_A T_3^{0.5}\right)(\Delta P_L/P_3)^{0.5}\right) \qquad [2.11]$$

$$\therefore \eta_m \propto \left(\frac{\rho A_{ref}}{\dot{m}_A}\right)\left(\frac{T_3 \Delta P_L}{P_3}\right)^{0.5} \quad [4.30]$$

$$\therefore \eta_m \propto \left(\frac{\rho}{\dot{m}_A}\right)\left(\frac{T_3(\rho v^2)}{P_3}\right)^{0.5} \quad [4.31]$$

$$\therefore \eta_m \propto \left(\frac{\rho A_{ref} v}{\dot{m}_A}\right) \quad [4.32]$$

Assuming a fixed dimensionless ratio to exist between the area of the liner air holes and the combustor reference area (A_{ref}), the numerator is also equal to the air mass flow rate. This indicates that both τ_{res} and τ_{mix} are proportional to $1/\dot{m}_A$.

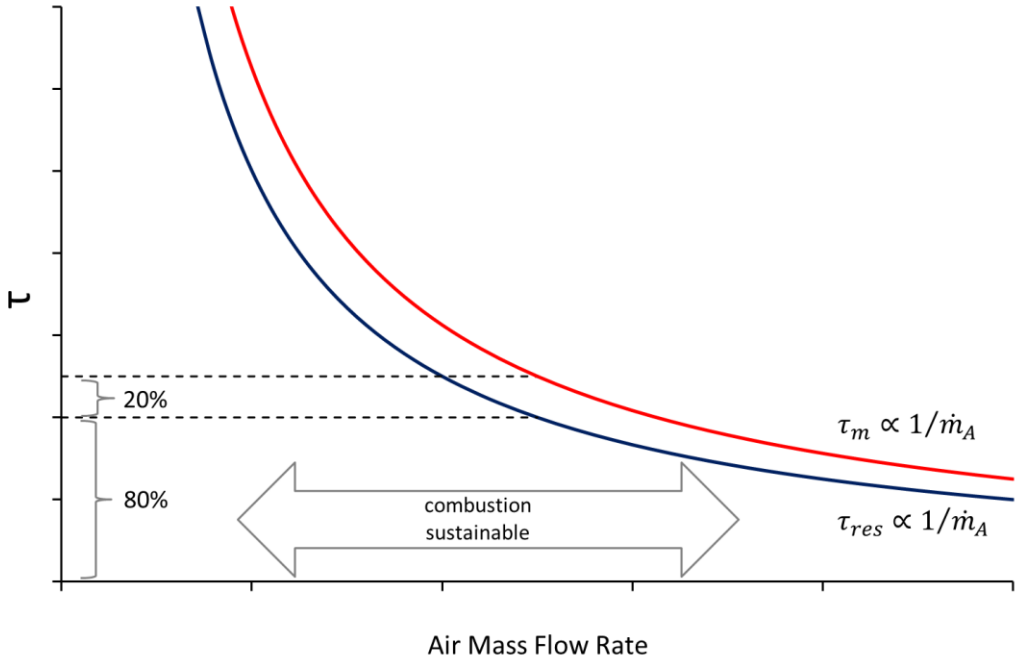

Figure 4.7: Illustrative timescales in a mixing limited system with fixed inlet pressure and temperature

For any given pressure and temperature condition, the efficiency is nominally independent of air mass flow rate and is essentially dependent only on the ratio of the area of the liner air holes to the combustor cross-section area.

4.4.3 Reaction-controlled efficiency

Rearranging Equation 2.31 for reaction-controlled combustion efficiency yields Equation 4.27.

$$\eta_\theta \propto V e^{-E/RT} \rho^{1.75} / \dot{m}_A \quad [2.31]$$

$$\therefore \eta_\theta \propto \left(\frac{\rho V}{\dot{m}_A}\right)\ \left(e^{-E/RT} P^{0.75}\right) \qquad [4.27]$$

The first term on the right hand side of the equation is again equivalent to the residence time, τ_{res} , while the second term is the inverse of a common expression for the reaction induction time or so-called ignition delay time, τ_θ [57]. The combustion efficiency is therefore in fact simply being expressed as the air residence time divided by the combustion induction time which is equivalent to the Damköhler number, Da:

$$\eta_\theta = \frac{Air\ residence\ time}{Combustion\ induction\ time} = \frac{\tau_{res}}{\tau_\theta} \equiv Da \qquad [4.28]$$

In a laboratory model-combustor operating at constant pressure and temperature the fluid-mechanic timescale or air residence time becomes a function of the inverse of the air mass flow rate while the chemical timescale will be constant. Figure 4.8 represents this diagrammatically for a system where the limiting combustion efficiency has again been assumed to be at 80%. Combustion can be sustained as long as the residence time is greater than 80% of the ignition delay which dictates a maximum air mass flow rate at which blowout occurs and beyond which combustion is impossible.

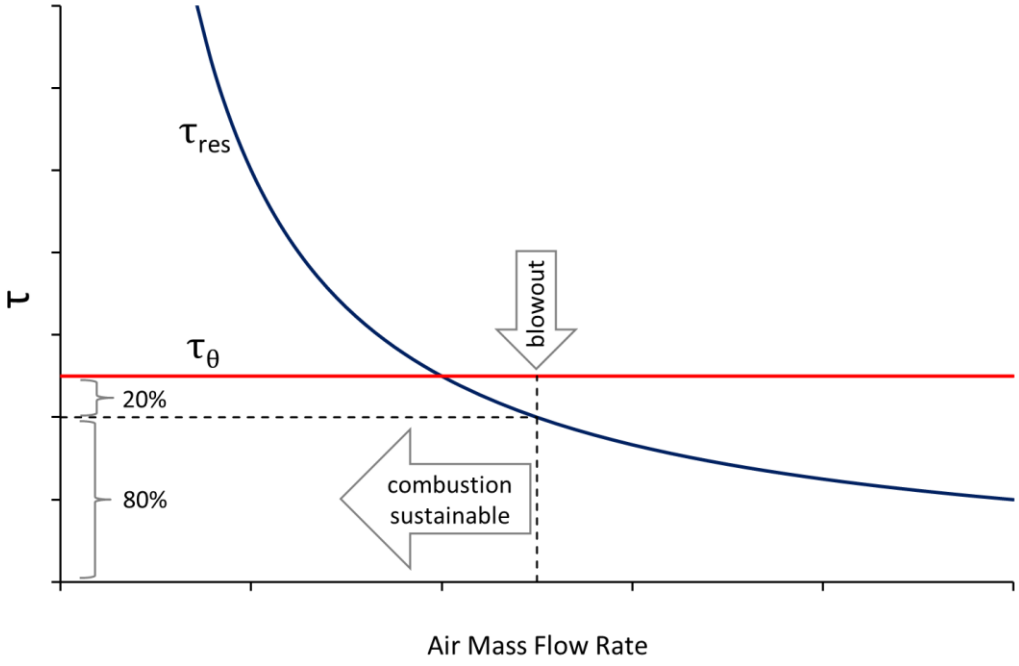

Figure 4.8: Illustrative timescales in a chemical reaction limited system with fixed inlet pressure and temperature.

The diagrams presented in this section were chosen to illustrate the relative timescale behaviour in a combustor having fixed inlet pressure and temperature. Obviously one could consider the relative timescale behaviour under other scenarios such as fixed air mass flow and varying inlet pressure or temperature. However, it was the principle of viewing the efficiency as the ratio of two competing timescales that is useful in this present work.

The subsequent chapter details the experimental approach that was designed to interrogate the thesis hypotheses by examining how the theoretical evaporation- and reaction-controlled combustion efficiencies translate to practical combustion behaviour.

5 Experimental Design

An experimental programme was designed based on the insights gained from the theoretical treatment and literature review to provide data to explore how fuel properties can impact combustion efficiency and extinction under representative gas turbine combustion conditions. The programme was also intended to provide data for answering the hypotheses and explaining the LBO differences that were observed during the fully synthetic jet fuel (FSJF) certification tests. It consisted of the following main components:

- Design of a test fuel matrix
- Physical and chemical characterisation the fuel matrix
- Evaluation of the test fuel LBO behaviour in a laboratory-scale model-combustor
- Evaluation of the test fuel spray behaviour in a laboratory-scale model-combustor

5.1 Test fuel matrix

The theoretical assessment implicitly proposed a research strategy for revealing the root cause if it were possible to evaluate a number of fuels that exhibit independently varied properties relating to evaporation and reaction behaviour. It is, however, virtually impossible to change fuel properties entirely orthogonally which complicates the selection of appropriate test fuels and the interpretation of test results. The design of the test fuel matrix was influenced by a combination of the desire to include fuels that were representative of those employed during the FSJF certification process and results from previous laboratory-scale extinction and ignition work [7, 58] which included both full boiling range and single component test fuels. The primary goal was to investigate the relative influence of fuel properties on evaporation rate and reaction rate independently in a combustion environment. It was therefore important to differentiate key properties to as large a degree as possible, while still employing fuels that resembled current commercial jet fuels. The resultant matrix entailed a selection of eight fuels that were nominally representative of either crude-derived or viable alternative jet fuel formulations. It included fuels that complied fully with the Jet A-1 specification such as crude-derived and Fischer–Tropsch (FT) derived synthetic commercial fuels as well as fuels that were formulated to intentionally breach the specification on selected properties that were of interest. Table 5.1 reflects the test fuel

matrix with a selection of crude-derived Jet A-1, synthetic paraffinic kerosene, linear paraffinic solvents, aromatic solvents and pure compounds. While the matrix included some synthetic jet fuel formulations, the primary focus was on fuel properties regardless of the production pathways employed to produce the fuels.

Table 5.1: Test fuel matrix

CJF	Crude-derived Jet A-1
CJF/D	Jet A-1 + 50% n-dodecane
SJF1	FSJF (certification)
SJF2	FSJF (commercial)
SJF2+	FSJF (commercial) + 1.5% HCPP
LTSK	Experimental GTL kerosene
HTSK	Synthetic paraffinic kerosene (SPK)
HN	Heavy naphtha refinery stream

CJF was a commercial crude-derived Jet A-1 while CJF/D was a 50:50 blend of CJF and n-dodecane. SJF1 was formulated to be representative of the FSJF that was used during the 2006 certification process and the associated test program, while SJF2 was representative of a FSJF formulation that would comply with the distillation gradient specification that was introduced for FSJF as part of DEFSTAN 91-91 [59] in 2008. SJF2+ was a blend of 98.5% SJF2 and 1.5% hydrogenated cat-poly petrol (HCPP) which was added to investigate the influence of flash point. HTSK was a Synthetic paraffinic kerosene stream that is typically employed in both fully and semi-synthetic jet fuel. HN was a heavy naphtha refinery stream and LTSK a gas-to-liquids (GTL) kerosene that were both included to assist in evaluating non-orthogonal changes in the various fuel properties. LTSK was of further interest due to the fact that it nominally resembled a fuel that could also be produced via a renewable synthetic jet fuel manufacturing process. The influence of the LTSK's largely linear paraffin structure on ignition delay, cetane, and LBO was also of interest in light of the observations that have been highlighted by literature as discussed in Chapter 3 [8, 10, 11].

5.2 Physical characterisation of test fuel matrix

The test fuel matrix was characterised employing the standard test methods employed in the aviation industry as specified by ASTM D1655 [60]. While full-specification analyses were performed, the physical properties that were of primary interest included density, viscosity, flash point, and the distillation profiles. Concerns have been raised within the aviation industry regarding the sensitivity of the D86 method that is stipulated by ASTM D1655 for determining distillation profiles. Therefore, apart from the conventional D86 method, a GC-based simulated distillation was also conducted according to ASTM D2887 [61]. Surface tension measurements were performed at 25°C and 40°C, and refractive indices were determined to be employed by the Phase Doppler Anemometry (PDA) measurements during the fuel spray characterisation.

5.3 Chemical characterisation of test fuel matrix

In addition to the normal (physical) jet fuel specification tests a number of measurements were conducted to characterise the chemical composition and reactivity of the test fuels. Comprehensive two–dimensional gas chromatography (GCxGC), where two independent separations are applied to a single sample injection, is considered to be the most accurate means to obtain detailed compositional information for complex petrochemical mixtures. This technique offers structured separations, high sensitivity and high peak capacity. Complex fuels are traditionally analysed in the so-called “normal” GCxGC mode where a non–polar column is used in the first dimension to perform a boiling-point based separation. A thermal modulator is used to focus the effluent from the first column onto a polar column which provides separation in the second dimension based on polarity. For this study the analyses were performed in the so-called “inverse mode” where the first dimension employs a polar column and the second dimension employs a non–polar column. This sequence is considered to be less orthogonal but has been demonstrated to extend the separation space when used to characterise FT fuels and the aromatic fractions in petroleum middle–distillates resulting in improved resolution [62]. Chemical structures were elucidated by time–of–flight mass spectrometry (TOF–MS), and a flame ionisation detector (FID) was used for quantification. The two-dimensional gas chromatography results provided information about the test fuel chemical compositions and were used to determine carbon to

hydrogen ratios that were required to calculate the stoichiometric fuel/air ratio (FAR) for each test fuel.

Tests were also conducted to characterise the chemical reactivity of the fuels. An IQT™ combustion bomb (manufactured by AET, Canada) was employed to determine ignition delay times of the test fuel matrix. This automated test method is used for the quantitative determination of the ignition characteristics of specifically middle-distillate fuels and fuel blending components. The IQT™ utilises a constant-volume combustion chamber that is pre-heated electrically to 843 K. Test fuel is injected directly into the chamber filled with synthetic air at 2.1 MPa. An empirical calibration formula, as specified in ASTM D 6890 [63], is used to convert the measured ignition delay to a derived cetane number. This is a combustion quality indicator used primarily in diesel engine applications.

Laminar flame speed (LFS) has been suggested as a combustion indicator that could potentially be appropriate for evaluating gas-turbine performance [42, 43, 64]. A pressure-based method making use of a spherical bomb was employed to measure the LFS and Markstein length of the test fuels. Tests were conducted at ambient initial pressure and two initial temperatures with six different air-fuel ratios spanning the range from lean to rich. A minimum of six repeat combustion pressure records of approximately 90 data points were obtained for each test fuel which yielded a database of over 6000 individual calculations of LFS from which the relevant parameter coefficients could be calculated using a regression technique. The experimental hardware and analysis methodology are described in greater detail by Yates et al. [64]. Peak LFS values were calculated at an equivalence ratio of $\phi = 1.075$ and reference conditions of 298.15 K and 101.325 kPa.

Ignition delays were determined by the Institute of Combustion Technology at the German Aerospace Centre (DLR) in Stuttgart, Germany. A high pressure shock tube was employed with an internal diameter of 98.2 mm. The 5.18 m long driver section and 11.12 m long driven section were separated by aluminium diaphragms. A turbo-molecular pump was used to evacuate the driven section to pressures below 10-6 mbar. Gas mixtures were prepared manometrically in an evacuated stainless steel storage cylinder at pressures below 10-6 mbar. Four piezo-electric pressure sensors at 20 cm intervals were used to calculate the incident shock speed. A one-dimensional shock model was used to calculate the temperature and pressure behind the reflected shock

wave from the measured incident shock speed and the speed attenuation. The resultant uncertainty in the calculated reflected shock temperature was less than 10 K. Piezo-electric pressure sensors (PCB® 113A24 and Kistler® 603B) located 1 cm from the end flange, were used to observe the pressure profiles associated with ignition.

OH*-emission (at 308 nm) and CH*-emission (at 431 nm) were measured using a photomultiplier and narrow band filter (full width at half maximum - FWHM of 5 nm). The ignition delay time values were calculated as the time elapsed between the system being initiated by the reflected shock wave and the maximum OH*-emission being recorded. Ignition delay times of up to 6.5 ms can be measured by the experimental setup depending on the temperature. All tests were performed at initial pressures of 1.6 MPa ± 10% with synthetic air (20%v O2 in N2). Reaction mixtures were diluted 1:2, i.e. one part undiluted mixture and one part N2.

5.4 Gas turbine model-combustor: LBO evaluation

The LBO behaviour of the eight test fuels were evaluated using a laboratory-scale model-combustor at the German Aerospace Centre (DLR). The combustor was based on previous spray burner research [65] and was designed to be representative of the primary zone encountered in real aero-engines. The scaling of the combustor was a compromise to accommodate practical laboratory constraints while retaining technical relevance. The resultant rig was designed for thermal powers of approximately 10 kW at atmospheric pressure conditions.

The core of the combustor consisted of the burner nozzle shown in Figure 5.1. A common air plenum supplied air to inner and outer air swirlers that produced two co-axial, co-rotating swirl flows that were separated by a thin annular ring with a sharp edge. A pressure-swirl atomiser produced a hollow cone of fuel spray through two swirl channels that was sprayed onto the inside of the annular ring. A fuel film formed on the surface and was transported to the lip of the ring where it re-atomised. This so-called prefilming airblast atomisation concept is widely used in current combustion systems [66].

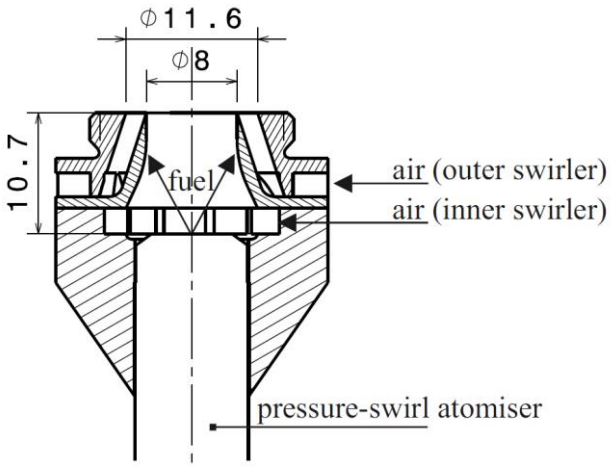

Figure 5.1: Laboratory-scale model burner nozzle (configuration B) [65]

The combustion chamber consisted of four quartz windows that were held in place by steel posts. The resultant optical access allowed the application of a host of optical and laser-based diagnostic techniques. A top plate secured the windows and posts. The 19 mm diameter exit port in the top plate exhausted to atmospheric pressure. The chamber had a cross section of 85 mm by 85 mm and a length of 169 mm which was sufficient to fully contain combustion throughout the operating conditions that were investigated. Specific care was taken to ensure cylindrical symmetry of the spray cone and resultant combustion zone.

The experimental layout of the model-combustor is shown in Figure 5.2. A mass flow controller (Bronkhorst EL-FLOWselect F-203AV) was used to regulate supply of dry compressed air to the air plenum. The air temperature was controlled by an electric pre-heater based on the temperature inside the air plenum measured using a K-type thermocouple. A sonic nozzle decoupled the combustor acoustically from the air feed line while meshes were used to homogenise the air flow into the plenum. The test fuel was supplied from a piston driven stainless steel cylinder which ensured that the nitrogen driver gas was not in contact with the test fuel. The test fuel was also degassed prior to testing by applying a mild vacuum to the supply cylinder. A mass flow controller (Bronkhorst mini CORI-FLOW M14) regulated the fuel supply to the fuel pressure atomiser via a water-cooled fuel lance. The fuel temperature control was based on the temperature measured just upstream of the atomiser exit. The development of the test apparatus is discussed in greater detail by Grohmann et al. [65].

Two burner configurations (A and B) were tested with different swirl numbers. The swirl number is defined as the ratio of the angular momentum flux, G_θ, divided by the axial momentum flux, G_y, and a characteristic radial distance, R [67, 68].

$$S = \frac{G_\theta}{G_y R} \quad [5.1]$$

Subsequent to the completion of the LBO tests with burner configuration A, stereoscopic particle image velocimetry (PIV) measurements were conducted of the non-reacting and reacting flows during an unrelated test program at DLR. The PIV results revealed the absence of a strong central recirculation zone as would be present in typical real aero-engine combustors. This was ascribed to lower geometric swirl with a centre swirl number of $S_c = 0.6$. The burner was modified, and the resultant second configuration (B) exhibited a well-developed central recirculation zone with a geometrical swirl number of $S_c = 1.17$ for the centre flow and $S_a = 1.22$ for the annular flow.

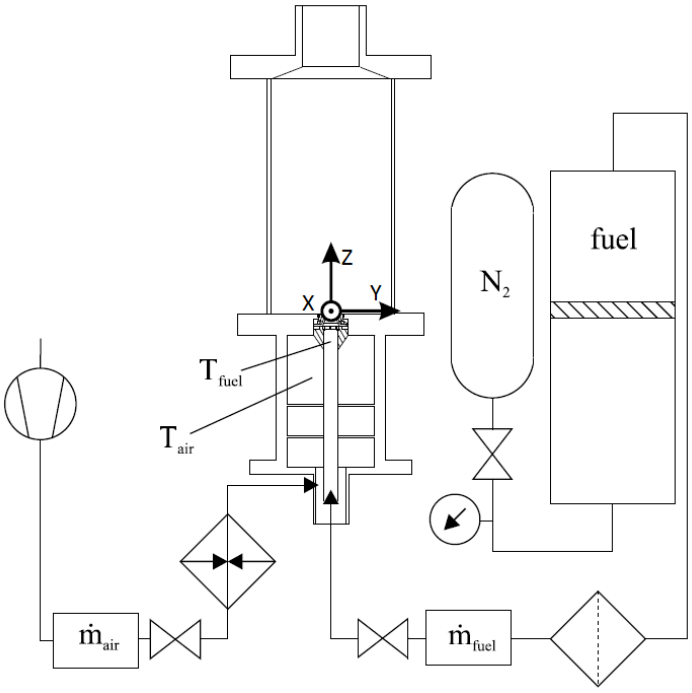

Figure 5.2: Laboratory-scale model-combustor layout [65]

The LBO tests of configuration A were conducted at two air pre-heat temperatures, 323 K and 413 K, while the tests of configuration B were only conducted at 323 K due to the limited volume of test fuel available. The fuel temperature was controlled to 303 K

for the low air pre-heat tests and to 323 K for the high air pre-heat tests. For each air pre-heat condition, a series of tests were conducted over range of air flow rates ranging from 2.2 g/s to 12.9 g/s. The air mass flow rate was kept constant for each test point operating condition. Combustion was established at a stoichiometry of approximately ϕ = 0.7, well within the stable combustion operating envelope, following which the fuel mass flow rate was reduced at a controlled rate of 0.5 (g/h)/s up to the point of blowout. This corresponded with a ϕ reduction rate of 0.001 s^{-1} to 0.0001 s^{-1} depending on the air mass flow rate. The stoichiometry and air mass flow rate at the point of extinction was recorded as the LBO point. A minimum of three repeat tests were conducted at each operating condition. The model-combustor set-up and a stoichiometric Jet A-1 reference flame are shown in Figures 5.3 and 5.4 respectively.

Figure 5.3: Model-combustor setup

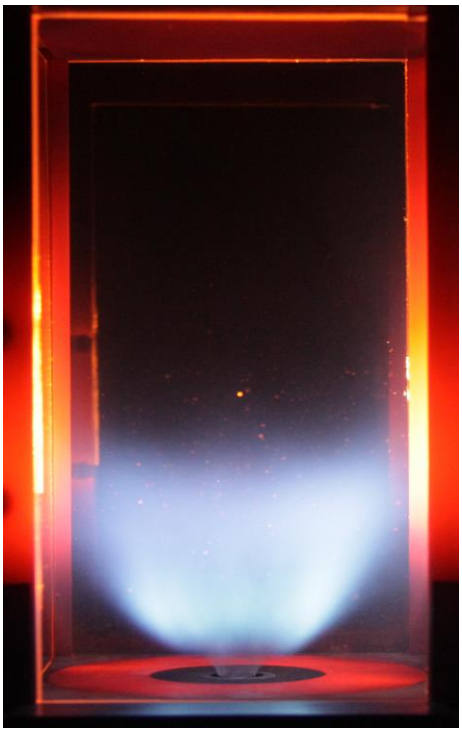

Figure 5.4: Reference Jet A-1 flame (ϕ = 1, T_{air} = 323 K)

5.5 Gas turbine model-combustor: fuel spray evaluation

A three component Phase Doppler Anemometry (PDA) system by Artium Technologies Inc. (PDI-300 MD) was used to investigate the fuel spray in the model-combustor. The droplet diameters as well as radial, axial and circumferential velocity components of the

droplets were measured during combustion close to LBO. Three pairs of laser beams were generated by three diode pumped solid state lasers contained in the two transmitting units: 532 nm for axial velocity and diameter measurements, and 491 nm and 561 nm both for radial and circumferential velocity measurements. Negative velocity measurements were enabled by frequency shifting one beam of each of the beam pairs using a Bragg cell. The receiving unit collected the signal in a 45° forward scatter configuration. The focal length of the optics was 350 mm with the beam waist in the measurement volume of between 150 and 180 µm depending on the 3 wavelengths. Droplet measurements of between 0.7um and 100um were attainable with the spatial aperture of 500um that was applied. The characterisation of smaller droplets was optimised by adjusting the amplifier voltages of the signal receiving photo multipliers based on local measurement requirements which minimised saturation of the photo multipliers while still maximising small droplet signal. A refractometer was used to determine the refractive indices of the eight test fuels at room temperature.

Measurements were conducted at two stoichiometric air-fuel ratios: one at the LBO stoichiometry plus 5% and another at a stoichiometry of $\phi = 0.6$. This allowed both investigation of the spray behaviour as close to blowout as practical, as well as a comparison between all fuels at exactly the same stoichiometric air-fuel ratio. For each stoichiometric set point, measurements were performed at two air flow rates: 2.2 g/s and 6.5 g/s which allowed evaluation both below and above the flow rate range where a distinct air flow-related influence was detected in the LBO behaviour as discussed in the following chapter.

The combustor was mounted on a three-axis traversing stage that was driven by stepper motors. This allowed the positioning of the measurement volume within the combustion zone. The coordinate system is shown in Figure 5.2. Measurements were performed at three distances from the nozzle exit plane: z = 15 mm, z = 25 mm, and z= 35 mm. At each z-axis location the combustor was traversed along the y-axis in 2 mm increments. A minimum of 2500 droplet measurements, that were coincident for all three channels, were recorded at each measurement point. This resulted in diameter values being based on between 3000 and 135000 readings per position depending on the position and operating conditions.

6 Results

The results of the various test programmes are presented in the following chapter. The general fuel characterisation is presented first followed by the results of the LBO and PDA measurements that were conducted in the model-combustor.

6.1 Physical characterisation results

Comprehensive fuel property analysis results are reported in Appendix B. The most relevant properties are listed below in Table 6.1, and the distillation profiles are shown in Figure 6.1.

Table 6.1: Test fuel characterisation: key physical properties from specification analysis

Test Fuel		CJF	CJF/D	SJF1	SJF2	SJF2+	LTSK	HTSK	HN
Flash point	[K]	315.5	320.0	315.5	326.5	311.0	311.0	319.5	320.0
T_5	[K]	437.3	454.2	436.4	446.4	442.3	427.8	442.9	436.6
T_{50}	[K]	468.7	478.6	445.7	469.6	469.2	441.8	451.0	438.7
T_{90}	[K]	508.1	494.6	468.7	514.5	515.2	461.0	469.4	445.3
T_{50}-T_{10}	[K]	25.3	18.0	9.6	19.7	25.2	12.7	6.8	2.0
T_{90}-T_{10}	[K]	64.7	34.0	32.6	64.6	71.2	31.9	25.2	8.6
Density @ 20°C	[kg/l]	0.793	0.773	0.795	0.812	0.810	0.730	0.757	0.756
Viscosity @ 40°C	[cSt]	1.20	1.29	1.05	1.46	1.42	0.91	1.16	0.91
Surface tension @ 25°C	[mN/m]	25.68	25.61	24.06	25.97	25.94	23.45	23.85	24.25

6.2 Chemical characterisation results

The results of the comprehensive two–dimensional gas chromatography (GCxGC) characterisation, the laminar flame speed (LFS) measurements, the derived cetane numbers (DCN) acquired in the IQT™, and shock tube ignition delays corresponding to three reference temperatures are summarised in Table 6.2.

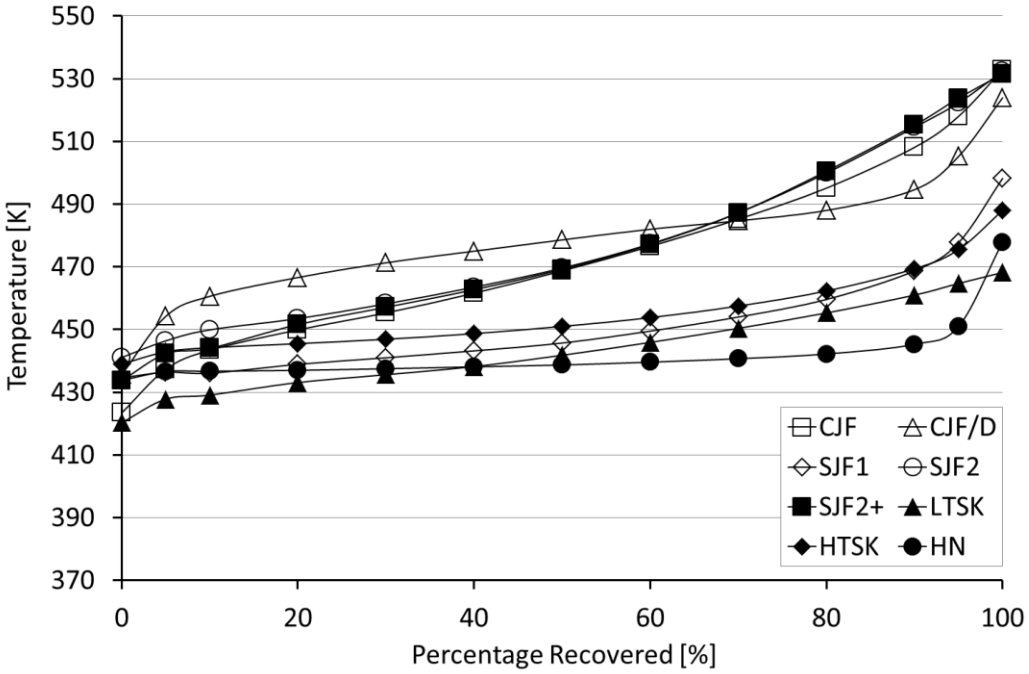

Figure 6.1: Test fuel volatility: distillation profiles.

Table 6.2: Test fuel characterisation: GCxGC speciation, DCN, LFS and shock tube ignition delays

Test Fuel		CJF	CJF/D	SJF1	SJF2	SJF2+	LTSK	HTSK	HN
normal-paraffins	[wgt%]	24.0	60.3	8.2	2.5	2.4	67.9	0	38.1
iso-paraffins	[wgt%]	28.3	14.9	65.1	43.6	44.5	31.1	92.0	34.7
cyclic paraffins	[wgt%]	20.4	10.6	9.1	14.4	14.3	1.0	7.6	17.6
bicyclic paraffins	[wgt%]	4.6	2.3	2.8	20.8	20.4	0	0	1.6
tricyclic paraffins	[wgt%]	0.3	0	0	7.5	7.4	0	0	0
alkyl benzenes	[wgt%]	15.7	8.2	12.8	2.9	2.9	0	0	7.6
cyclic alkyl benzenes	[wgt%]	4.4	2.3	1.8	8.0	7.8	0	0	0.4
naphthalenes	[wgt%]	2.3	1.2	0	0.3	0.3	0	0	0
C/H ratio		1.93	2.04	2.02	1.95	1.95	2.20	2.16	2.09
LFS	[$m.s^{-1}$]	0.358	0.353	0.345	0.351	0.350	0.338	0.345	0.352
ID_{IQT}	[ms]	4.50	3.45	6.68	7.06	7.14	3.24	7.14	3.88
DCN		45.9	58.5	32.4	30.9	30.6	62.0	30.6	52.6
$ID_{1250\,K}$ (1000/T = 0.8)	[ms]	0.29	0.31	0.34	0.26	0.26	0.22	0.32	0.24
$ID_{1000\,K}$ (1000/T = 1.0)	[ms]	2.52	2.61	3.05	2.34	2.31	1.94	2.92	2.07
$ID_{833\,K}$ (1000/T = 1.2)	[ms]	13.25	9.08	22.90	17.07	15.09	10.08	21.11	9.94

The IQT™-measured ignition delays (ID_{IQT}) were converted to DCN values using the empirical calibration described by Equation 6.1 [69].

$$DCN = 83.99\left(ID_{IQT} - 1.512\right)^{-0.658} + 3.547 \quad [6.1]$$

The constant 1.512 ms offset that was applied to all the measured ignition delays accounted for the evaporation and mixing delays that are intrinsic to the heterogeneous injection in the IQT™ bomb.

While the physical characterisation, compositional analyses, laminar flame speed, and IQT™ ignition delay results could be used without significant processing, the data from the shock tube ignition delay experiments had to be analysed further. The data points spanned both the high-temperature and low-temperature regimes with a number but not all of the fuels recording delays into the negative temperature coefficient (NTC) region. Yates et al [70] proposed a convenient method of describing the ignition delays in each of the distinct temperature regimes using generic Arrhenius functions having the form:

$$\tau_i = A_i p^{n_i} e^{\frac{B_i}{T}} \quad [6.2]$$

Where τ_i represents the ignition delay, A, n and B, are constants and p and T are the pressure and temperature respectively. They treated the two sequential stages in the low-temperature regime (low temperature and NTC) as the arithmetic sum of the individual delays, $\tau_1 + \tau_2$. The high temperature delay, τ_3, represented an alternative competing pathway and the overall ignition delay for both low and high-temperature was expressed by Equation 6.3.

$$\tau_{overall} = \left((\tau_1 + \tau_2)^{-1} + (\tau_3)^{-1}\right)^{-1} \quad [6.3]$$

This approach was applied to the shock tube results to smooth over the experimental noise and intrinsic test-to-test variation in measurement conditions in order to facilitate direct comparisons between the various fuels. It also facilitated the inclusion of the ignition delay results in correlation analysis of the fuel properties and LBO test results.

The values of the coefficients A and B for each of the stages were determined by means of a regression analysis. The pressure dependence was ignored ($n_i = 0$) due to all tests being conducted at a common pressure. The shock tube data set did not contain results that extended into the linear portion of the low-temperature region for all the test fuels, which essentially reduced the three-Arrhenius to a two-Arrhenius treatment without

influencing the model fit or accuracy in the NTC or high-temperature regions. An example of the measured results and modelled ignition delay for one of the fuels (test fuel CJF) is presented in Figure 6.2. The results, modelled ignition delay curves, and model coefficients for the full fuel matrix are presented in Appendix C. The modelled ignition delay results for the full matrix are presented in Figure 6.3 while values calculated for each fuel at 833 K, 1000 k and 1250 K (corresponding with 1000/T values of 1.2, 1.0 and 0.8 respectively) are included in Table 6.2.

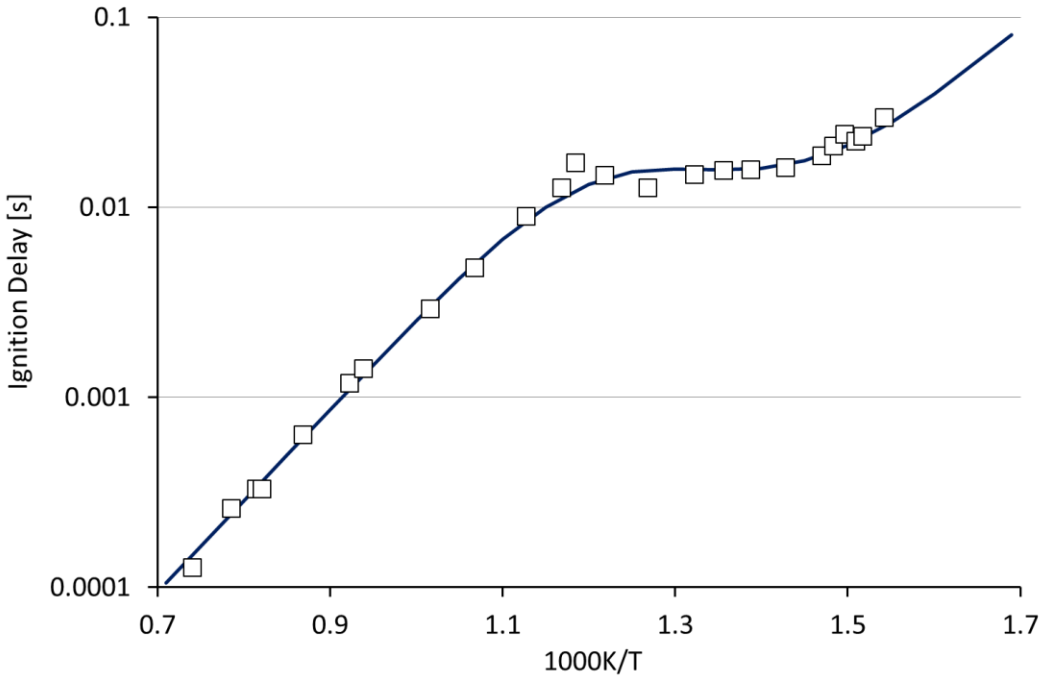

Figure 6.2: Test fuel CJF: Shock tube measured (markers) and modelled (curve) ignition delay results based on eq. 6.3.

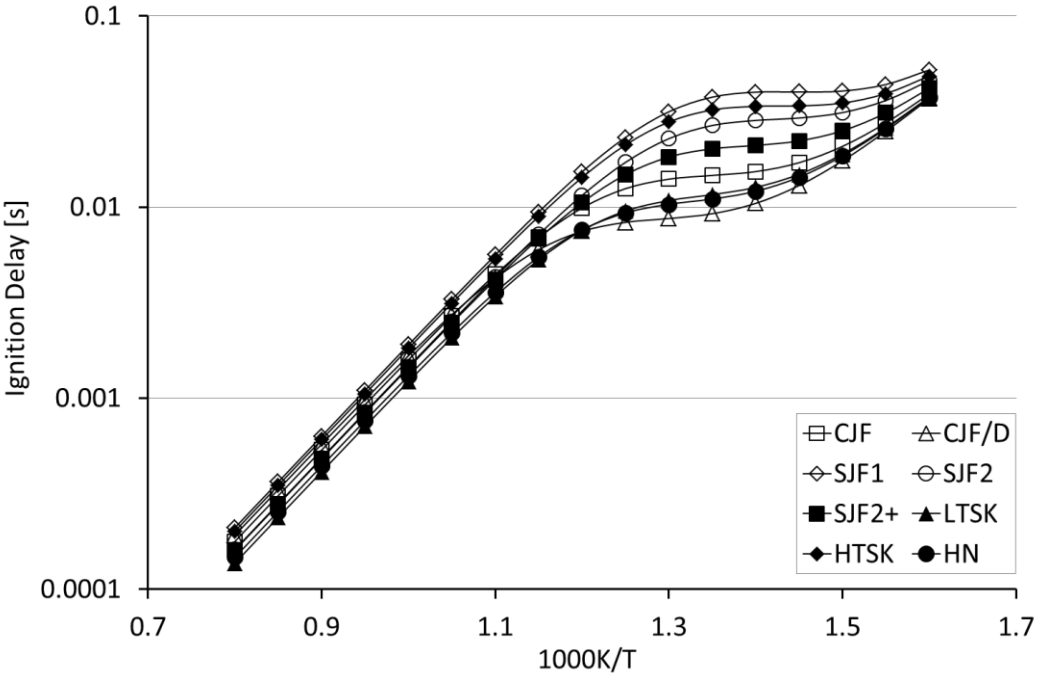

Figure 6.3: Modelled ignition delay results for the full tests fuel matrix

The differences in the absolute values of the ignition delays measured in the homogeneous shock tube and heterogeneous IQT™ are a manifestation of the inherent differences in operating conditions. It can, however, be expected that fuels with similar evaporative behaviour exhibit a correlation between IQT™ and shock tube ignition delays under similar pressure and temperature conditions by virtue of the fuel-to-fuel differences in the IQT™ ignition delays being reduced primarily to differences in chemistry. The shock tube measurements in this study were conducted at 16 bar which did not allow direct comparison with the delays that were measured at 21 bar in the IQT™ without applying a pressure correction. As mentioned above it was not possible to calculate an exact pressure correction for each individual fuel due to all the tests being conducted at the same starting pressure. A reasonable approximation can, however, be made by applying the pressure dependence of the reaction-controlled combustion efficiency as expressed in Equation 2.31. The shock tube results also needed to be adjusted to account for the nitrogen dilution. This was done based on experimental and modelling work by Zeng et al. [71] which indicated that a correction factor of 0.529 was applicable. The shock tube ignition delays ($ID_{843\ K}$) were thus converted to IQT™ conditions ($ID_{843\ K}'$) by applying the relationship expressed in Equation 6.4 and are compared with the IQT™-measured delays in Figure 6.4.

$$ID_{843\,K}{}' = 0.529\, ID_{843\,K} / \left(\frac{P_{IQT}}{P_{ST}}\right)^{1.75} \quad [6.4]$$

where 0.529 is the dilution correction factor [71]. It is interesting to note that the constant evaporation and mixing delay offset contained in the calculation of DCN values (Equation 6.1), was also revealed as a constant offset in the best-fit linear trend line in the comparison with the shock tube ignition delays.

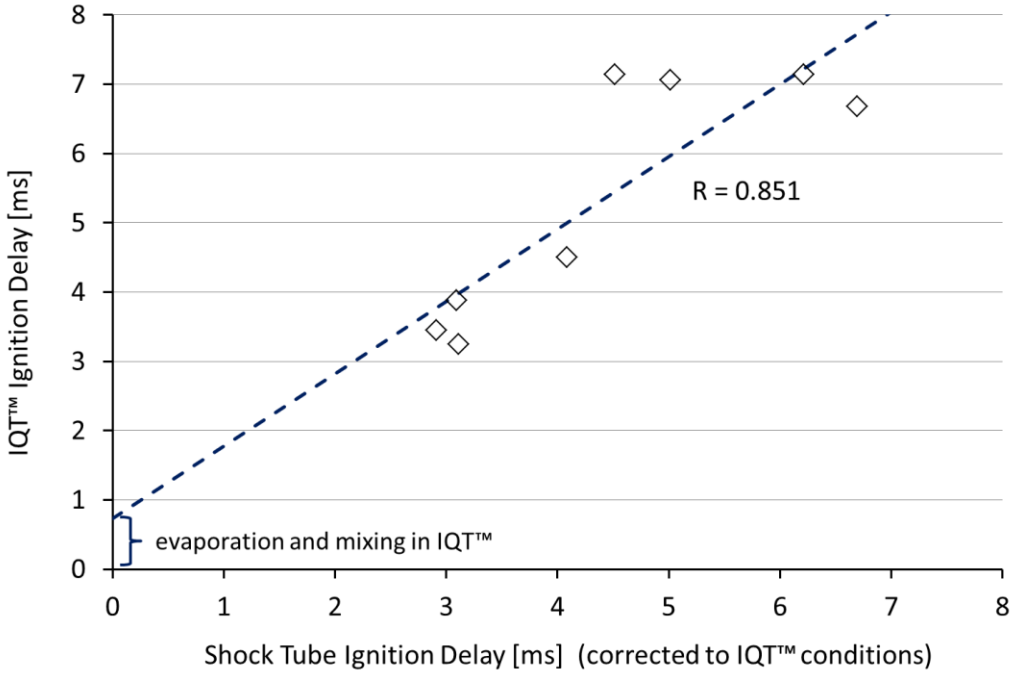

Figure 6.4: Comparison of IQT™ and shock tube ignition delays

The various ignition delay measurements were compared using a correlation matrix analysis (see Table 6.3) which confirmed that the shock tube ignition delays at 833 K correlated very strongly with the delays converted to IQT™ conditions ($ID_{843\ K}$'). (Absolute coefficients greater than 0.7 were considered indicative of strong correlations while 0.5 to 0.7 were considered to be indicative of weak but significant correlations.) The analysis also revealed a strong positive correlation between IQT™ delays and the shock tube results at 833 K (1000/K = 1.2), but weak correlations in the high temperature regime, 1000/K = 1.0 and 0.8. While this is not an unqualified result it confirmed confidence in the ignition delay data sets measured in both the shock tube and IQT™. Due to the very strong positive correlation revealed between the 1000 K and 1250 K shock tube delays which indicated that these results were essentially covariant, only the 1000 K metric was used in the subsequent analyses. Similarly the 833 K shock

tube delays were subsequently considered to also be a reasonable proxy representation of results converted to the IQT™ temperature and pressure operating conditions

Table 6.3: Correlation analysis of IQT™ and shock tube ignition delay results

	$ID_{1250\ K}$	$ID_{1000\ K}$	$ID_{833\ K}$	$ID_{843\ K}$'	ID_{IQT}
$ID_{1250\ K}$ (1000/T = 0.8)	1				
$ID_{1000\ K}$ (1000/T = 1.0)	0.99	1			
$ID_{833\ K}$ (1000/T = 1.2)	0.66	0.76	1		
$ID_{843\ K}$'	0.67	0.78	1.00	1	
ID_{IQT}	0.40	0.51	0.86	0.85	1

-0.5 to 0.5	-0.7 to -0.5 ; 0.5 to 0.7	<-0.7 ; >0.7

6.3 Gas turbine model-combustor: LBO evaluation results

The results of LBO evaluation in the model-combustor are shown in Figures 6.5 to 6.7. It reports the global equivalence ratios at which the blowout events were detected as a function of the air mass flow rate for the three different combinations of burner configuration and air pre-heat temperature.

While there were marked differences in the characteristic shape-functions associated with the three different combustor test series, they each exhibited statistically consistent trends for all eight test fuels. Clear differences were observed between the eight test fuels and superficially these differences appeared to carry through consistently over the greater part of the air mass flow range and between different test series.

However, a transition was observed between the results at the lowest air mass flow rates and the results at higher air mass flow rates above approximately 5 g/s. This was broadly in line with the behaviour that was predicted by the theoretical treatment in Section 4.3 as illustrated by Figure 4.3 which showed combustion limits being constrained by evaporation below a critical air mass flow rate. These results will be explored in greater detail in a subsequent discussion section.

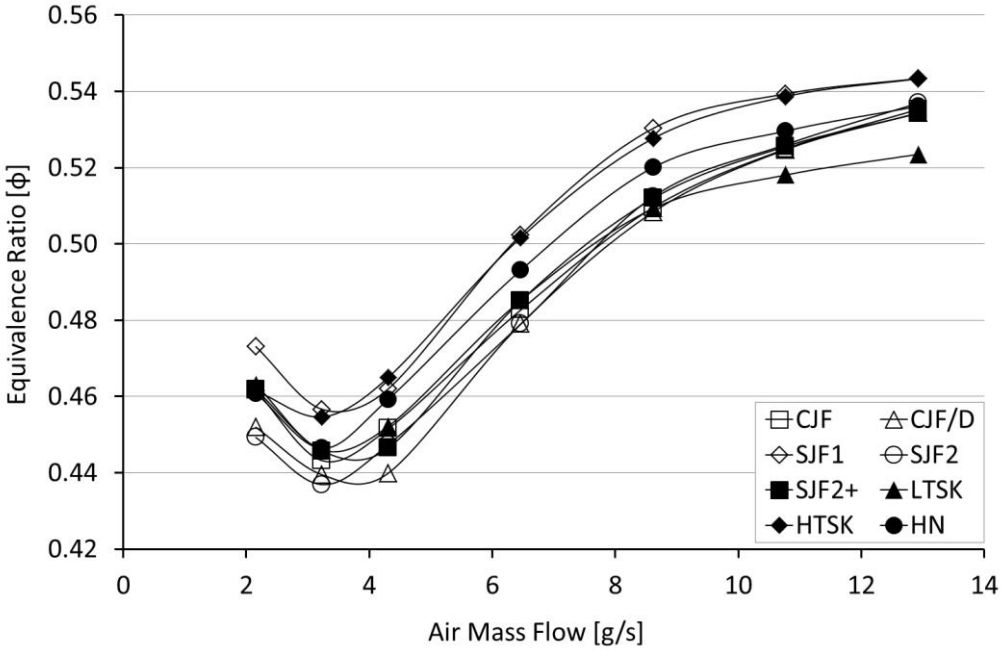

Figure 6.5: Model-combustor LBO results - burner configuration A, 323 K air pre-heat

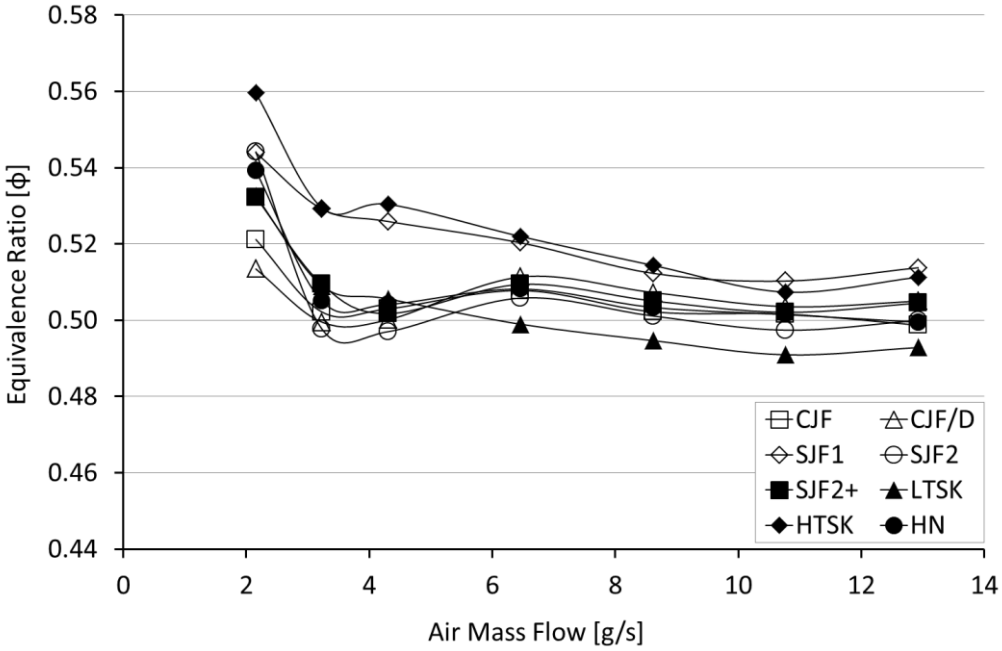

Figure 6.6: Model-combustor LBO results - burner configuration A, 413 K air pre-heat

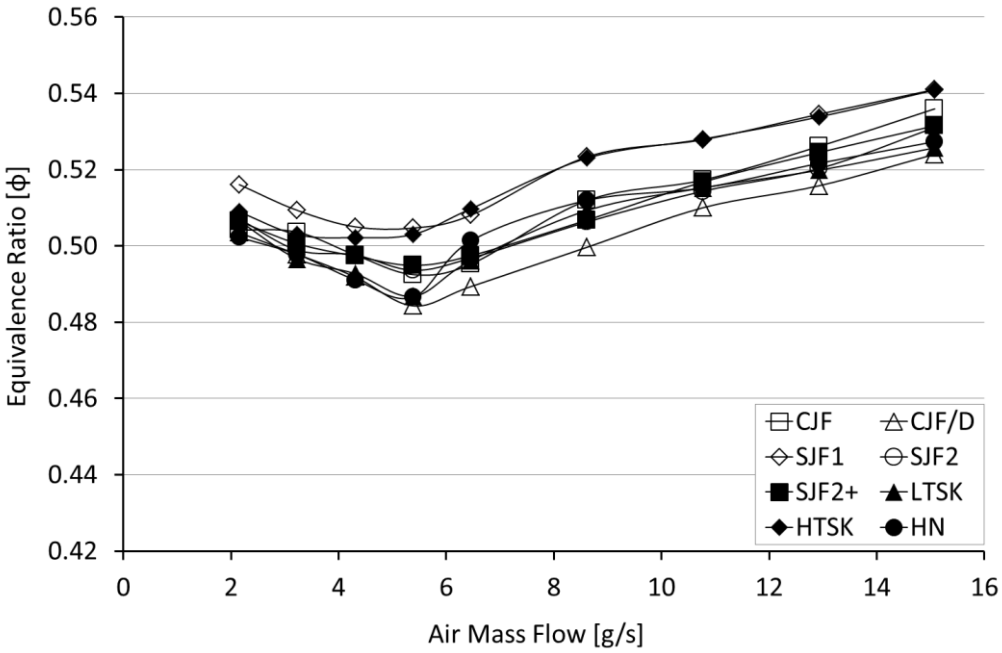

Figure 6.7: Model-combustor LBO results - burner configuration B, 323 K air pre-heat

6.4 Gas turbine model-combustor: fuel spray evaluation results

The PDA spray measurements in the laboratory-scale model-combustor were conducted at two stoichiometric air-fuel ratios: one at 5% rich of the LBO stoichiometry and another at a stoichiometry of $\phi = 0.6$. This allowed both investigation of the spray behaviour as close to blowout as practical, as well as a comparison between all fuels at exactly the same stoichiometric air-fuel ratio. For each stoichiometric set point, measurements were performed at two air mass flow rates (2.2 g/s and 6.5 g/s) and three distances from the nozzle exit plane (z = 15 mm, z = 25 mm , and z= 35 mm). The combustor was traversed along the y-axis at each z-axis location in 2 mm increments. The PDA test results are summarised in Appendix D, which reports Sauter mean diameter (SMD), D_{32}, values to capture the diameter distribution for each fuel, combustion condition, and measurement position as a single representative number. There were no significant differences in the measured behaviour between the two stoichiometric conditions. The measurements at 6.5 g/s air mass flow rate revealed clear fuel-specific trends that applied across all test conditions and measurement positions. All eight test fuels displayed similar distributions over the measurement area at the higher flow rate.

The measurements at the lower air mass flow rate (2.2 g/s) displayed greater variability and considerably larger droplet diameters. The spray distributions were also not consistent across all eight test fuels, with HN deviating from the distribution displayed by the rest of the test fuels at the lower flow rate.

Figures 6.8 and 6.9 show representative SMD results for ϕ = 0.6 and an air mass flow rate of 6.5 g/s at the maximum and minimum axial measurement positions. Figure 6.10 reflects the SMD results for an air mass flow rate of 2.2 g/s at ϕ = 0.6 at a distance of 15 mm from the nozzle exit plane. (Note the increase in the vertical scale for Figure 6.10 relating to the lower air mass flow.)

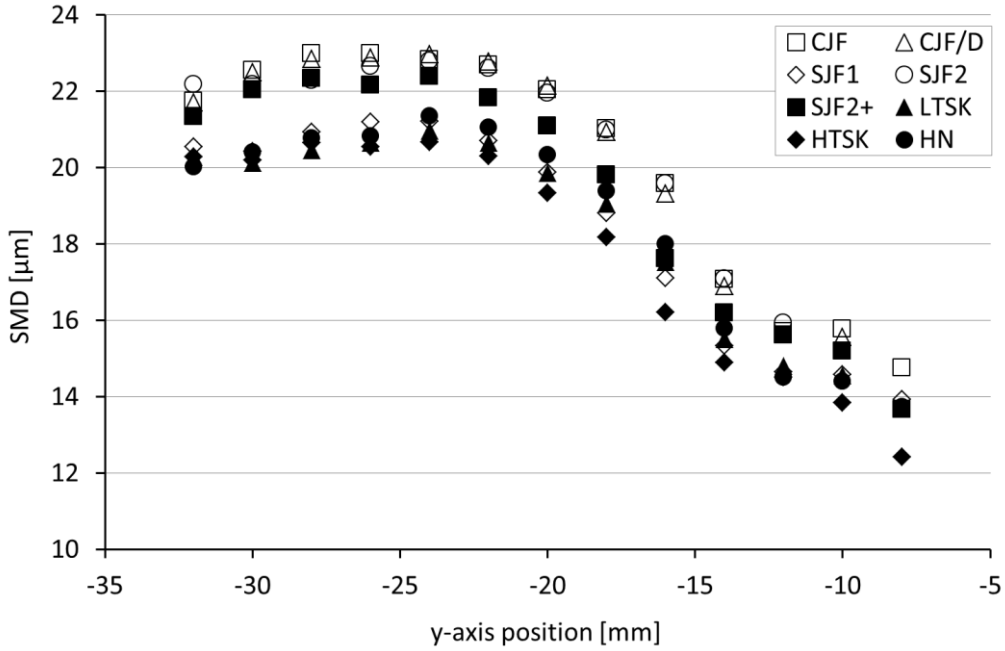

Figure 6.8: Radial SMD profiles (ϕ = 0.6, $\dot{m}_A$ = 6.5 g/s, z = 15 mm from exit plane)

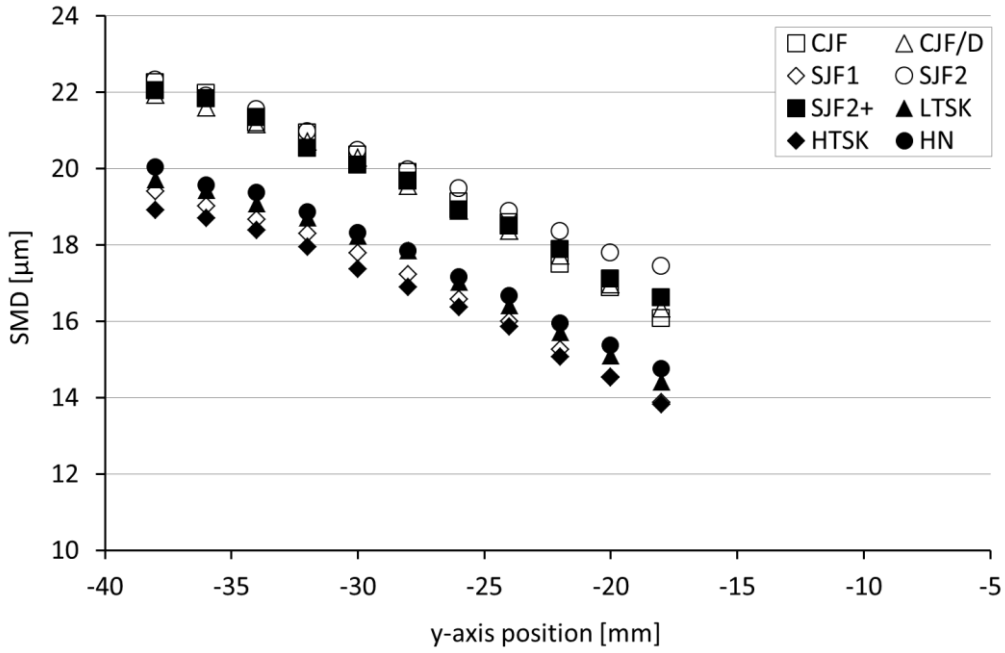

Figure 6.9: Radial SMD profiles (ϕ = 0.6, $\dot{m}_A$ = 6.5 g/s, z = 35 mm from exit plane)

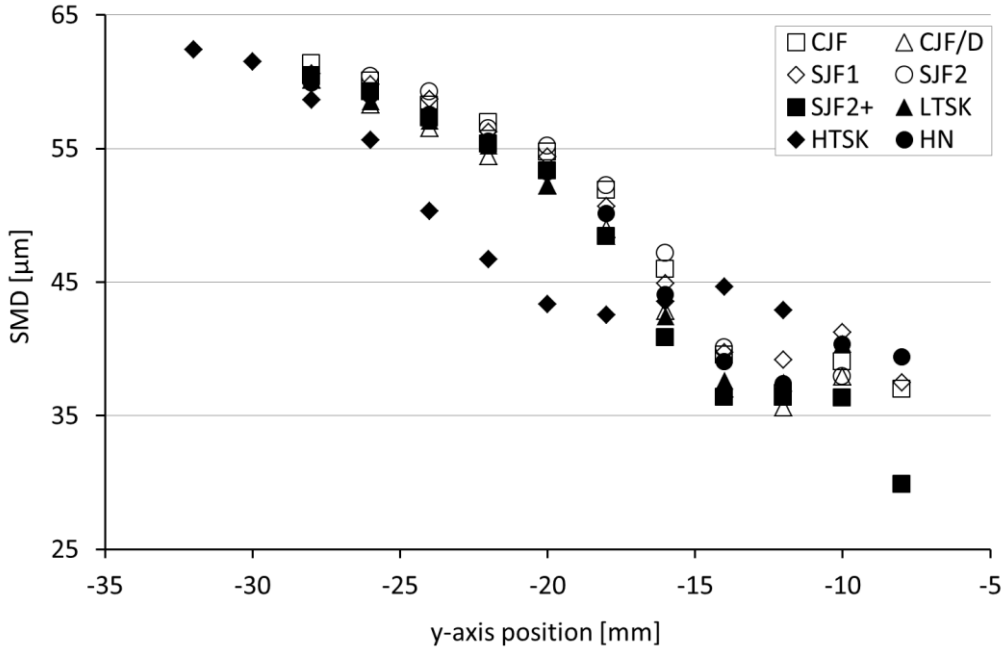

Figure 6.10: Radial SMD profiles (ϕ = 0.6, $\dot{m}_A$ = 2.2 g/s, z = 15 mm from exit plane)

7 Analysis and Discussion of Results

In the following discussion the results from the different aspects of the experimental programme are combined to interrogate the influence of various fuel properties on LBO behaviour. In contrast with the preceding sections, the spray and evaporation behaviour of the fuels are discussed first because they are important in the evaluation of the so-called chemical differences. The physical properties and spray behaviour were evaluated against the theoretical combustion efficiency in an evaporation-controlled system, while the chemical differences were examined by testing the assumption that the LBO results had been driven by a reaction-controlled system.

7.1 Spray and evaporation-controlled system analysis of LBO results

The results of the PDA measurements were used to calculate relative SMD values at each air mass flow condition and for both stoichiometry conditions with CJF as references. Radial measurements were averaged for each axial measurement positions and overall for all axial positions. The lower air mass flow rate condition did not yield sufficient data at the z = 35 mm position for calculating relative SMD numbers. As can be seen in Table 7.1 the average z-axis values were credible representations of the measurements at the individual z-axis positions and there was no significant difference in the relative SMD results between the two stoichiometry conditions. The subsequent analyses were therefore performed using the average values for the ϕ_{LBO}+5% case as being representative of the PDA performance at the two air mass flow rates.

The spray behaviour was evaluated by comparing the experimental PDA results with theoretical evaporation-controlled combustion efficiencies for different fuels. Recalling Equation 2.6, the relative evaporation-controlled combustion efficiencies for two fuels can be expressed as Equation 7.1.

$$\eta_e = {\rho_A \lambda_{eff} V}\Big/{D_0^2 f_c \dot{m}_A} \qquad [2.6]$$

$$\therefore {\eta_{e_2}}\Big/{\eta_{e_1}} = {\lambda_{eff_2}}\Big/{\lambda_{eff_1}} \left(\frac{1}{{D_{0_2}}/{D_{0_1}}} \right)^2 \qquad [7.1]$$

Table 7.1: PDA spray measurements: Relative SMD values averaged per axial measurement position

ϕ	z	Air mass flow [g/s]	Test Fuel							
			CJF	CJF/D	SJF1	SJF2	SJF2+	LTSK	HTSK	HN
ϕ_{LBO} + 5%	15	2.2	1	0.990	1.042	1.016	0.969	0.998	0.949	1.008
ϕ_{LBO} + 5%	25	2.2	1	0.993	1.031	1.004	0.963	1.014	1.006	1.009
ϕ_{LBO} + 5%	Ave	2.2	1	0.991	1.036	1.010	0.966	1.006	0.978	1.009
ϕ_{LBO} + 5%	15	6.5	1	0.987	0.910	1.005	0.971	0.924	0.880	0.929
ϕ_{LBO} + 5%	25	6.5	1	0.996	0.883	1.022	0.980	0.915	0.880	0.912
ϕ_{LBO} + 5%	35	6.5	1	0.983	0.864	1.021	0.992	0.897	0.866	0.899
ϕ_{LBO} + 5%	Ave	6.5	1	0.989	0.886	1.016	0.981	0.912	0.875	0.913
0.6	15	2.2	1	0.959	1.006	1.003	0.943	0.973	0.936	0.993
0.6	25	2.2	1	1.001	1.041	1.015	0.975	1.038	1.021	1.024
0.6	Ave	2.2	1	0.980	1.024	1.009	0.959	1.005	0.978	1.008
0.6	15	6.5	1	0.996	0.915	0.997	0.959	0.910	0.885	0.920
0.6	25	6.5	1	0.998	0.885	1.017	0.986	0.911	0.866	0.889
0.6	35	6.5	1	0.995	0.869	1.023	1.000	0.893	0.856	0.903
0.6	Ave	6.5	1	0.996	0.890	1.012	0.982	0.905	0.869	0.904

The effective evaporation constants were calculated using Equation 7.2 which was derived empirically from plots by Chin and Lefebvre that relate effective evaporation constants to normal boiling point, droplet size, velocity, pressure and ambient temperature [20]. They presented effective evaporation constants versus boiling point (T_{bn}) for various values of droplet size-velocity products (UD_0) at three pressures and three ambient temperatures.

$$\lambda_{eff} \propto \frac{P^{0.124}\, T^{1.652}}{T_{bn}{}^{0.501}} \qquad [7.2]$$

The 100 kPa plots were employed as representative of the atmospheric pressure conditions under which the PDA measurements were performed. Unlike the earlier treatment, fuel-specific volatility differences were taken into account by including the boiling point, T_{bn}. The boiling point of each fuel was approximated as the distillation temperature at which 50% is recovered. Chin and Lefebvre acknowledged that while a single fuel property cannot fully describe evaporation characteristics of any given fuel, average boiling point has the benefit of being directly related to vapour pressure and fuel volatility. The PDA measurements revealed that the products of velocity and droplet size, UD_0, ranged between 150 and 1000 depending on the test conditions and

measurement position. For any given test point, the fuel-to-fuel variation of UD_0 was, however, relatively insignificant, which implied that nominally representative values could be used with confidence to calculate evaporation constants over the full spectrum of test conditions. Comparison of different system temperatures revealed that while the absolute values of the effective evaporation constants were influenced strongly, the relative numbers were insensitive to system temperature. This enabled the use of nominally representative values of system temperature with confidence.

The relative SMD values were modelled based on Equation 2.28. By comparing relative SMD numbers, the influence of velocity and the characteristic dimension were cancelled. Air/liquid ratios (ALRs) at the relevant stoichiometry conditions ($\phi = 0.6$ and $\phi = \phi_{LBO}+5\%$ respectively) were employed although it should be noted that the relative results were not significantly impacted.

$$SMD \propto \left(\frac{\sigma}{\rho_A {U_A}^2 D_P}\right)^{0.5} \left(1 + \frac{1}{ALR}\right) \qquad [2.28]$$

The results of the modelled relative effective evaporation constants, SMDs, and evaporation-controlled combustion efficiencies are presented in Table 7.2. Due to the use of relative normalised metrics the influence of air mass flow was largely eliminated with only the ALR values introducing differences at the two test conditions. These differences were, however, of the order of 1% and lower. The relative values were, therefore, averaged over the test burner configurations, air pre-heat set points, and the two air mass flow rates at which PDA measurement were performed.

Table 7.2: Average relative effective evaporation constants, SMDs, and evaporation-controlled combustion efficiencies of the test fuel matrix.

Test Fuel	CJF	CJF/D	SJF1	SJF2	SJF2+	LTSK	HTSK	HN
$\lambda_{eff.(rel)}$	1	0.978	1.064	0.998	0.999	1.078	1.047	1.090
$SMD_{(rel)}$	1	0.996	0.970	1.008	1.003	0.953	0.955	0.967
$\eta_{e(rel)}$	1	0.986	1.132	0.982	0.992	1.188	1.147	1.164

An analysis was performed of the linear correlation between these calculated relative spray and evaporation metrics and the relative experimental PDA results from Table 7.1. The results of this analysis are presented in Table 7.3 with $SMD_{(rel)}$ referring to the averaged calculated relative SMD values and $PDA_{(rel)}$ referring to the measured relative SMD values. The air mass flow rate conditions (2.2 g/s and 6.5 g/s) are identified

as “LF” (low flow) and “HF” (high flow) respectively. The two stoichiometric ratios at which the PDA measurements were conducted are identified as “LBO” for the $\phi_{LBO}+5\%$ test condition and “0.6” for the $\phi = 0.6$ test condition.

Table 7.3: Correlation analysis of relative spray and evaporation metrics and the relative experimental PDA results.

	$\lambda_{eff.(rel)}$	$SMD_{(rel)}$	$\eta_{e(rel)}$	$PDA_{(rel)}$ $(LF;\ LBO)$	$PDA_{(rel)}$ $(LF;\ 0.6)$	$PDA_{(rel)}$ $(HF;\ LBO)$	$PDA_{(rel)}$ $(HF;\ 0.6)$
$\lambda_{eff.(rel)}$	1						
$SMD_{(rel)}$	-0.874	1					
$\eta_{e(rel)}$	0.964	-0.972	1				
$PDA_{(rel)(LF;\ LBO)}$	0.441	-0.198	0.320	1			
$PDA_{(rel)(LF;\ 0.6)}$	0.520	-0.265	0.397	0.967	1		
$PDA_{(rel)(HF;\ LBO)}$	-0.840	0.930	-0.913	-0.231	-0.243	1	
$PDA_{(rel)(HF;\ 0.6)}$	-0.871	0.946	-0.937	-0.221	-0.255	0.996	1

-0.5 to 0.5	-0.7 to -0.5 ; 0.5 to 0.7	<-0.7 ; >0.7

The relative PDA measurements that were conducted at the higher air mass flow rate showed a strong correlation with the calculated SMD values and strong negative correlations with the calculated effective evaporation constants and evaporation efficiencies. This confirmed that the measured spray behaviour was in agreement with the theoretical treatment for a prefilming airblast atomiser. The lower air mass flow test data revealed no correlation with the higher air mass flow data or with the theoretical calculated values. This indicated that the spray behaviour deviated significantly from the theoretical optimal (design) operation at the lower flow condition.

The relative PDA measurements exhibited a very high correlation between the two stoichiometry test conditions for both air mass flow rates which enabled the use of the data set from either one of the two test conditions as representative of the relative spray behaviour. (The $\phi_{LBO}+5\%$ results were used in the subsequent analyses.)

Figure 4.3 theoretically predicted the influence of evaporation efficiency on the experimental LBO boundaries, and the experimental LBO results resembled this behaviour to a large degree. Based on this the possibility was investigated of LBO behaviour at the lower air mass flow rate being governed by evaporation. The operating range of the burner, as well as the experimental noise at very low air mass flow rates,

resulted in a very limited set of data points in the low flow region that was of interest. This limited the value that could be gained from comparing LBO trends in this range with theoretical evaporation efficiencies. An alternative approach was followed by considering the postulate that the effect of evaporation efficiency resulted in a relative offset in blowout extinction boundaries and that this would be proportional to the differences in LBO behaviour in the lowest air mass flow rate while the higher flow region was shown to be governed by the chemical reaction rate (Figure 4.4). The magnitude of the "offset" was therefore represented by the numerical difference in extinction stoichiometries at the lowest air mass flow rate of 2.2 g/s and the 8.6 g/s test point. The results were then normalised for each test configuration by subtracting the results of the CJF fuel in that particular configuration. The two low-preheat temperature test configurations were chosen because they were likely to represent the more extreme fuel evaporation situation where the fuel differences would be more readily discerned. It was not considered to be technically defensible to include the higher pre-heat case. These measured phi "offset" values were compared against theoretical phi values that were calculated with Equation 7.3 which was derived from equations 2.6, 7.2 and 2.28.

$$\phi \propto \left(\frac{P^{0.124}\, T^{1.652}}{{T_{bn}}^{0.501}\eta_e \sigma}\right)^{0.5} - 1 \qquad [7.3]$$

By applying an appropriate proportionality constant the correlation between theoretical and experimental phi values could be determined. Both burner configurations revealed positive correlations. Configuration A revealed a weaker and configuration B a stronger positive correlation. The results from these two burner configurations were, therefore, combined to reduce the influence of experimental scatter. The fact that a combination of the two data sets resulted in an improved maximum correlation indicated the benefit of reducing the influence of experimental noise as reflected by Figure 7.1 graphically. Figure 7.2 reports the correlation at the optimal combination of the two data sets comprising of 75% B and 25% A.

Regardless of whether the configurations are viewed individually, numerically averaged, or the optimal combination of the data sets is used, the correlations supported the hypothesis that the LBO behaviour at low air mass flow was governed by evaporation efficiency.

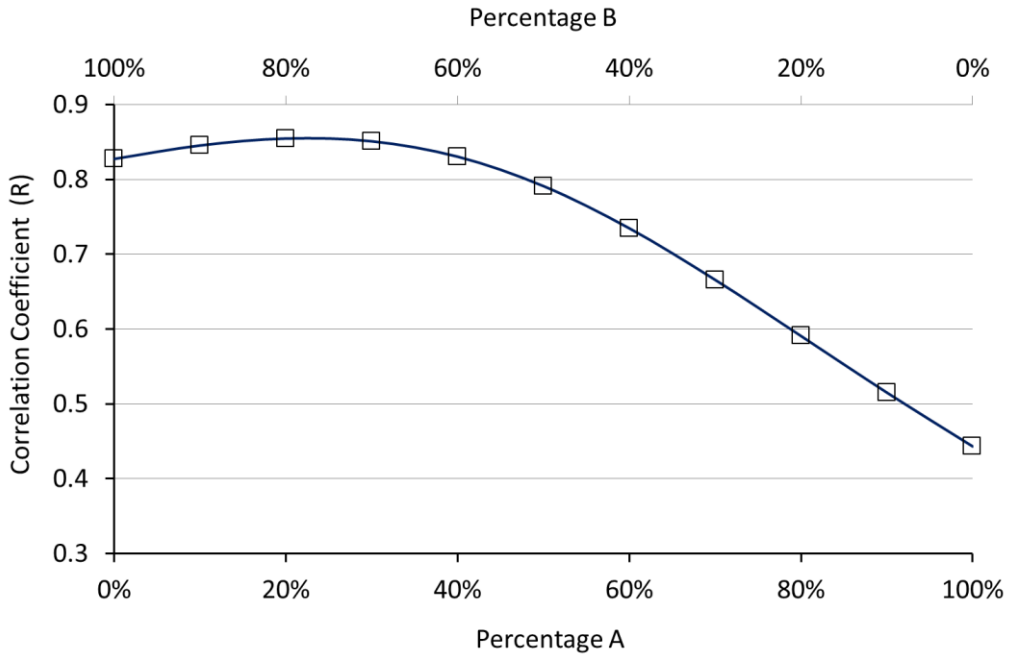

Figure 7.1: Correlation of experimental and theoretical stoichiometric values (effect of proportional representation of configurations A and B)

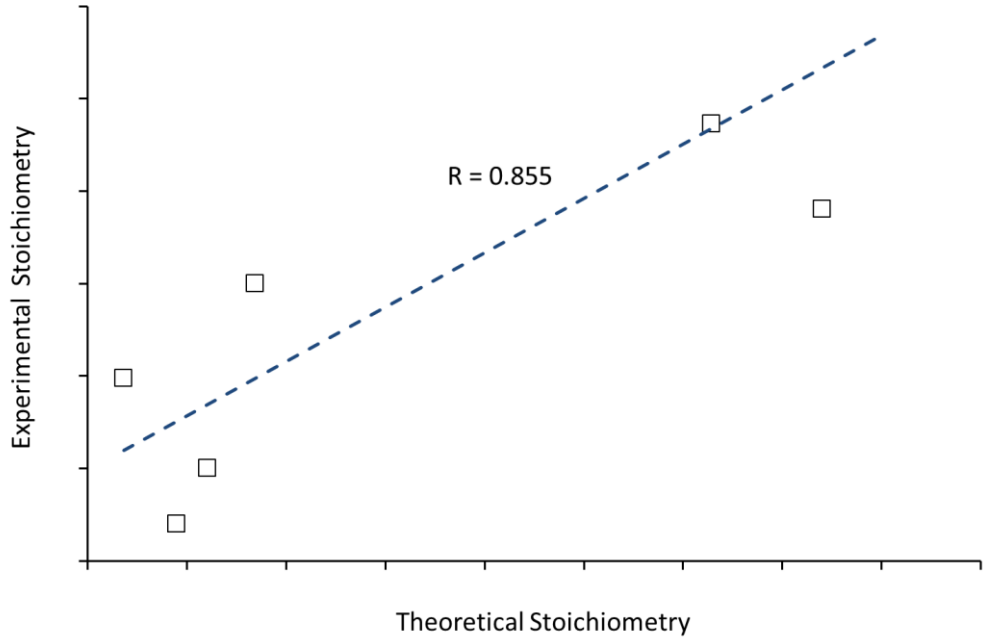

Figure 7.2: Correlation of experimental and theoretical stoichiometric values (75% configuration B and 25% configuration A)

7.2 Reaction-controlled system analysis of LBO results

The possibility of ignition delay differences influencing the LBO differences that were recorded in the model-combustor was investigated by recalling the model treatment of a well-stirred homogeneous reactor (representative of a reaction-controlled system) as developed in Chapter 4. The relationship between the volumetric flow rate through the combustor and the combustion efficiency (the extent to which combustion was completed during the available residence time) are described by Equations 4.18 and 4.23 for lean and rich combustion respectively. These expressions were used to generate Figures 4.2 and 4.3 to illustrate theoretical differences in LBO behaviour driven by differences in AFT and proportionality constants which in turn were based on ignition delay differences.

The model-combustor LBO results were evaluated using the same theoretical treatment to calculate the best fit values for the proportionality constant of each test fuel. These constants were subsequently employed in a correlation analysis with fuel properties (including ignition delay results) and results from the preceding spray behaviour analysis. Equation 4.18 provided the relevant expression for the relationship between the volumetric flow rate through the combustor and the combustion efficiency under the lean conditions that are implicit during LBO.

$$\frac{\dot{m}_A}{VP^{i+j}} = K\frac{(1-\eta_\theta)^i\phi^{i-1}(1-\eta_\theta\phi)^j}{T^{i+j}\eta_\theta}e^{-E/RT} \qquad [4.18]$$

The adiabatic flame temperatures at blowout would have been influenced by both the test fuel composition and stoichiometry. For each test fuel the GCxGC based C/H ratio was used to calculate the adiabatic flame temperature (AFT) and air fuel stoichiometry at each LBO point. Heptane-toluene surrogates were used to match the test fuel C/H ratios as explained previously. A regression analysis of the calculated and measured air mass flow was then employed to determine the proportionality constant, K, for every LBO point. The volume was based on the combustor volume, and pressure was atmospheric, both of which were constant for all fuels. Figure 7.3 represents an example of these proportionality constants for burner configuration B with air pre-heated to 323 K. The detailed results for all three test configurations are presented in Appendix E.

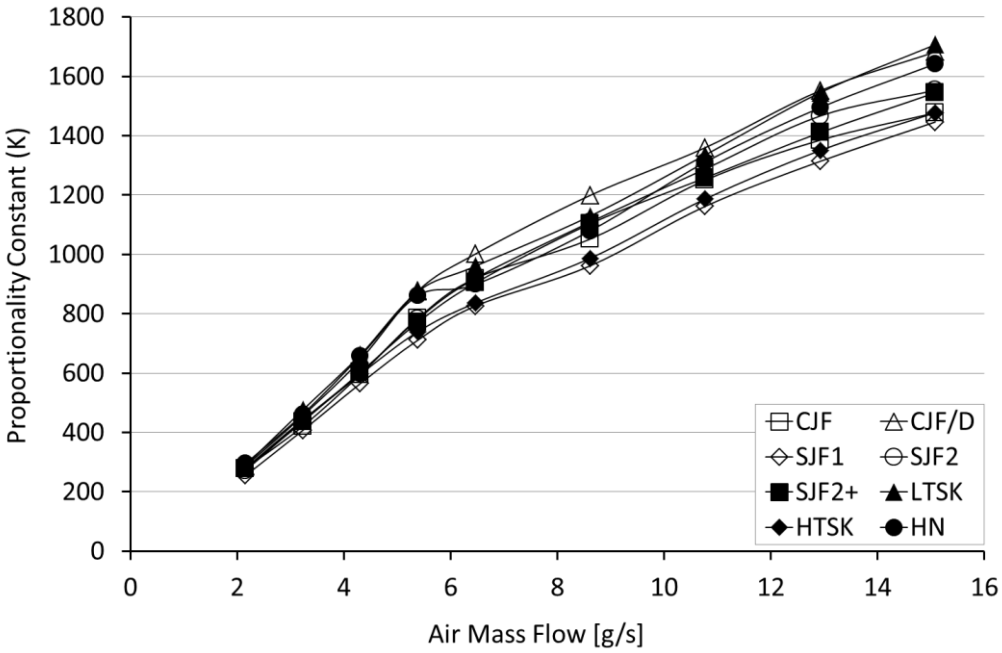

Figure 7.3: Proportionality constants for modelled combustor airflow based on LBO test data - burner configuration B, 323 K air pre-heat

The calculated proportionality constants exhibited a flow dependence that would not be expected in a homogeneous perfectly-stirred reactor. This is indicative of the homogeneous perfectly-stirred treatment oversimplifying the conditions relevant to the experimental spray combustor. It was not surprising and could be ascribed to the additional evaporation, mixing and heat transfer delays that are inherent in the spray combustor but not applicable in a stirred reactor. These various delay elements would be influenced by air mass flow rate to different degrees. It was shown in Section 4.4 that the mixing delay, for example, would be essentially independent of the air mass flow rate while the evaporation delay would be inversely proportional to the square of the air mass flow rate. As discussed previously, burner configuration A did not possess a strong central recirculation zone as would be present in typical real aero-engine combustors. This was in contrast to configuration B that did exhibit a well-developed central recirculation zone which resulted in differences in the amount of air and combustion products being recirculated into their respective primary zones at high flow rates. Furthermore by increasing air temperature (pre-heat) air viscosity is increased which influences the entrainment of air into the primary zone. The calculated proportionality constants of the three burner configuration / pre-heat combinations would therefore be expected to exhibit different degrees of dependence on air mass

flow rate. This was explored by investigating a modified expression which incorporated both air mass flow dependent and independent delays.

In the earlier theoretical assessment Equation 4.27 expressed combustion efficiency in terms of the air residence time and the ignition delay:

$$\eta_\theta = \left(\frac{\rho V}{\dot{m}_A}\right)\ \left(K e^{-E/RT} P^{0.75}\right) \qquad [4.27]$$

By rearranging 4.27, the reaction proportionality constant can be expressed as:

$$K = \frac{\rho V/\dot{m}_A}{\eta_\theta e^{-E/RT} P^{0.75}} \qquad [7.4]$$

A modified proportionality constant which incorporates an additional, fixed delay term to allow for the physical mixture preparation can then be defined by introducing a constant delay, τ_c, into the air residence time in a manner similar to the treatment of the IQT™ ignition delay calibration curve (Equation 6.1) discussed in Section 6.2.

$$K_\theta = \frac{\rho V/\dot{m}_A - \tau_c}{\eta_\theta e^{-E/RT} P^{0.75}} \qquad [7.5]$$

$$\therefore \quad \frac{K_\theta}{K} = \frac{\rho V/\dot{m}_A - \tau_c}{\rho V/\dot{m}_A} \qquad [7.6]$$

$$K_\theta = K(1 - C_\theta \dot{m}_A) \qquad \text{where} \quad C_\theta = \frac{\tau_c}{\rho V} \qquad [7.7]$$

Modified proportionality constants were calculated for each fuel by appropriate selection of C_θ to minimise the standard deviation in the higher air mass flow region where the effects of evaporation are diminished, and one could reasonably expect the modified proportionality constant to be independent of air mass flow rate. The results for all three configuration / pre-heat combinations are presented in Appendix E. The modified proportionality constants for burner configurations A and B with 323 K air pre-heat are shown in Figures 7.4 and 7.5. Configuration A without the strong recirculation exhibited relatively constant values at air mass flow rates above 6.5 g/s, but configuration B retained a small measure of flow rate dependence. At the higher pre-heat temperature, the test results with burner configuration A exhibited even greater air mass flow dependence. The residual dependence of the modified proportionality constants on air flow rate could possibly be ascribed to increased entrainment of secondary air under higher flow turbulence conditions, but importantly does not significantly impact the relative performance of the different fuels.

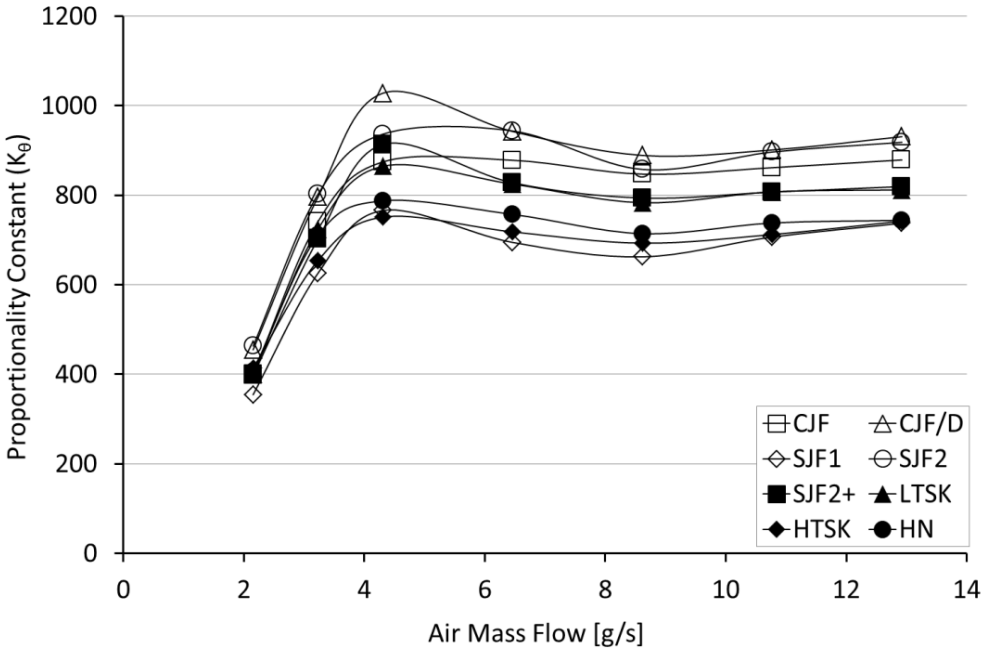

Figure 7.4: Modified proportionality constants (K_θ) for modelled combustor airflow based on LBO test data - burner configuration A, 323 K air pre-heat

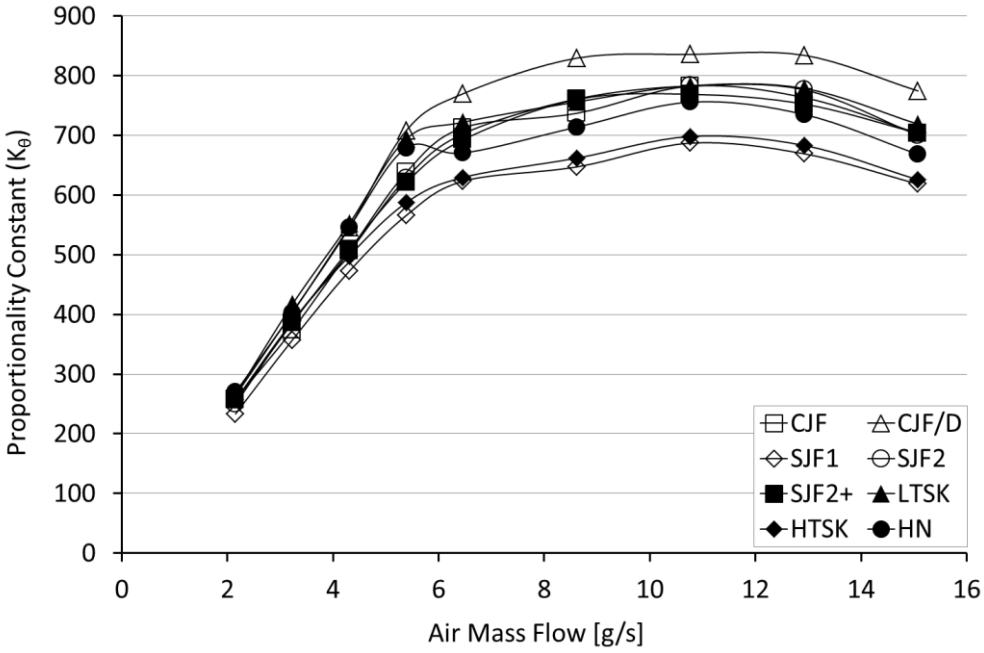

Figure 7.5: Modified proportionality constants (K_θ) for modelled combustor airflow based on LBO test data - burner configuration B, 323 K air pre-heat

The modified and unmodified proportionality constants (as reported in Table E1, Appendix E) were compared by conducting a correlation analysis of the averaged values

for all three test configurations at flow rates above 8 g/s. Both modified and unmodified proportionality constants exhibited deviations at air mass flows below 6 g/s which agreed with the preceding conclusion that evaporation efficiency impacted the blowout results at low air flow rates. The relative ranking of the fuel constants were similarly achieved by normalising them to a common reference: Test Fuel CJF. The correlation analysis results reported in Table 7.4 revealed that the normalised proportionality constants (K) of the three test configurations correlated strongly with each other and with their respective modified constants (K_θ). The modified constants of the two low air pre-heat cases also correlated strongly, but the correlation between the low and high pre-heat cases were much weaker. The K and K_θ values averaged over their three test configurations all correlated very strongly the individual configuration rankings with the exception of the modified constants for the higher pre-heat case of configuration A. Based on these results the unmodified relative proportionality constants averaged over all configurations, K_{Ave}, were selected for use as the optimal representation of the chemical reaction rate in subsequent analyses to represent the relative LBO performance of the fuels.

Table 7.4: Correlation analysis of normalised LBO proportionality constants (K) and modified proportionality constants (K_θ)

	K (A, 323 K)	K (B, 323 K)	K (A, 413 K)	K_{Ave}	K_θ (A, 323 K)	K_θ (B, 323 K)	K_θ (A, 413 K)	$K_{\theta Ave}$
K (A, 323 K)	1							
K (B, 323 K)	0.892	1						
K (A, 413 K)	0.848	0.714	1					
K_{Ave}	0.976	0.930	0.906	1				
K_θ (A, 323 K)	0.712	0.660	0.331	0.614	1			
K_θ (B, 323 K)	0.874	0.900	0.521	0.823	0.893	1		
K_θ (A, 413 K)	0.873	0.742	0.990	0.922	0.380	0.571	1	
$K_{\theta Ave}$	0.922	0.866	0.647	0.871	0.920	0.963	0.692	1

-0.5 to 0.5	-0.7 to -0.5 ; 0.5 to 0.7	<-0.7 ; >0.7

As a preliminary check on the self-consistency within the various experimental data, the influence of fuel properties on LBO behaviour was interrogated by analysing the

correlation between the relative LBO proportionality constants (K_{Ave}), the relative spray behaviour ($SMD_{(rel)}$) and the metrics that were used to define the combustion chemistry of the fuel matrix (LFS, ID_{IQT}, $ID_{1000\,K}$, $ID_{833\,K}$). The results of the analysis are reported in Table 7.5. The following conclusions were drawn from the results of this analysis:

- The $SMD_{(rel)}$ was chosen to represent the spray behaviour at higher air mass flow rates because of the very strong correlation with the relative PDA measurements (as reported in Table 7.3). Under these conditions the spray was fully developed and adhering to the theoretical treatment for a prefilming airblast atomiser. There was absolutely no correlation between the LBO proportionality constants and the relative spray behaviour of the different fuels which confirmed that there was no discernable influence of evaporation or spray on the blowout results in the high air mass flow regime.

Table 7.5: Correlation analysis of average relative LBO behaviour, fuel spray, LFS and ignition delays

	K_{Ave}	$SMD_{(rel)}$	LFS	ID_{IQT}	$ID_{833\,K}$	$ID_{1000\,K}$
K_{Ave}	1					
$SMD_{(rel)}$	0.07	1				
LFS	-0.08	0.74	1			
ID_{IQT}	-0.71	0.22	-0.05	1		
$ID_{833\,K\,(1000/T\,=\,1.2)}$	-0.87	-0.11	-0.23	0.86	1	
$ID_{1000\,K\,(1000/T\,=\,1.0)}$	-0.84	-0.01	0.07	0.51	0.76	1

-0.5 to 0.5	-0.7 to -0.5 ; 0.5 to 0.7	<-0.7 ; >0.7

- Similarly there was absolutely no correlation between the LBO proportionality constants and LFS which discredited the relevance of LFS being used to predict the LBO behaviour of different fuels. This provided clarification of the contradictions in literature regarding the impact of LFS on LBO, that were identified in Chapter 4.
- Relative LBO behaviour, K_{Ave}, exhibited a strong inverse correlation with IQT™ ignition delays and even stronger with the two shock tube ignition delays. However, as was also reported in Table 6.3, while IQT™ delays correlated strongly with the lower intermediate temperature shock tube ignition delays, the correlation was weaker with the higher temperature delays. Viewed in

combination these results would suggest that while the IQT™ is providing a reasonable indication of the LBO performance, it could possibly provide an even better metric if the IQT™ apparatus were operated at a higher temperature.

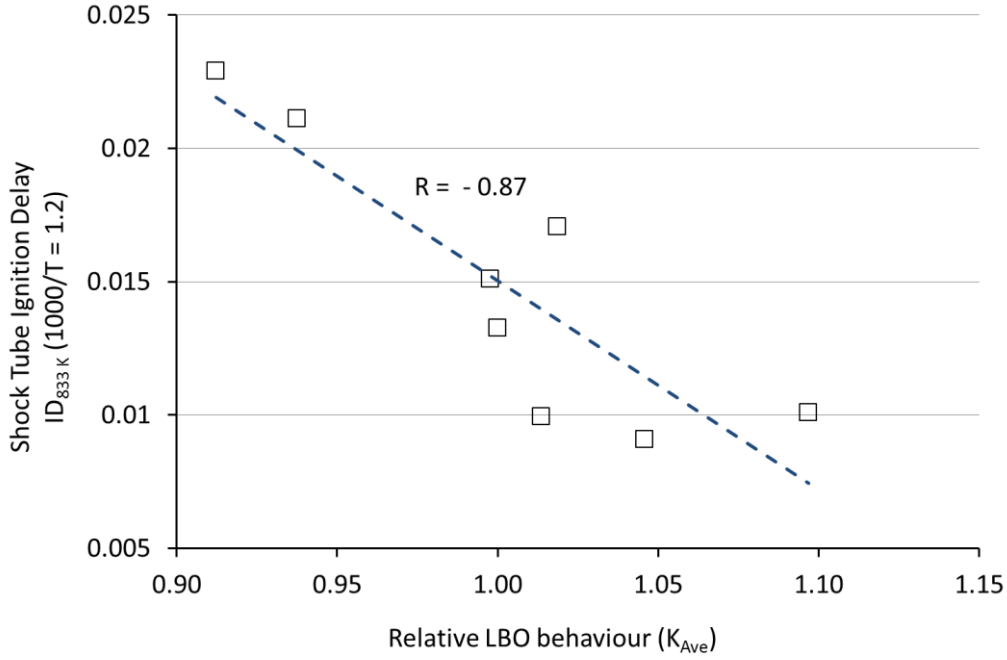

Figure 7.6: Correlation of relative LBO proportionality constants (K_{Ave}) and intermediate temperature shock tube ignition delay ($ID_{833\,K}$)

7.3 Interpretation of the experimental results

The experimental programme was designed to interrogate the hypothesis that jet fuel properties relating to evaporation and reaction behaviour could have a detectable and significant influence on high altitude extinction behaviour. Analysis of the experimental results provided the necessary data required to perform this task and were interpreted by recalling the theoretical operating envelope, demarcated by the reaction and evaporation-controlled extinction limits that was presented in Figure 2.6. The test programme was not designed to yield the absolute values of the reaction and evaporation-controlled extinction limits; however, by examining the relative behaviour of different fuels it was possible to explain the altitude extinction results that were observed during the FSJF certification tests.

First the relative LBO behaviour in the model-combustor was used to model the theoretical relative reaction-controlled operating envelope. The proportionality constant of the crude-derived jet fuel CJF, K'_{CJF}, was chosen such that the extinction

boundary (based on Equation 2.31) passed through the blowout extinction point that was recorded by the crude-derived test fuel (AVTUR) during the Rolls-Royce test campaign: Mach 0.99 at 10760 m (35300 ft.) altitude [13]. The fuel-specific relative LBO proportionality constants (K_{Ave}) that were calculated in the preceding section were employed in Equation 7.8 to produce the relative extinction limits for the rest of the test fuel matrix.

$$\eta_\theta \propto V e^{-E/RT} \rho^{1.75} / \dot{m}_A \qquad [2.31]$$

$$\eta_\theta = K'_{CJF}\, K_{Ave}\, V\, e^{-E/RT} \rho^{1.75} / \dot{m}_A \qquad [7.8]$$

The results are shown graphically in Figure 7.7 resulting in a number of observations that can be made. As mentioned, test fuel SJF1 was nominally identical to the synthetic test fuel that was employed in the FSJF certification tests (SFSAK). A blowout extinction limit of approximately Mach 0.95 at 10270 m (33700 ft.) altitude was reported for the SFSAK fuel [13]. The modelled extinction behaviour of SJF1 confirmed this impaired extinction limit relative to the crude-derived reference CJF/ AVTUR with its extinction boundary passing through Mach 0.95 at an altitude of 10150 m. (The AVTUR and SFSAK blowout extinction points are included in figures 7.7 to 7.9 to contextualise the results.)

It is interesting to note that the relative proportionality constants for SJF1 represented a 9 to 12 % reduction in air mass flow at blowout which compares well with the observation from the altitude test report which stated an almost 6% difference in relative air flow at first sector blowout and more than 10% difference in final sector blowout.

The modelled performance of the production synthetic jet fuel formulation, SJF2, was marginally better than the reference CJF while the low-temperature FT kerosene, LTSK achieved the highest extinction boundaries.

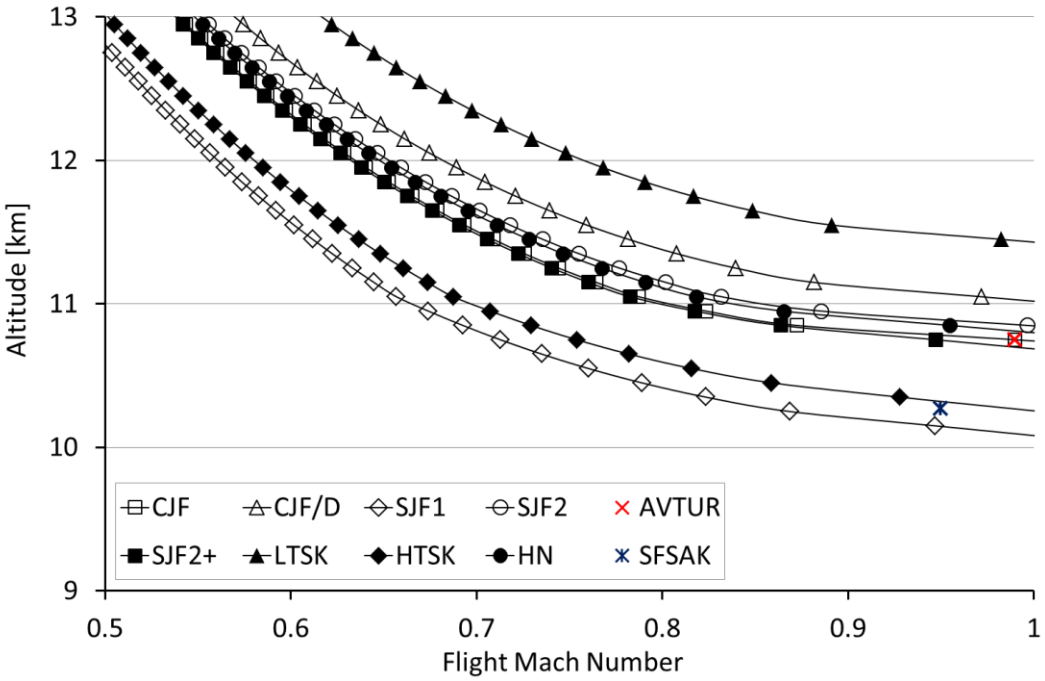

Figure 7.7: Theoretical relative reaction-controlled extinction limits

Similarly a theoretical relative evaporation-controlled operating envelope was modelled based on relative spray behaviour and relative effective evaporation constants, again using CJF as the reference. Incorporating $SMD_{(rel)}$ and the effective evaporation constants from Equation 7.2 into Equation 2.6 yields Equation 7.9 which was used to model the relative evaporation-controlled extinction limits. The proportionality constant $K"_{CJF}$ was again chosen such that the extinction boundary of CJF passed through the blowout extinction point that was recorded by the AVTUR fuel during the Rolls-Royce test campaign: Mach 0.99 at 10760 m (35300 ft.) altitude. The resultant extinction boundaries for all eight test fuels are reported in Figure 7.8.

$$\eta_e = {K"_{CJF}\, P^{1.124}\, T^{0.652}} \Big/ {T_{bn}{}^{0.501}\, SMD_{rel}{}^{2}\, \dot{m}_A} \qquad [7.9]$$

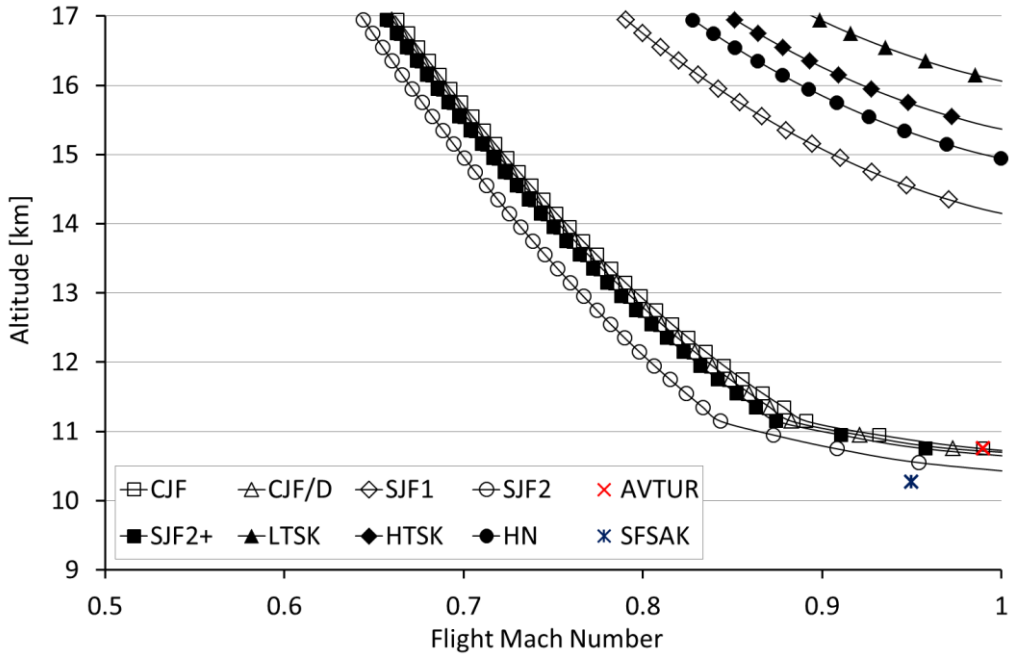

Figure 7.8: Theoretical relative evaporation-controlled extinction limits

The use of T_{50} as representative of the boiling point resulted in potentially exaggerated spread in the relative performance of the different fuels, but it does not undermine the modelled trends and relative performance.

The modelled extinction boundary of test fuel SJF1 was considerably improved over the reference CJF. The production synthetic jet fuel formulation, SJF2, was marginally worse than the reference CJF while the low-temperature FT kerosene, LTSK achieved the highest extinction boundaries. The SFSAK blowout extinction point was not supported by the evaporation-controlled boundary of SJF1. This clearly indicates that the location of the impaired SFSAK extinction point was not associated with an evaporation-controlled limit.

The relative spray behaviour and evaporation-controlled boundary of SJF1 also agreed with the observation made by the Honeywell test report that the atomisation of the FSJF was as good as or better than the Jet A reference fuel [15].

Interestingly SJF2 recorded impaired extinction limits relative to SJF1 in spite of conforming to the distillation gradient restriction that was introduced partially in reaction to the FSJF (SJF1) altitude relight results.

The flash point modified SJF2+ reported improved evaporation limited extinction boundaries relative to SJF2, but it was primarily ascribed to the relative SMD behaviour of the two fuels with the distillation only playing a secondary role. The apparent sensitivity to distillation could be increased slightly by using the flash point instead of T_{50} as the representative boiling point temperature in Equation 7.9. This would widen the difference in relative performance of the two fuels slightly (as would be expected) and would result in SJF2+ recording marginally better extinction limits than CJF, but it was not considered to be a technically justified representation.

It can therefore be concluded that the reaction-controlled extinction limits were in agreement with the altitude relight differences that were observed during the Rolls-Royce FSJF tests, while the evaporation-controlled extinction limits were in direct opposition to the FSJF altitude extinction results. The relative atomisation results of SJF1 were in fact in agreement with the atomisation results during the FSJF certification tests: The atomisation of the FSJF was reported to be as good as or better than the Jet A reference fuel for both airblast and pressure type fuel atomisers.

These results indicate that the relative impact of the reaction and evaporation efficiency limits on altitude extinction blowout were such that the reaction-controlled limits dominated and limited the overall altitude-Mach number envelope. Figure 7.9 compares both evaporation- and reaction-controlled extinction limits for four of the test fuels. As before, the proportionality constants were chosen such that the extinction boundaries of CJF passed through the blowout extinction point of the AVTUR test fuel. The relative performance of the other test fuels then serves to illustrate the relative impact of their evaporation and reaction boundaries.

It is interesting to examine the effect of introducing SJF2 to compensate for the lower blowout extinction performance recorded by SJF1. In spite of the focus on distillation gradient differences, a chemical ignition delay improvement resulted in the reaction-controlled extinction behaviour being improved to marginally better than the reference CJF. The evaporation-controlled extinction limits were, however, impaired and suggests that overall blowout extinction limits could be compromised at higher flight Mach numbers in excess of Mach 0.85 where the evaporation boundary drops below the reaction boundary. Consistent with the argument that was offered in the original certification report, this effect appears beyond the typical flight envelope and the resultant blowout extinction limits are projected to lie between the AVTUR and SFSAK

results. It should also be noted that it is unlikely that both evaporation and extinction boundaries would have come into play simultaneously with the AVTUR which means that the absolute evaporation limits for all the test fuels could potentially be greater.

The largely linear paraffin structure of LTSK has been associated in literature with shorter ignition delays and higher DCN values. Compared to the rest of the test fuel matrix, LTSK recorded the best performance in both evaporation-limited and reaction-limited efficiency boundaries by significant margins. This is of particular interest due to LTSK nominally resembling a fuel that could also be produced via a renewable synthetic jet fuel manufacturing process.

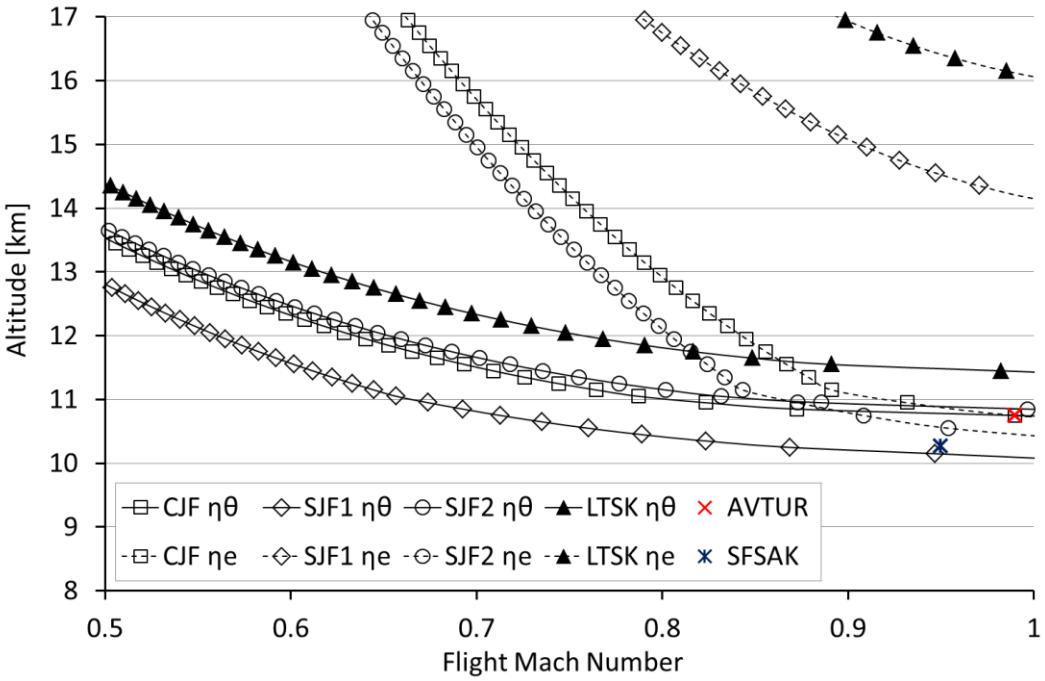

Figure 7.9: Theoretical relative evaporation- and reaction-controlled extinction limits

8 Summary, Conclusions, and Recommendations

This study investigated the influence of alternative jet fuel properties on aviation gas turbine performance at threshold combustor operating conditions. It was motivated by previously unexplored anomalous altitude extinction results that were observed during an industry evaluation of synthetic jet fuel as well as inconsistencies in literature dealing with this subject.

The research methodology was based on the use of a fundamental theoretical treatment to interpret results generated by an experimental design which adopted a novel approach of formulating a test fuel matrix to reflect real-world alternative fuel compositions while still enabling a targeted evaluation of the influences of both physical and chemical reaction properties. A comprehensive characterisation was performed of all the test fuels detailing their physical properties and chemical reaction properties. The extinction and spray behaviours of the fuels were then evaluated in a laboratory scale combustor and the various experimental data sets were interpreted within the context of the theoretical analyses.

The relative performance of alternative jet fuel formulations under laboratory burner conditions was translated to predict relative real world altitude performance. This approach was validated against results from the abovementioned industry evaluation and demonstrated to be very credible. This study enabled the following conclusions to be drawn:

- All three project hypotheses were substantiated.

  Hypothesis 1: While most of the eight test fuel blends conformed to the legislated physical jet fuel specifications, the non-conforming blends were deliberately included for technical reasons. The spectrum of blends successfully achieved significant independent variation in properties relating to evaporation and chemical reaction behaviour.

  Hypothesis 2: The test fuels recorded significant differences in spray formation, evaporation, and blowout extinction which resulted in significant and measurable combustion efficiency and blowout differences. Through the application of an appropriate theoretical model these differences were shown to impact altitude blowout results which were validated by comparison with real altitude test results.

Hypothesis 3: Chemical ignition delays measured in a shock tube were shown to correlate strongly with altitude blowout performance. The chemical ignition delays measured in an IQT™ recorded slightly weaker correlations with LBO performance, but also provided an accurate metric of the relative blowout extinction behaviour of different fuels.

- A critical analysis of the test data provided a technically defensible explanation for the altitude relight results that were observed in the Rolls-Royce test campaign that was conducted during the FSJF certification process. A credible case has been made for the relative extinction limits being ascribed to the relative chemical ignition delays of the fuels.
- The fuel spray evaluation discredited the probability of volatility (distillation profile) and fuel physical properties playing a significant role in the impaired altitude performance that was recorded during the Rolls-Royce tests.
- DCN ignition delays were shown to correlate strongly with the LBO results obtained in a technically relevant gas turbine model-combustor supporting its use as a chemical reaction rate proxy.
- The 1000 K shock tube ignition delays recorded even stronger correlations with the LBO results.
- Laminar flame speed was shown not to correlate with LBO and no support was found for its use as a proxy for reaction rate.
- Evaporation-controlled combustion efficiency was shown to become a significant factor at low air mass flow rates or when the fuel evaporation is degraded.
- Different synthetic jet fuel formulations recorded wide ranging results with low temperature Fischer Tropsch GTL kerosene (LTSK) recording the best performance in both evaporation-limited and reaction-limited efficiency boundaries by significant margins.
- The results of this study support the importance of chemical ignition delays being considered when evaluating the blowout behaviour of alternative jet fuel formulation options.

Based on these conclusions, the following recommendations are made:

- It is recommended that DCN values (based on the IQT™-measured ignition delays) provide a practical and convenient metric for provisionally ranking jet fuel ignition delay and for highlighting potential altitude extinction concerns.

- It is recommended that the development of a higher temperature version of the IQT™ be investigated to provide an even more representative screening tool. This could potentially be implemented more readily than shock tube testing which would be prohibitively complex for wider industry use.
- Future certification processes should afford due consideration to the chemical ignition delay character of a candidate fuel.

Appendix A: Evaporation-controlled System

In a system where the mixing and reaction rates are sufficiently fast for the fuel evaporation to be the rate-controlling step, the fuel is assumed to instantly mix and burn with the surrounding air as soon as it evaporates. Under such conditions the evaluation of evaporation and droplet lifetime is of interest since it determines the residence time required for combustion to occur.

The evaporation of a spherical droplet is accepted to consist of an unsteady state or heat-up period during which the droplet temperature increases with time until the drop attains its wet-bulb temperature. This transient period is followed by relatively steady-state evaporation during which the droplet diameter, D, changes according to the so-called "D^2 law of droplet evaporation" that was first formulated by Godsave [17]. Typical assumptions include: that the droplet is spherical, that the fuel is a pure single boiling point liquid and that radiant heat transfer is negligible. The mathematical expression of the law is provided in equation A.1 where λ represents the evaporation constant, t the time elapsed and D and D_0 the instantaneous and starting droplet diameters respectively [18].

$$D_o^2 - D^2 = \lambda t \qquad \text{[A.1]}$$

Figure A.1 shows this relationship between D^2 and time as generated by Wood et al. for kerosene and JP-4 droplets [19]. The evaporation constant corresponds to the slope of the graph which is very small during the initial heat-up stage while the majority of the heat supplied is used to raise the droplet temperature. As the liquid temperature rises the slope gradually increases with time until a stage is reached where all the heat transferred to the droplet is used as heat of vaporization and the droplet attains a steady-state at the wet-bulb temperature. Beyond this the slope of the curve remains virtually constant for the remainder of the droplet's life. Figure A.1 is based on measurements that were conducted at atmospheric pressure and 2000 K. under which conditions the initial heat-up period only constitutes a small portion of the total evaporation time. This is not necessarily the case for many fuels under high ambient temperature and pressure conditions where the unsteady heat-up period can be significant [18, 72].

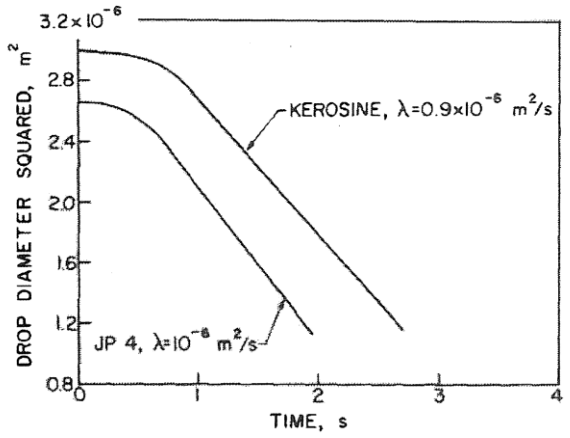

Figure A.1: Evaporation rate curves for kerosene and JP-4 [19]

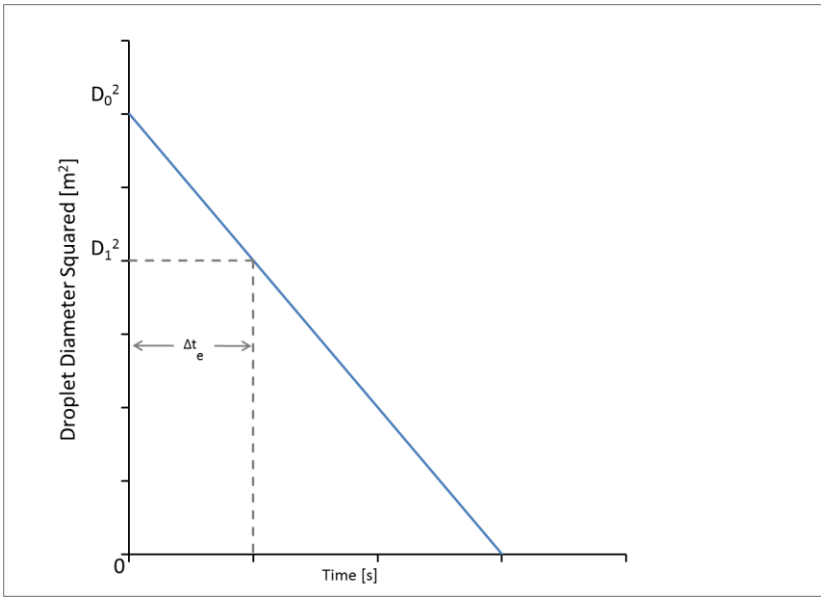

Figure A.2: Drop size vs time ignoring heat-up

From equation A.1 it follows that the evaporation constant, or slope of the curves in Figure A.1, are expressed by

$$\lambda = \frac{d}{dt}(D^2) \qquad [A.2]$$

$$\lambda = 2D\frac{d}{dt}(D) \qquad [A.3]$$

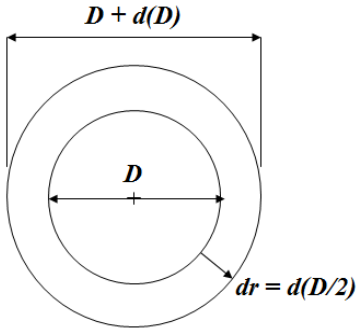

Figure A.3: Droplet shell

The evaporation of a fuel droplet and consumption of fuel during the steady burning of a stationary droplet in an oxidizing atmosphere is assumed to occur at a spherical surface that is established around the droplet. The volume, V, of this droplet shell is given by:

$$V = Surface\ area\ .\ d\left(\frac{D}{2}\right) = \pi D^2\ d(\frac{D}{2}) \quad [A.4]$$

The rate of volume and mass change due to evaporation can therefore be expressed as

$$\frac{dV}{dt} = \dot{V} = \frac{\pi}{2} D^2\ \frac{d}{dt}(D) \quad [A.5]$$

$$\frac{dm}{dt} = \dot{m} = \frac{\pi}{2} \rho_F D^2\ \frac{d}{dt}(D) \quad [A.6]$$

Where ρ_F is the fuel density. By substituting the evaporation constant from A.3 the volume and mass flow rates simplifies to

$$\dot{V} = \frac{\pi}{2} D^2\ \frac{\lambda}{2D} = \frac{\pi}{4} D\lambda \quad [A.7]$$

$$\dot{m} = \frac{\pi}{4} \rho_F D\lambda \quad [A.8]$$

The mass change between the initial droplet diameter ($D = D_0$; $m = m_0$) and droplet extinction ($D = 0$; $m = 0$) can be derived by integration of A.6.

$$dm = \frac{\pi}{2} \rho_F D^2\ d(D) \quad [A.9]$$

$$\int_{m_0}^{0} dm = \int_{D_0}^{0} \frac{\pi}{2} \rho_F D^2\ d(D) \quad [A.10]$$

$$m_0 = \frac{\pi}{2} \rho_F \left[\frac{{D_o}^3}{3}\right] = \frac{\pi}{6} \rho_F D_0^3 \quad [A.11]$$

By assuming λ to be constant, integration of A.2 yields the droplet lifetime, t_e.

$$t_e = {D_0^2}/{\lambda} \quad [A.12]$$

The evaporation constant was defined by Godsave for steady-state evaporation under quiescent conditions. Chin and Lefebvre defined an effective evaporation constant, λ_{eff}, to include the effects of the heat-up period and forced convection [20].

$$t_e = {D_0^2}/{\lambda_{eff}} \quad [A.13]$$

The average rate of droplet evaporation, $\dot{m}_{ave}$, follows from dividing the droplet mass evaporated by the droplet lifetime.

$$\frac{m_0}{t_e} = \frac{\pi}{6} \rho_F \left[\frac{{D_o}^3}{t_e}\right] = \frac{\pi}{6} \rho_F\ D_0 \left[\frac{{D_o}^2}{t_e}\right] \quad [A.14]$$

$$\therefore \dot{m}_{ave} = \frac{\pi}{6} \rho_F\ D_0 \lambda_{eff} \quad [A.15]$$

The average evaporation rate of n fuel drops with mean initial diameter of D_0 contained in a volume of air, can be expressed as

$$\dot{m}_{ave} = \frac{\pi}{6} n \rho_F D_0 \lambda_{eff} \quad [A.16]$$

By assuming that the mass of fuel is equivalent to the droplet mass multiplied by the number of droplets (n x 2.12), the fuel/air ratio, q, in the volume can be expressed as

$$q = {m_F}/{m_A} = {n \frac{\pi}{6} \rho_F D_0^3}/{V \rho_A} \quad [A.17]$$

The number of droplets in the volume can therefore be expressed in terms of the fuel/air ratio, densities and diameter (A.18) and substituted into A.16 to yield the average rate of evaporation of a fuel spray.

$$n = {6qV\rho_A}/{\pi \rho_F D_0^3} \quad [A.18]$$

$$\dot{m}_{ave} = \frac{\pi}{6} \rho_F D_0 \lambda_{eff} \cdot {6qV\rho_A}/{\pi \rho_F D_0^3} = {\rho_A \lambda_{eff} V q}/{D_0^2} \quad [A.19]$$

This expression for the average fuel spray evaporation rate can be employed in determining the combustion efficiency of a system in which the mixing and reaction rates are sufficiently fast for the fuel evaporation to be the rate-controlling step. The fuel is assumed to instantly mix and burn with the surrounding air as it evaporates. The combustion efficiency is therefore governed by the ratio of the rate of fuel evaporation within the combustion zone to the rate of fuel supply.

$$\eta_e = {\dot{m}_{ave}}/{q_{ov} \dot{m}_A} = {\dot{m}_{ave}}/{f_c q_c \dot{m}_A} \quad [A.20]$$

Where f_c is the fraction of the total combustor airflow that takes part in combustion and q_{ov} and q_c are the overall and combustion zone fuel/air ratios respectively. Substituting A.19 into A.20 yields

$$\eta_e = {\rho_A \lambda_{eff} V q}/{D_0^2 f_c q_c \dot{m}_A} = {\rho_A \lambda_{eff} V}/{D_0^2 f_c \dot{m}_A} \quad [A.21]$$

From [A.13] the effective evaporation constant can be expressed in terms of the evaporation time, t_e: $\lambda_{eff} = {D_0^2}/{t_e}$.

$$\eta_e = {\rho_A \lambda_{eff} V}/{D_0^2 f_c \dot{m}_A} = {\rho_A V}/{t_e f_c \dot{m}_A} \quad [A.22]$$

Since $\rho_A V$ is the mass of air in the combustor, ${\rho_A V}/{f_c \dot{m}_A} = \Delta t_r =$ the air residence time in combustor, which means that A.22 agrees with the logical argument that the combustion efficiency amounts to the ratio of residence time of the air in the combustor to the evaporation time for the droplets.

$$\eta_e = {\Delta t_r}/{\Delta t_e} \quad [A.23]$$

Equation A.21 expresses combustion efficiency in terms of the combustor operating conditions (ρ_A , λ_{eff} , $\dot{m}_A$), physical combustor dimensions (V), fuel spray characteristics (D_0) and fuel properties (D_0 , λ_{eff}). The equation, however, allows the evaporation efficiency to assume a value greater than 100%. This occurs when the time required for complete evaporation is less than the available time and the fuel within the primary recirculation zone is thus fully vaporised. Under these conditions the combustion efficiency should be assigned a value of 100%. Lefebvre proposes the use of a modified form similar to A.24 in order to avoid the abrupt discontinuity [21]. The two expressions are compared on the basis of combustion air residence in Figure A.4.

$$\eta_e = 1 - \exp\left({-B\rho_A \lambda_{eff} V}/{D_0^2 f_c \dot{m}_A}\right) \quad [A.24]$$

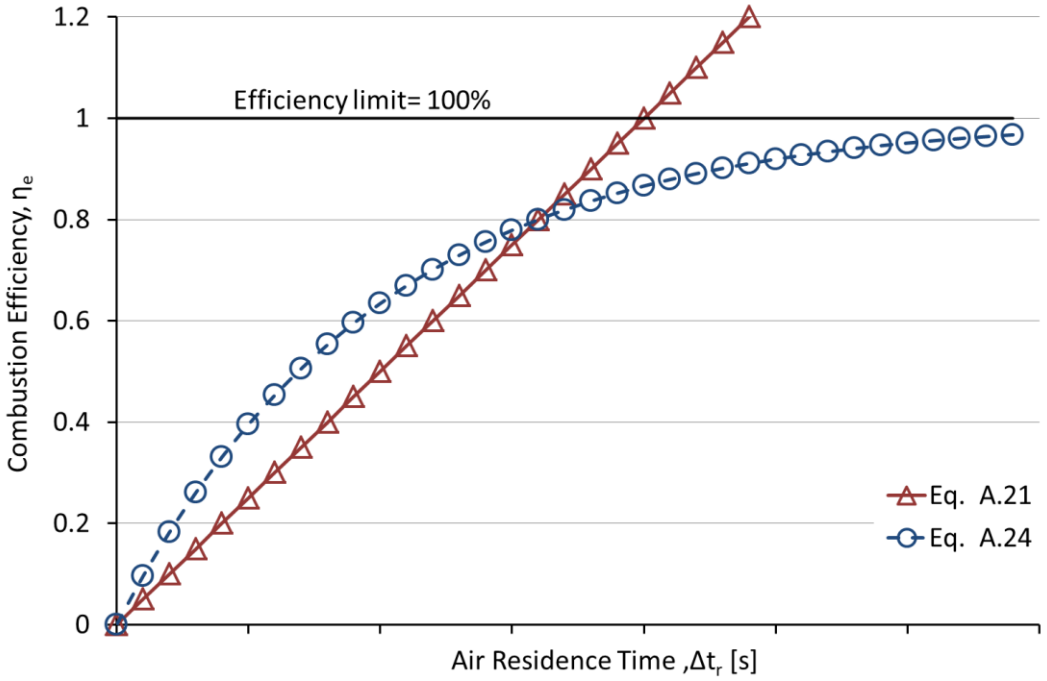

Figure A.4: Comparison of the direct (eq. A.21) and exponential (eq. A.24) expressions for evaporation efficiency

Appendix B: Comprehensive Fuel Property Analysis Results

Property	Units	Limits	CJF	CJF/D	SJF1	SJF2	SJF2+	LTSK	HTSK	HN
Appearance										
Appearance Visual		Report	PASS	PASS	PASS	PASS	PASS	PASS	PASS	PASS
Colour, Saybolt	-	Report	18	24	>+30	>+30	>+30	>+30	>+30	>+30
Particulate Contaminants	mg/l	1.0 max	0.6	0.3	2.1	0.2	<0.1	0.1	0.3	0.5
Particulate										
>= 4 µm (c)		Report	1423.0	1571.9	19605.9	194.3	1105.0	193.3	120.8	472.4
>= 6 µm (c)		Report	496.3	409.2	7636.2	82.3	422.6	62.9	69.9	16.0
>= 14 µm (c)		Report	79.9	30.2	375.6	10.5	61.7	6.5	18.2	4.0
>= 21 µm (c)		Report	29.1	8.5	36.2	2.4	16.5	1.9	6	1.6
>= 25 µm (c)		Report	15.1	3.6	10.3	1	7.4	1.1	2.8	0.9
>= 30 µm (c)		Report	6.5	1.3	3.1	0.4	3.2	0.2	1.1	0.4
Composition										
Total Acidity	mgKOH/g	0.015 max	0.002	0.001	0.002	0.001	<0.001	0.003	0.001	0.001
Total Aromatics	vol %	26.5 max	17.1	8.6	13.0	10.2	9.5	0.0	0.8	6.1
Paraffins	vol %	-	82.0	90.3	84.2	86.7	86.4	99.5	97.7	93.2
Olefins	vol %	-	0.9	1.1	2.8	3.1	4.1	0.5	1.6	0.8
Total Sulphur	mass%	0.30 max	0.12	0.07	<0.01	<0.01	<0.01	<0.01	<0.01	<0.01
Sulphur Mercaptan	mass%	0.0030 max	0.0016	0.0009	<0.0010	0.0010	<0.0010	<0.0010	<0.0010	<0.0010
Antioxidant	mg/l	-	<4	<4	<4	16	<4	4	<4	<4
API Gravity	degAPI	-	46.0	50.6	45.6	41.8	42.4	61.0	54.2	54.6
Combustion										
Specific Energy	MJ/kg	42.80 min	43.32	43.70	43.30	43.29	43.30	44.30	43.97	43.80
Smoke Point	mm	25.0 min	28.0	32.0	29.0	25.0	25.0	28.0	28.0	30.0
DCN ex IQT™		Report	45.9	58.5	32.4	30.9	30.6	62.0	30.6	52.6
JFTOT										
Control temperature	°C	260 min	-	-	-	-	-	-	-	-
Filter Pressure Diff	mmHg	25.0 max	0	0	0	0	0	0	0	0
Tube Deposit Rating		<3	1	<1	<1	<1	<1	<1	<1	<2
Filter Test		-	F	F	F	F	F	F	F	F

Property	Units	Limits	CJF	CJF/D	SJF1	SJF2	SJF2+	LTSK	HTSK	HN
Volatility										
Initial Boiling Point	°C	Report	150.4	162.6	161.6	168.1	160.7	147.3	166.0	160.8
5%	°C		164.3	181.2	163.4	173.4	169.3	154.8	169.9	163.6
10%	°C	205.0 max	170.4	187.6	163.1	176.9	171.0	156.1	171.2	163.7
20%	°C		176.9	193.6	165.9	180.5	178.6	160.1	172.5	164.0
30%	°C		182.3	198.3	168.0	185.2	184.1	162.6	173.9	164.5
40%	°C		188.6	202.0	170.2	190.5	189.7	165.2	175.7	165.1
50%	°C	Report	195.7	205.6	172.7	196.6	196.2	168.8	178.0	165.7
60%	°C		203.5	209.0	176.5	204.3	204.1	172.9	180.8	166.6
70%	°C		212.2	211.7	181.0	214.2	214.2	177.4	184.5	167.7
80%	°C		222.1	215.0	186.6	226.9	227.5	182.3	189.3	169.2
90%	°C	Report	235.1	221.6	195.7	241.5	242.2	188.0	196.4	172.3
95%	°C		245.0	232.2	204.7	249.3	250.8	191.7	202.5	178.0
Final Boiling Point	°C	300.0 max	259.9	250.9	225.2	259.3	258.5	195.2	215.0	204.9
Recovery	vol %		97.6	98.0	95.8	98.1	98.3	98.1	98.1	98.0
Residue	vol %	1.5 max	1.0	1.0	1	1.0	1.0	0.9	0.9	0.8
Loss	vol %	1.5 max	1.0	1.0	0.8	0.9	0.7	0.9	0.9	1.2
T50-T10	°C	> 15	25.3	18.0	9.6	19.7	25.2	12.7	6.8	2.0
T90-T10	°C	> 40	64.7	34.0	32.6	64.6	71.2	31.9	25.2	8.6
Flash pt. @ 101,3 kPa	°C	38.0 - 50.0	42.5	47.0	42.5	53.5	38.0	38	46.5	47.0
Density at 15 °C	g/mL	0.7750 - 0.8400	0.7961	0.7755	0.7979	0.8152	0.8128	0.7334	0.7604	0.7587
Density at 20 °C	g/mL	0.7710 - 0.8360	0.7931	0.7725	0.7949	0.8122	0.8098	0.7304	0.7574	0.7557
Fluidity										
Freezing Point	°C	-47.0 max	-50.4	-19.9	-71.2	-57.0	-57.3	-50.7	<-56.8	-45.3
Viscosity @ -20 °C	mm2/s	8.0 max	3.99	4.30	3.12	5.23	5.51	2.58	3.68	2.48
Viscosity @ 40 °C	cSt	-	1.20	1.29	1.05	1.46	1.42	0.91	1.16	0.91

Property	Units	Limits	CJF	CJF/D	SJF1	SJF2	SJF2+	LTSK	HTSK	HN
Contaminants										
Existent gum	mg/100 ml	7 max	2.4	0.6	0.8	0.9	0.1	1.2	1.0	0.8
Water content	mg/kg	80 max	43	37	21	33	20	39	23	12
Free water		-	<30	<30	<30	<30	<30	<30	<30	<30
Fuel with Static Dissipator Additive		70 min	76	84	-	-	-	-	-	-
Fuel without Static Dissipator Additive		85 min	-	-	89	98	99	98	94	98
Conductivity										
Electrical Conductivity	pS/m	50 - 450	97	40	33	1	1	1	14	1
Lubricity										
BOCLE, WSD	mm	0.85 max	0.68	0.71	0.80	0.71	0.72	0.69	0.70	0.83
Corrosion										
Copper Corrosion		1 max	1A	1A	1A	1A	1B	1A	1A	1B
Surface Tension										
S. Tension @ 25°C	mN/m		25.68	25.61	24.06	25.97	25.94	23.45	23.85	24.25
S. Tension @ 40°C	mN/m		24.3	24.1	22.8	24.69	24.47	22.07	22.16	22.78

Appendix C: Shock Tube Ignition Delay Results

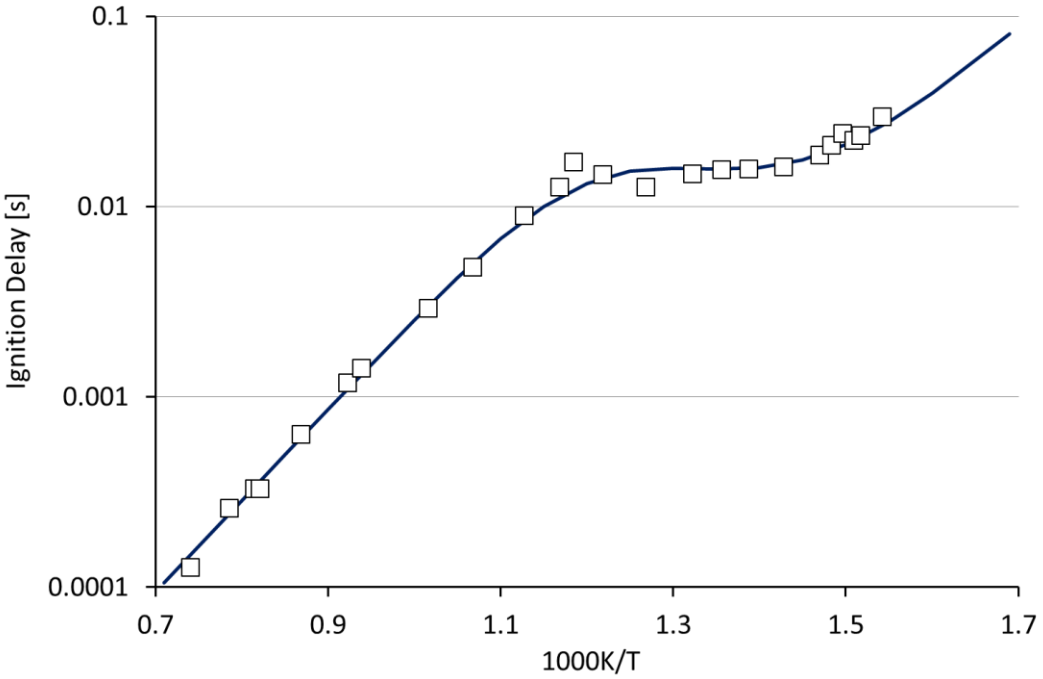

Figure C.1: Test fuel CJF: Shock tube measured (markers) and modelled (curve) ignition delay results based on eq. 6.3.

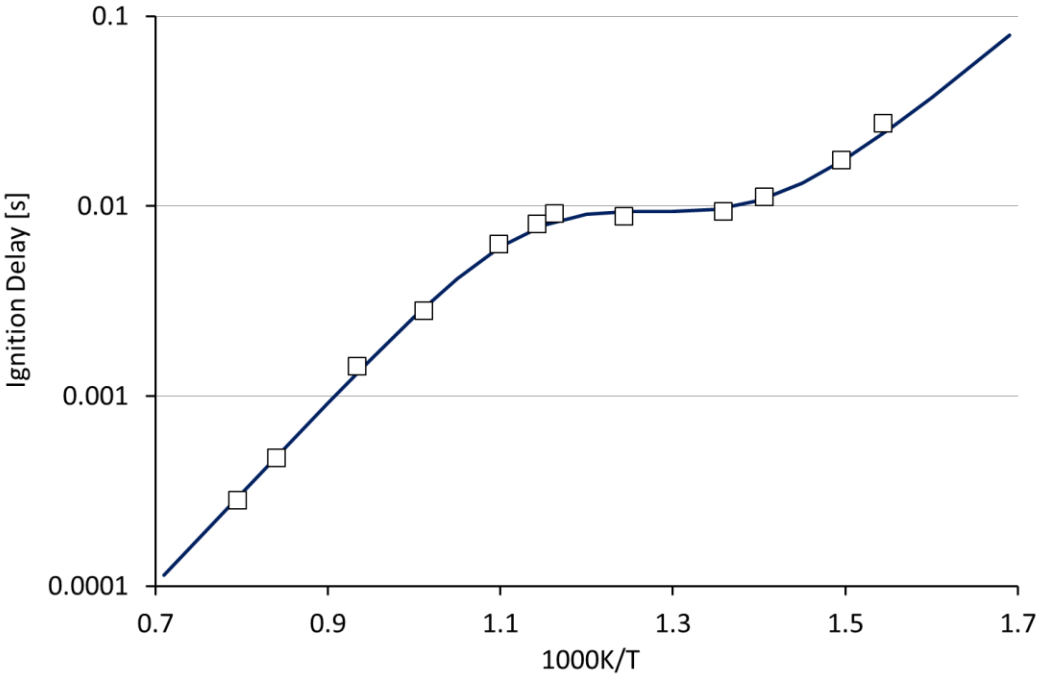

Figure C.2: Test fuel CJF/D: Shock tube measured (markers) and modelled (curve) ignition delay results based on eq. 6.3.

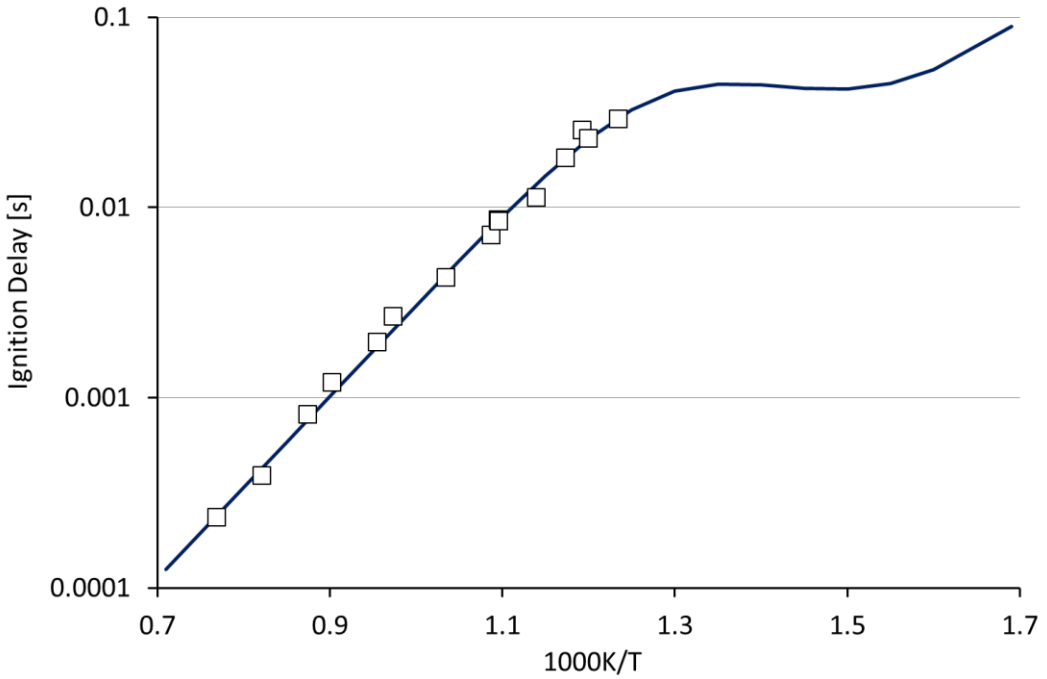

Figure C.3: Test fuel SJF1: Shock tube measured (markers) and modelled (curve) ignition delay results based on eq. 6.3.

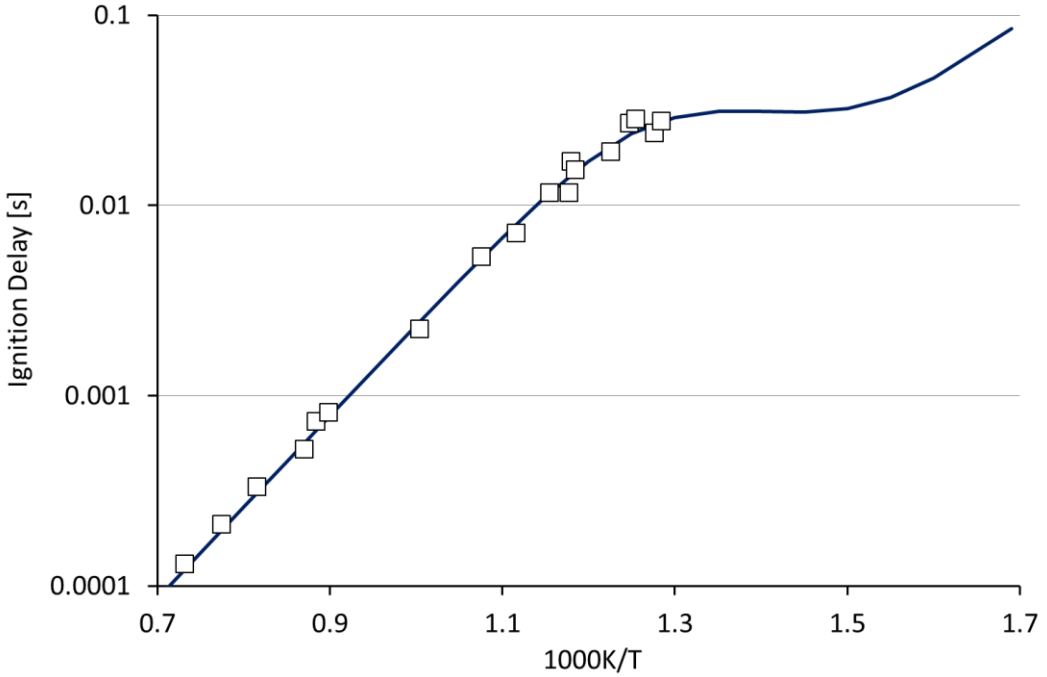

Figure C.4: Test fuel SJF2: Shock tube measured (markers) and modelled (curve) ignition delay results based on eq. 6.3.

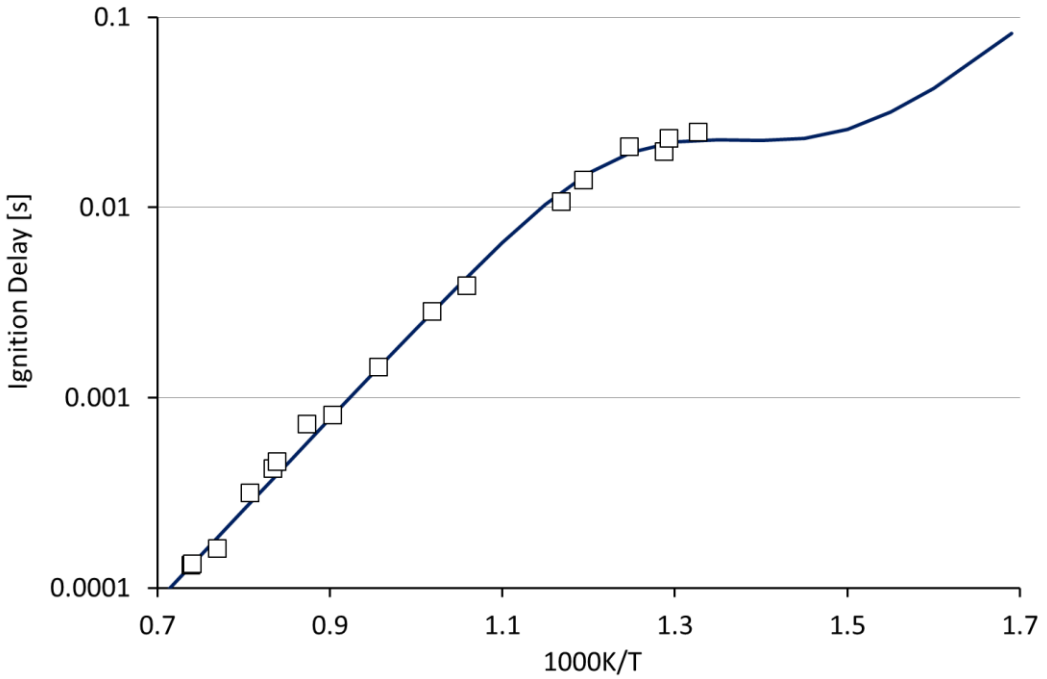

Figure C.5: Test fuel SJF2+: Shock tube measured (markers) and modelled (curve) ignition delay results based on eq. 6.3.

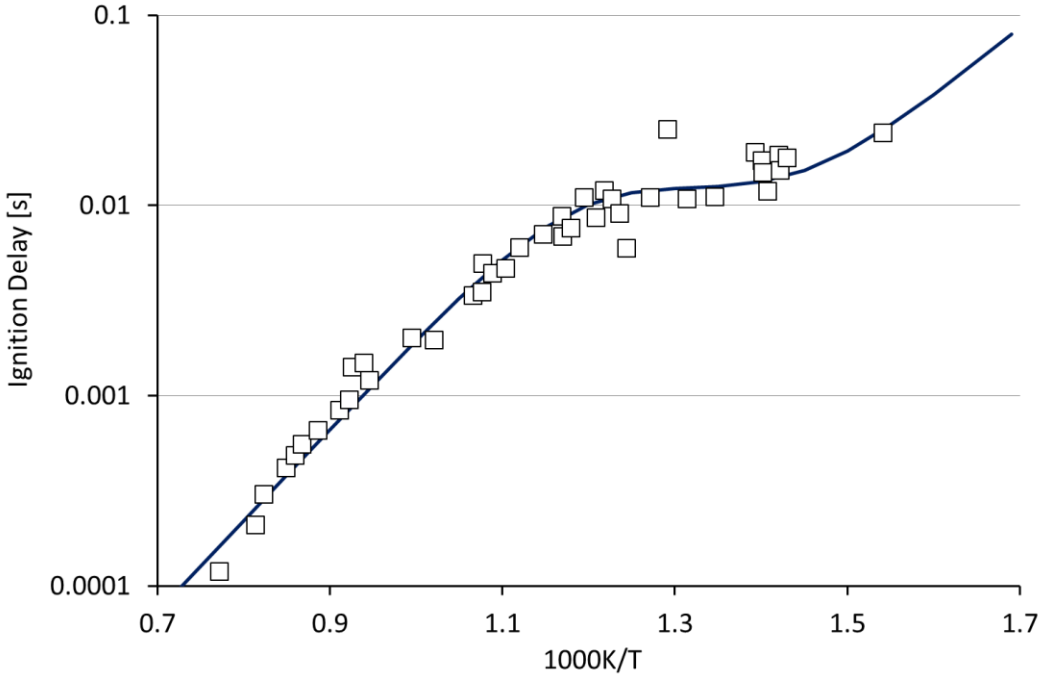

Figure C.6: Test fuel LTSK: Shock tube measured (markers) and modelled (curve) ignition delay results based on eq. 6.3.

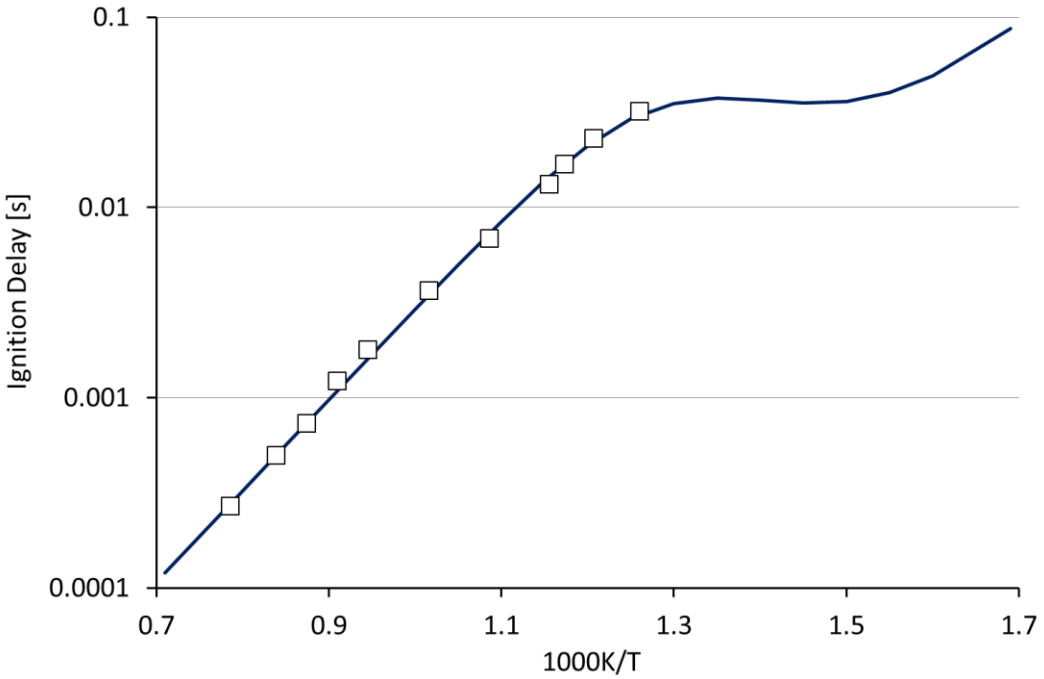

Figure C.7: Test fuel HTSK: Shock tube measured (markers) and modelled (curve) ignition delay results based on eq. 6.3.

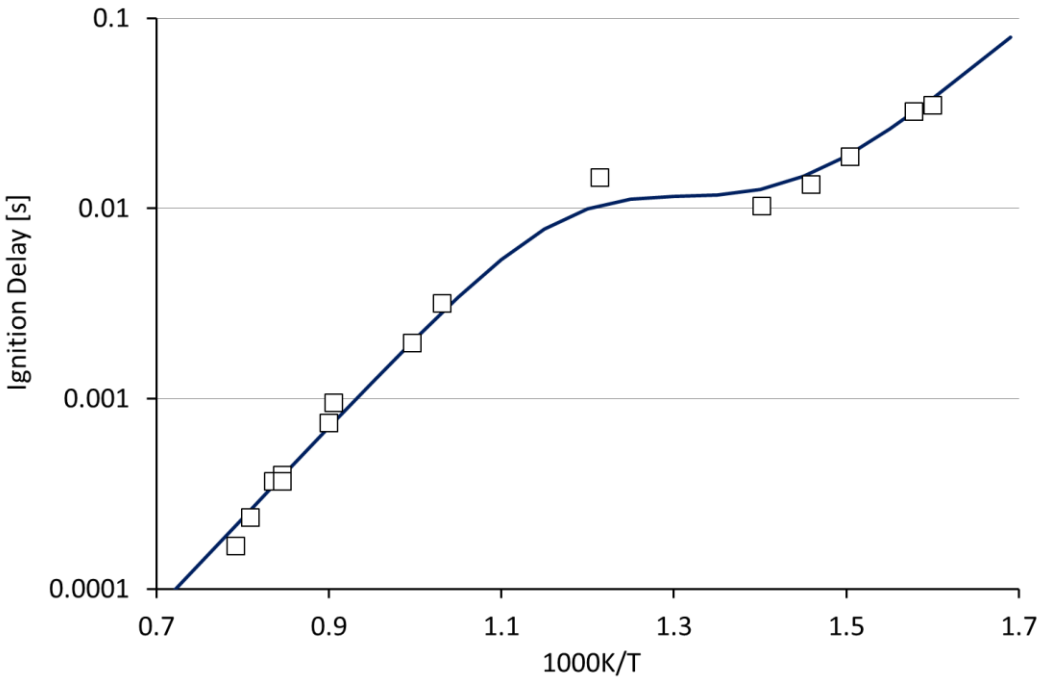

Figure C.8: Test fuel HN: Shock tube measured (markers) and modelled (curve) ignition delay results based on eq. 6.3.

Table C.1: Arrhenius function coefficients for modelled ignition delay

Fuel	$Ln(A_1)$	B_1	$Ln(A_2)$	B_2	$Ln(A_3)$	B_3
CJF	-17.262	8714	2.22	-4808.1	-12.15	11051
CJF/D	-17.262	8714	1.42	-4808.1	-12.07	11051
SJF1	-17.262	8714	3.68	-4808.1	-11.98	11051
SJF2	-17.262	8714	3.25	-4808.1	-12.24	11051
SJF2+	-17.262	8714	2.78	-4808.1	-12.25	11051
LTSK	-17.262	8714	1.92	-4808.1	-12.41	11051
HTSK	-17.262	8714	3.43	-4808.1	-12.02	11051
HN	-17.262	8714	1.81	-4808.1	-12.34	11051

Appendix D: PDA Spray Measurement Results

A selection of results from the PDA spray measurement that were conducted in the laboratory-scale model-combustor are summarised here as figures D.1 to D.12. Each figure represents a set combustion condition at a set stoichiometry, air mass flow rate and axial distance from the exit plane (z-axis). Measurements for each combustion condition were performed at radial (y-axis) increments of 2 mm. All tests were conducted under stable combustion conditions and at an air pre-heat temperature of 323 K. Two stoichiometric air-fuel ratios were evaluated: one at the LBO stoichiometry plus 5% and another at a stoichiometry of ϕ = 0.6. This allowed both investigation of the spray behaviour as close to blowout as practical, as well as a comparison between all fuels at exactly the same stoichiometric air-fuel ratio. Sauter mean diameter, D_{32}, (SMD) values are reported to capture the diameter distribution for each fuel, combustion condition, and measurement position as a single representative number.

Table D.1 reports the relative SMD values for each air mass flow condition and for both stoichiometric conditions. Radial measurements were averaged for each axial measurement positions and overall for all axial positions. The lower air mass flow rate condition did not yield sufficient data at the z = 35 mm position for calculating relative SMD numbers.

Table D.1: PDA spray measurements: Relative SMD values averaged per axial measurement position

ϕ	z	Air mass flow [g/s]	Test Fuel							
			CJF	CJF/D	SJF1	SJF2	SJF2+	LTSK	HTSK	HN
ϕ_{LBO} + 5%	15	2.2	1	0.990	1.042	1.016	0.969	0.998	0.949	1.008
ϕ_{LBO} + 5%	25	2.2	1	0.993	1.031	1.004	0.963	1.014	1.006	1.009
ϕ_{LBO} + 5%	Ave	2.2	1	0.991	1.036	1.010	0.966	1.006	0.978	1.009
ϕ_{LBO} + 5%	15	6.5	1	0.987	0.910	1.005	0.971	0.924	0.880	0.929
ϕ_{LBO} + 5%	25	6.5	1	0.996	0.883	1.022	0.980	0.915	0.880	0.912
ϕ_{LBO} + 5%	35	6.5	1	0.983	0.864	1.021	0.992	0.897	0.866	0.899
ϕ_{LBO} + 5%	Ave	6.5	1	0.989	0.886	1.016	0.981	0.912	0.875	0.913
0.6	15	2.2	1	0.959	1.006	1.003	0.943	0.973	0.936	0.993
0.6	25	2.2	1	1.001	1.041	1.015	0.975	1.038	1.021	1.024
0.6	Ave	2.2	1	0.980	1.024	1.009	0.959	1.005	0.978	1.008
0.6	15	6.5	1	0.996	0.915	0.997	0.959	0.910	0.885	0.920
0.6	25	6.5	1	0.998	0.885	1.017	0.986	0.911	0.866	0.889
0.6	35	6.5	1	0.995	0.869	1.023	1.000	0.893	0.856	0.903
0.6	Ave	6.5	1	0.996	0.890	1.012	0.982	0.905	0.869	0.904

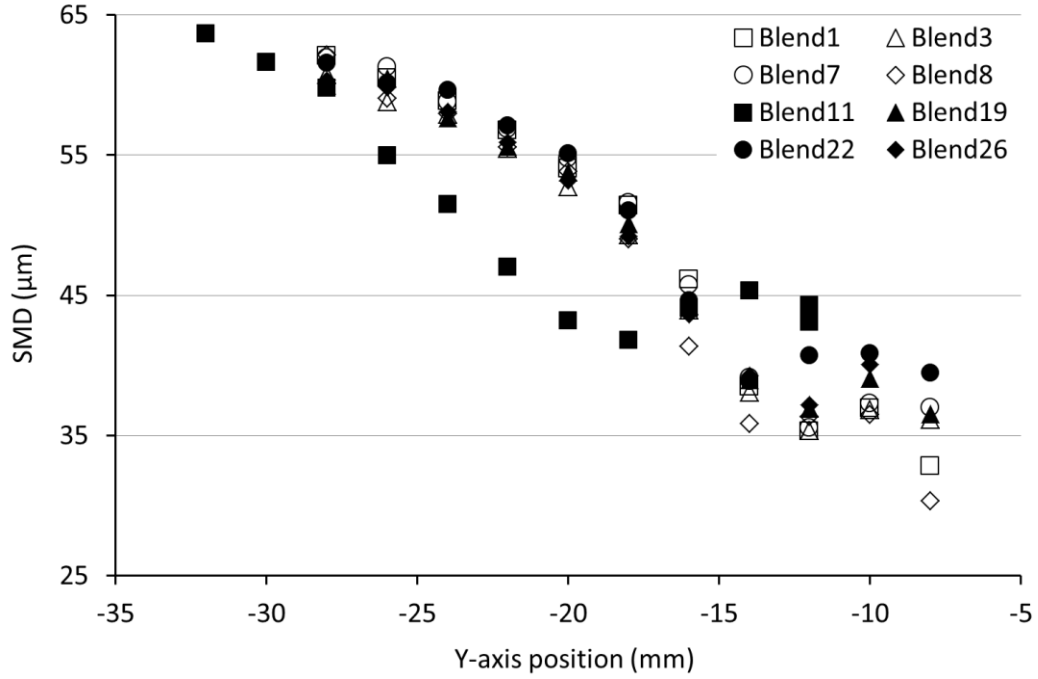

Figure D.1: Radial SMD profiles (ϕ = ϕ_{LBO}+5%, $\dot{m}_A$ = 2.2 g/s, z = 15 mm from exit plane)

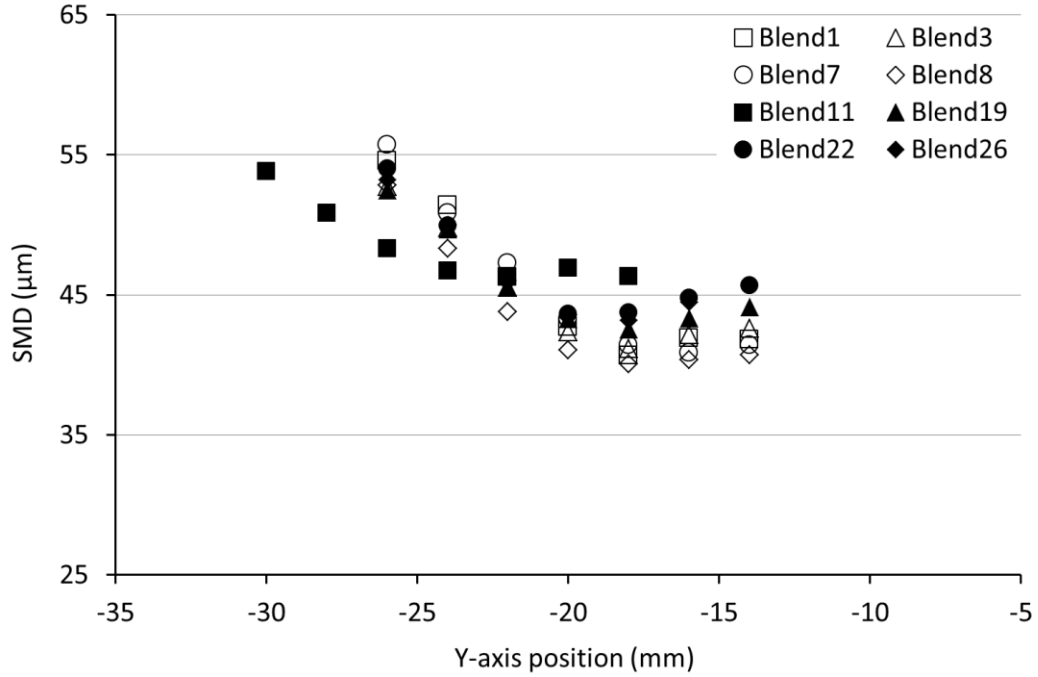

Figure D.2: Radial SMD profiles (ϕ = ϕ_{LBO}+5%, $\dot{m}_A$ = 2.2 g/s, z = 25 mm from exit plane)

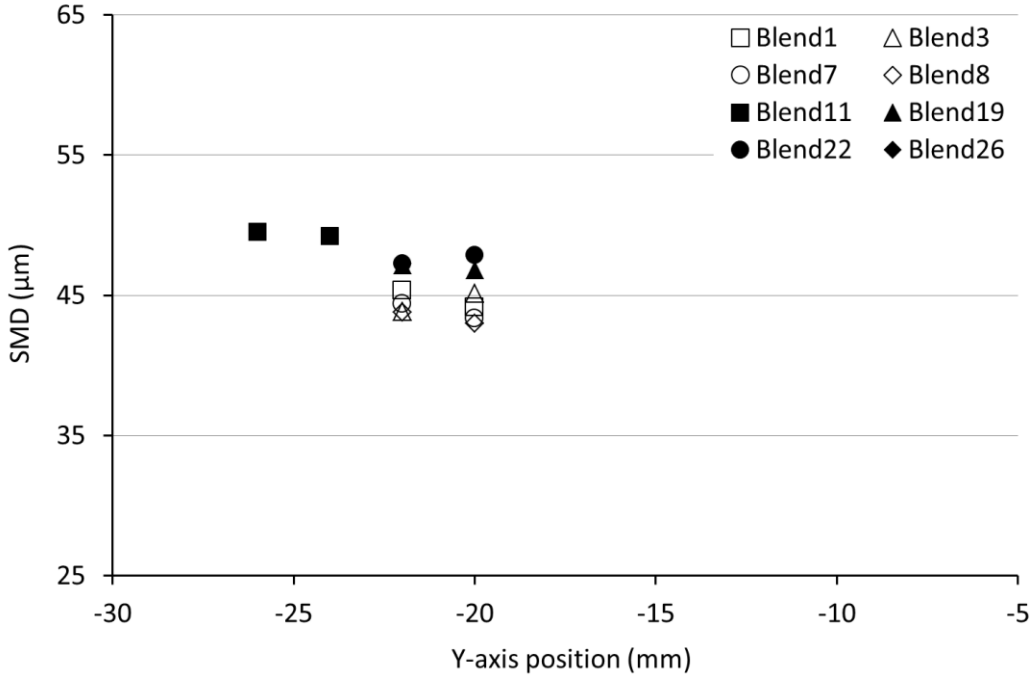

Figure D.3: Radial SMD profiles (ϕ = ϕ_{LBO}+5%, $\dot{m}_A$ = 2.2 g/s, z = 35 mm from exit plane)

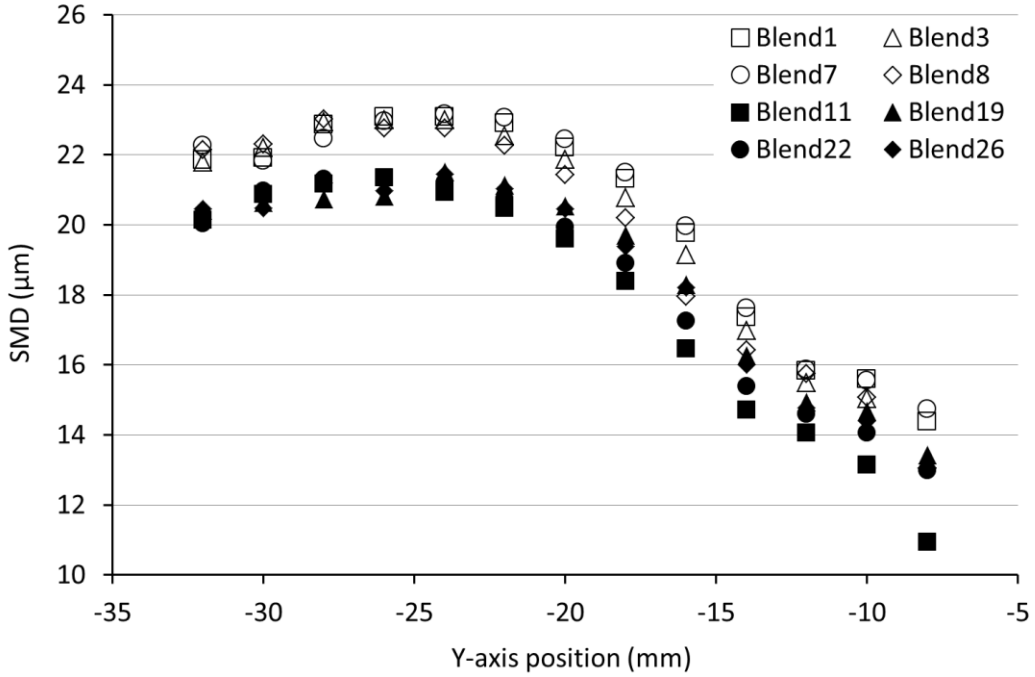

Figure D.4: Radial SMD profiles (ϕ = ϕ_{LBO}+5%, $\dot{m}_A$ = 6.5 g/s, z = 15 mm from exit plane)

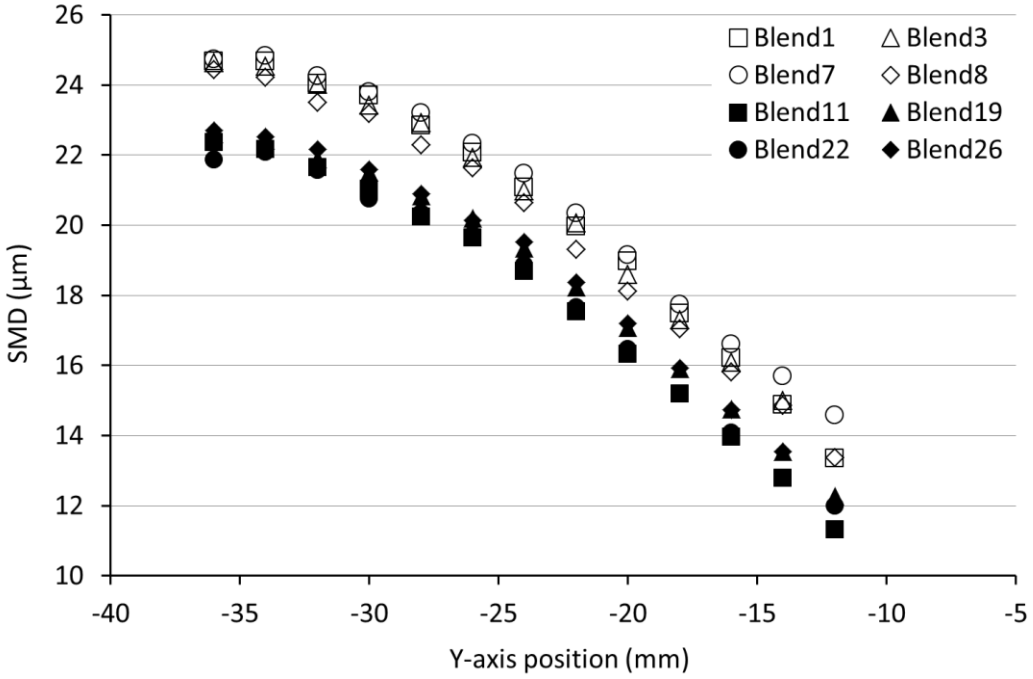

Figure D.5: Radial SMD profiles (ϕ = ϕ_{LBO}+5%, $\dot{m}_A$ = 6.5 g/s, z = 25 mm from exit plane)

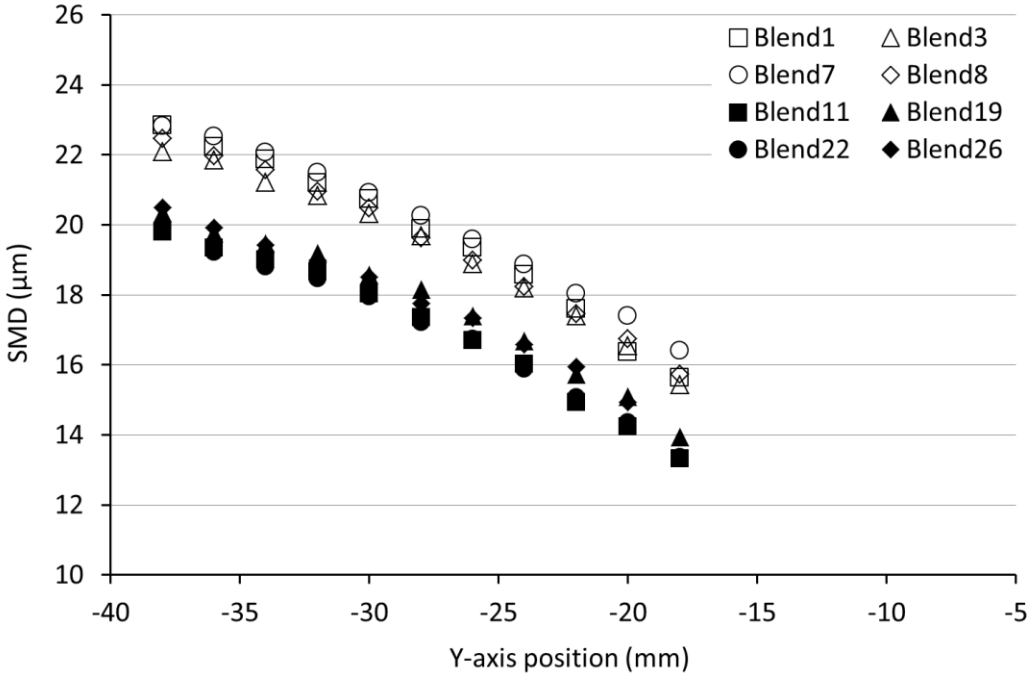

Figure D.6: Radial SMD profiles (ϕ = ϕ_{LBO}+5%, $\dot{m}_A$ = 6.5 g/s, z = 35 mm from exit plane)

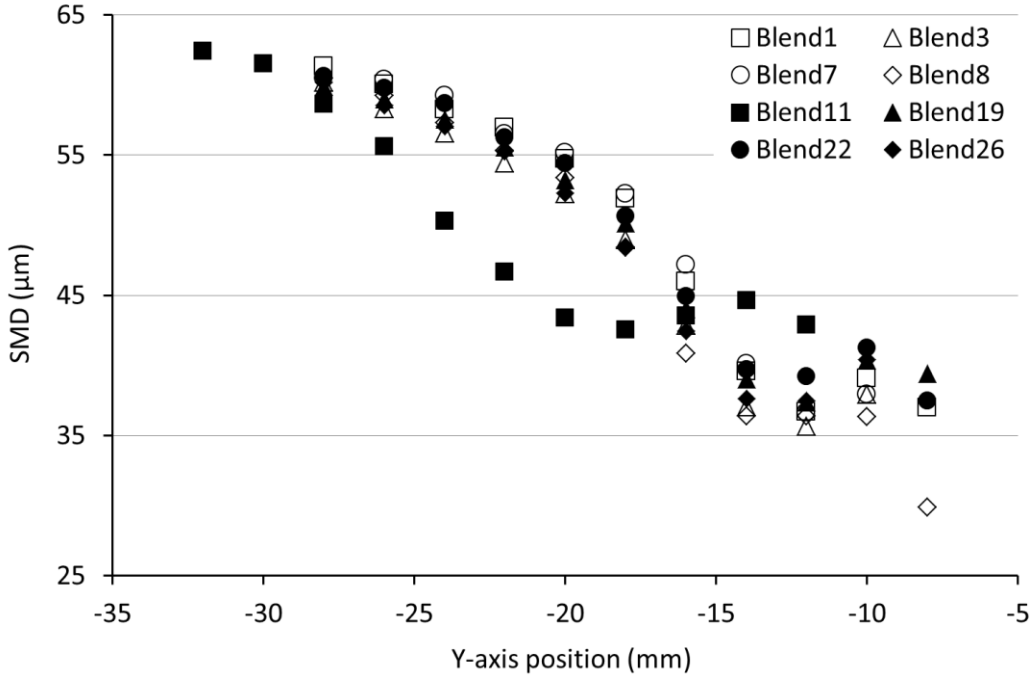

Figure D.7: Radial SMD profiles (ϕ = 0.6, $\dot{m}_A$ = 2.2 g/s, z = 15 mm from exit plane)

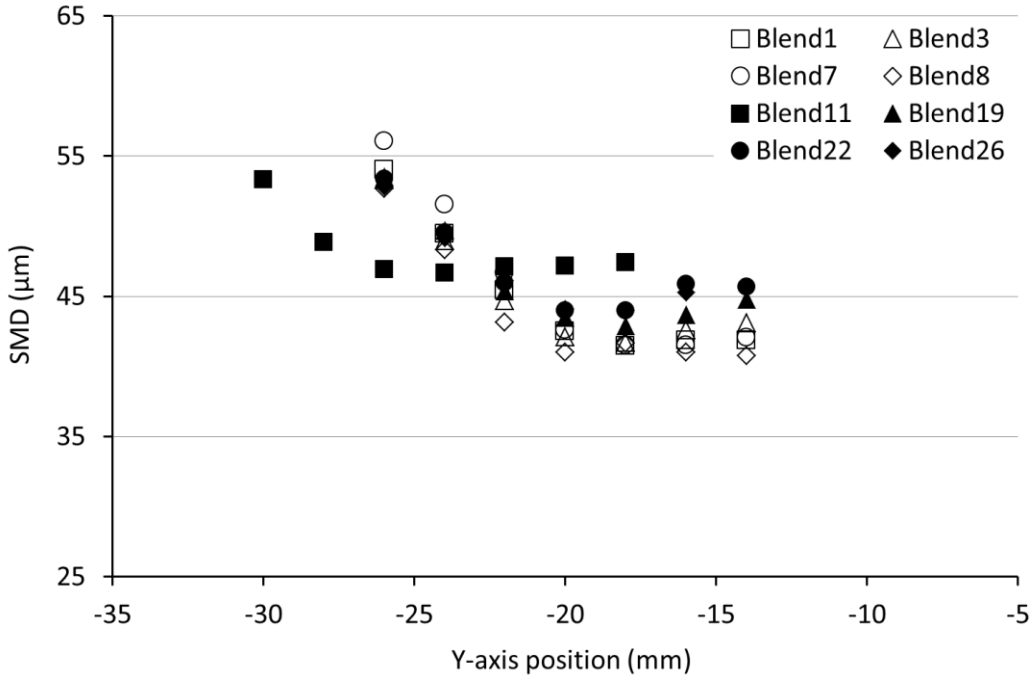

Figure D.8: Radial SMD profiles (ϕ = 0.6, $\dot{m}_A$ = 2.2 g/s, z = 25 mm from exit plane)

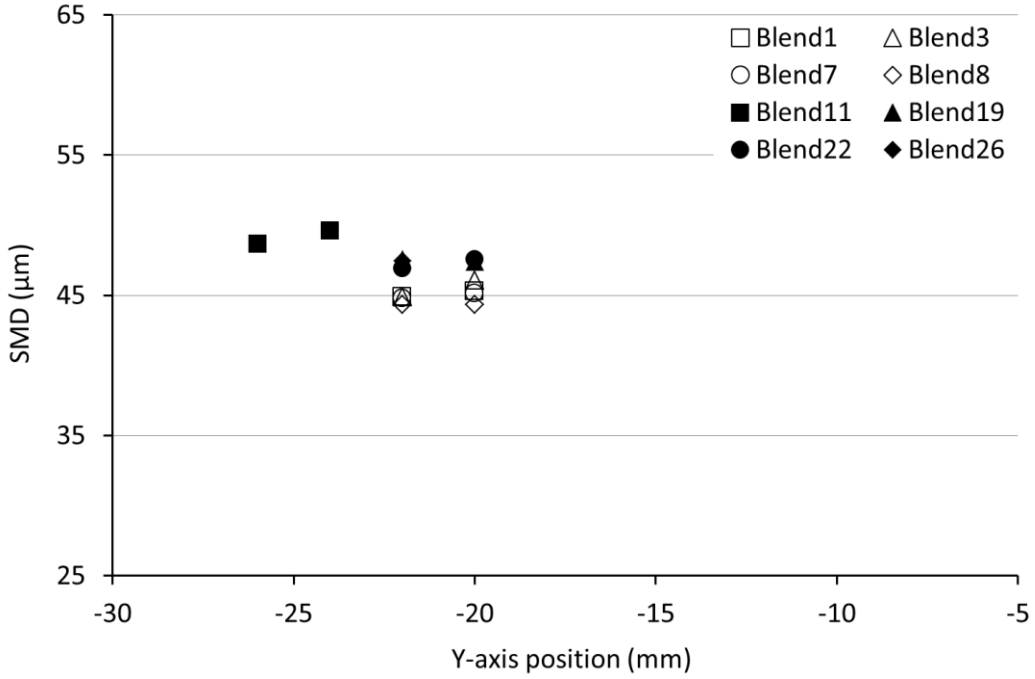

Figure D.9: Radial SMD profiles (ϕ = 0.6, $\dot{m}_A$ = 2.2 g/s, z = 35 mm from exit plane)

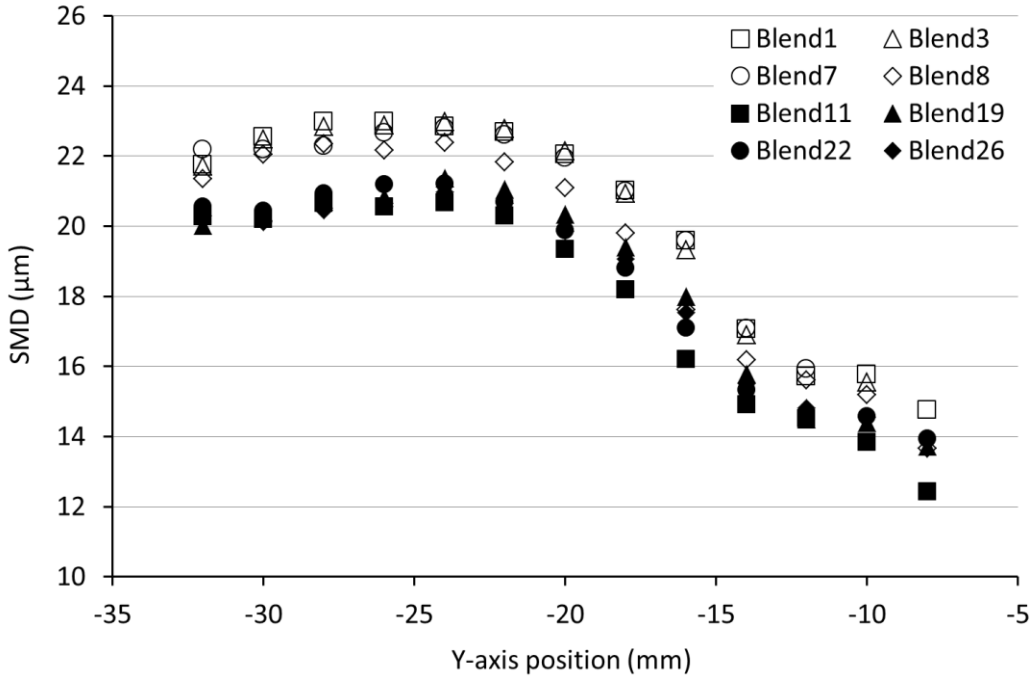

Figure D.10:Radial SMD profiles (ϕ = 0.6, $\dot{m}_A$ = 6.5 g/s, z = 15 mm from exit plane)

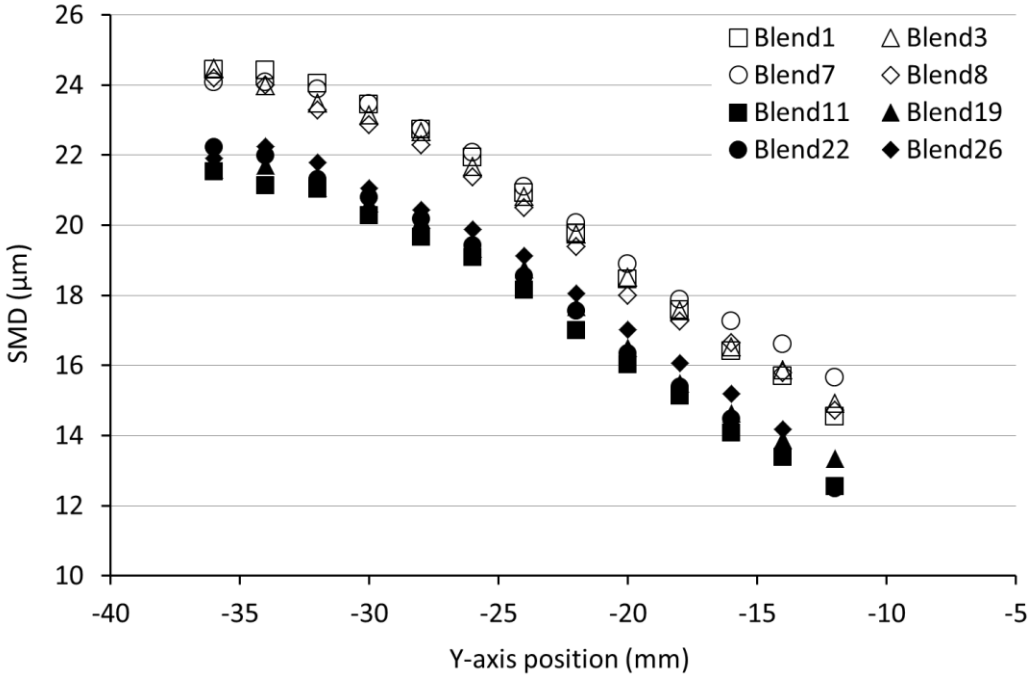

Figure D.11:Radial SMD profiles (ϕ = 0.6, $\dot{m}_A$ = 6.5 g/s, z = 25 mm from exit plane)

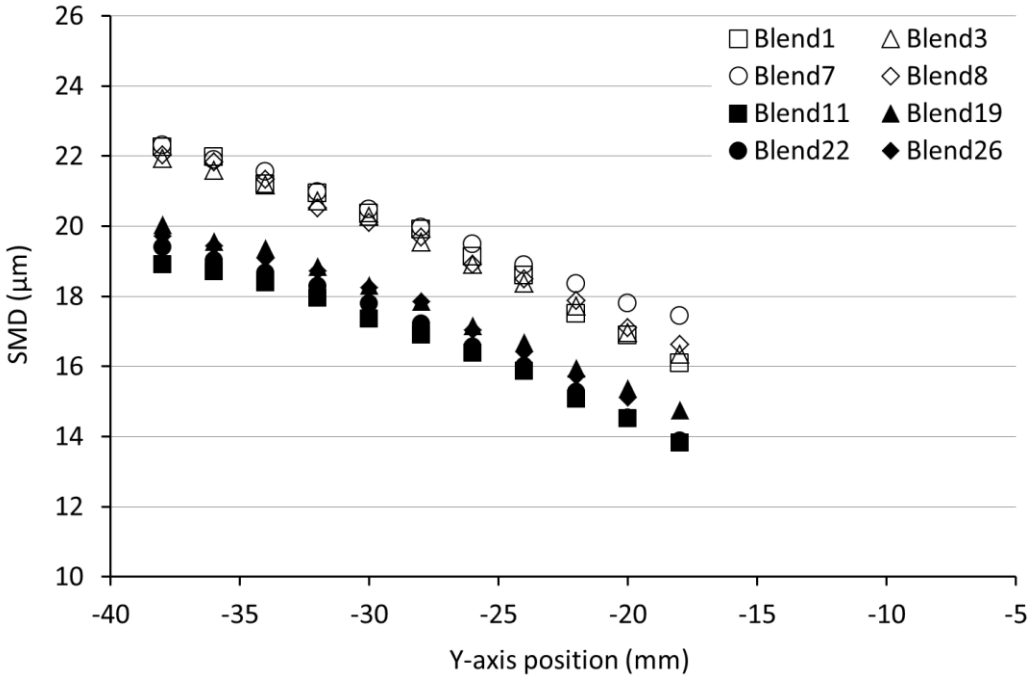

Figure D.12:Radial SMD profiles (ϕ = 0.6, $\dot{m}_A$ = 6.5 g/s, z = 35 mm from exit plane)

Appendix E: Modelled LBO Air Flow Proportionality Constants

Table E1: Normalised LBO proportionality constants and modified LBO proportionality constants

	CJF	CJF/D	SJF1	SJF2	SJF2+	LTSK	HTSK	HN
K (A , 323 K)	1.00	1.04	0.88	1.00	0.99	1.08	0.91	0.97
K (B , 323 K)	1.00	1.12	0.93	1.04	1.02	1.09	0.95	1.05
K (A , 413 K)	1.00	0.99	0.93	1.02	0.98	1.12	0.95	1.02
K_{Ave}	1.00	1.05	0.91	1.02	1.00	1.10	0.94	1.01
K_{θ} (A , 323 K)	1.00	1.06	0.81	1.04	0.94	0.93	0.83	0.85
K_{θ} (B , 323 K)	1.00	1.09	0.88	1.01	0.99	1.02	0.89	0.96
K_{θ} (A , 413 K)	1.00	0.99	0.93	1.02	1.00	1.12	0.93	1.02
$K_{\theta Ave}$	1.00	1.05	0.87	1.02	0.98	1.02	0.88	0.94

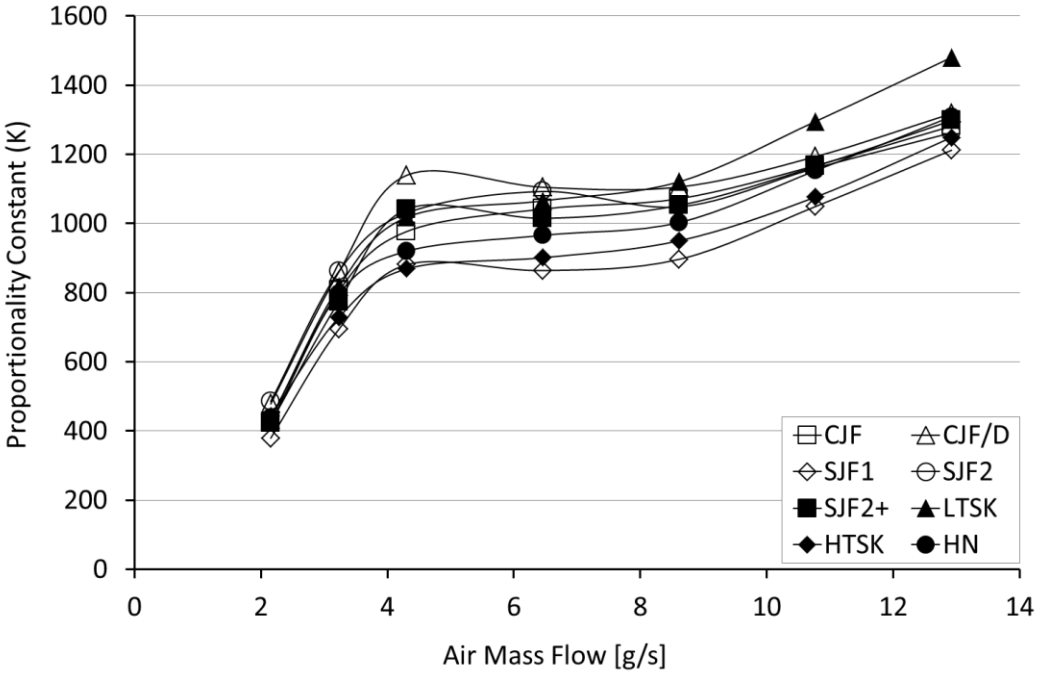

Figure E1: Proportionality constants for modelled combustor airflow based on LBO test data - burner configuration A, 323 K air pre-heat

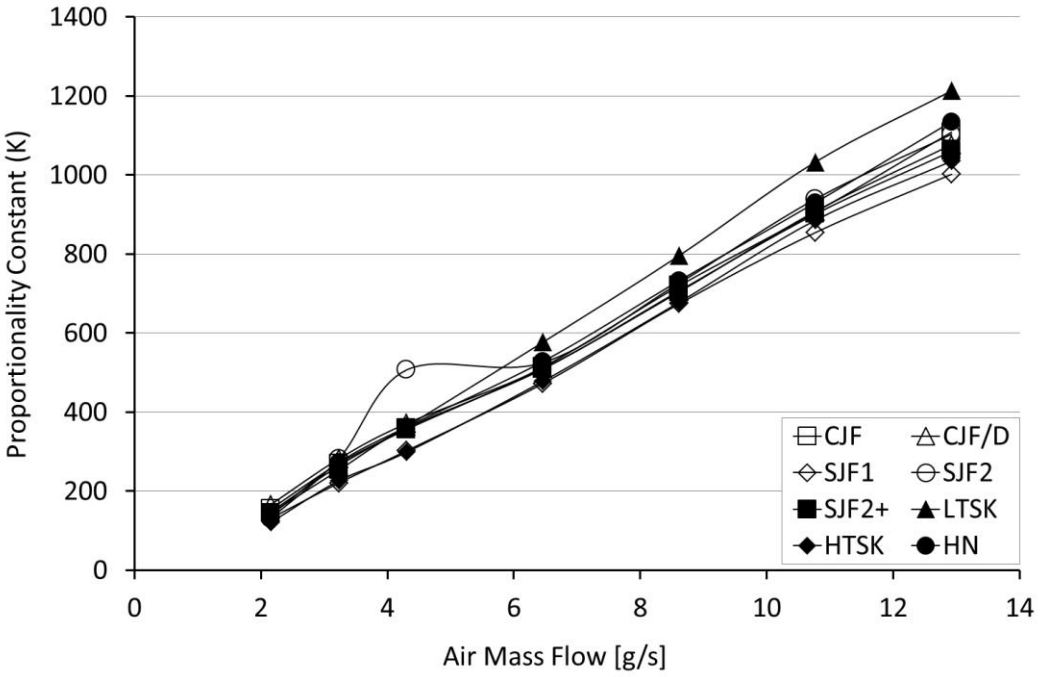

Figure E2: Proportionality constants for modelled combustor airflow based on LBO test data - burner configuration A, 413 K air pre-heat

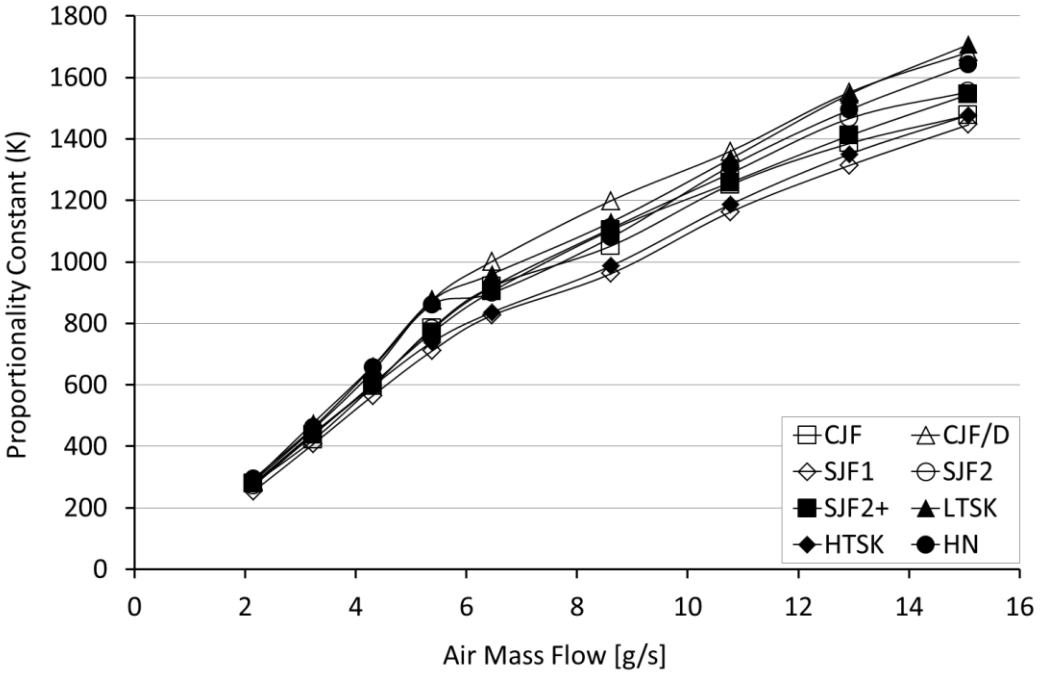

Figure E3: Proportionality constants for modelled combustor airflow based on LBO test data - burner configuration B, 323 K air pre-heat

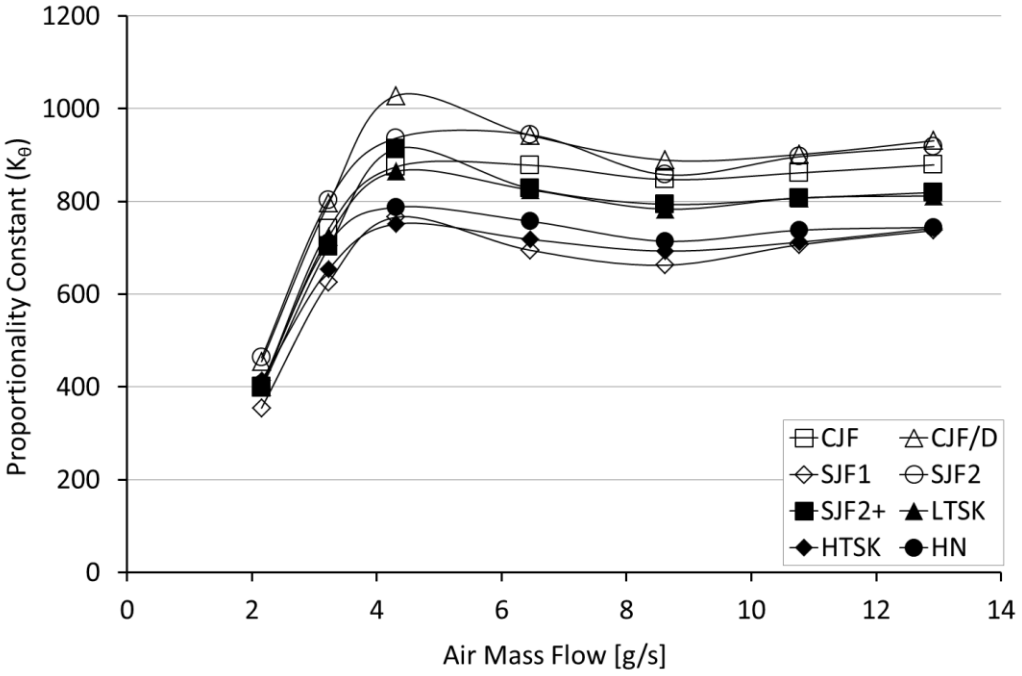

Figure E4: Modified proportionality constants (K_θ) for modelled combustor airflow based on LBO test data - burner configuration A, 323 K air pre-heat

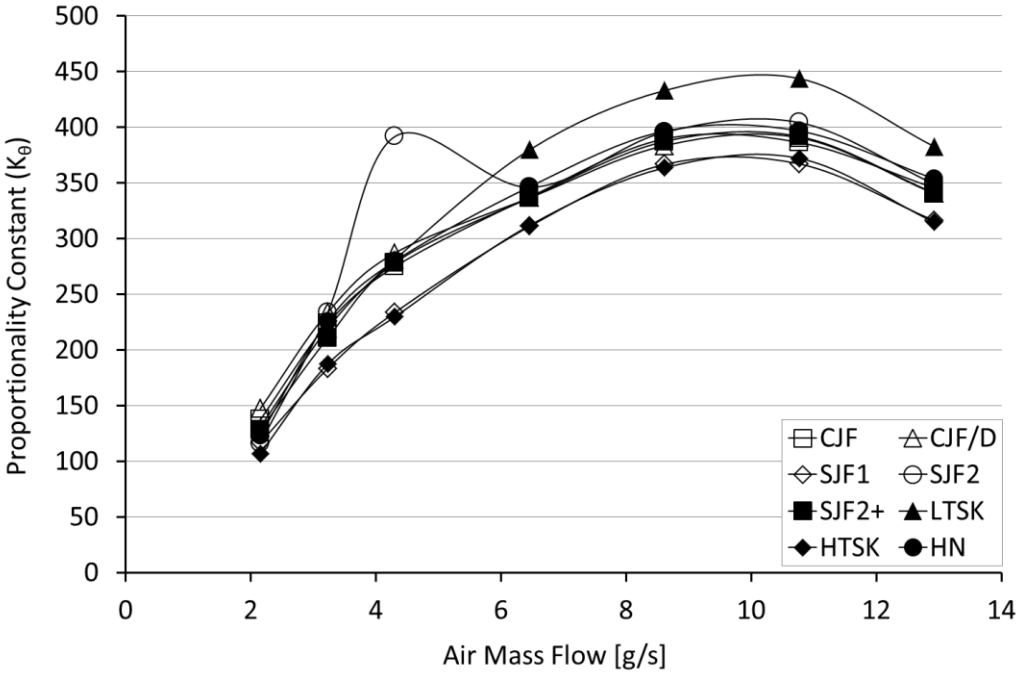

Figure E5: Modified proportionality constants (K_θ) for modelled combustor airflow based on LBO test data - burner configuration A, 413 K air pre-heat

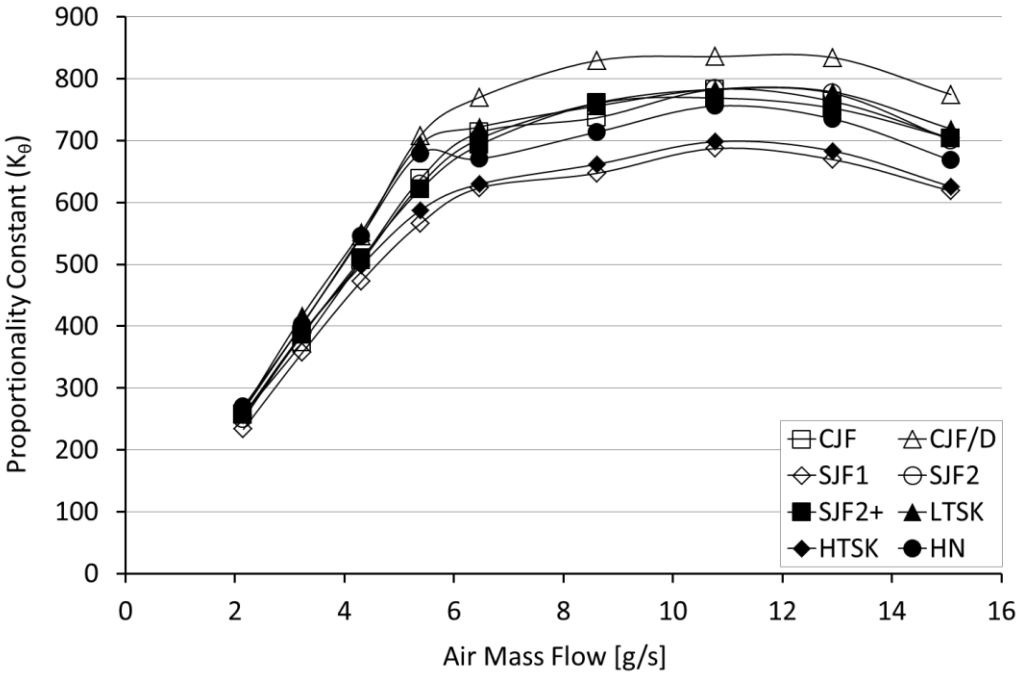

Figure E6: Modified proportionality constants (K_θ) for modelled combustor airflow based on LBO test data - burner configuration B, 323 K air pre-heat

References

[1] T. Edwards, "*Advancements in gas turbine fuels from 1943 to 2005*", Transactions of the ASME, Journal of Engineering for Gas Turbines and Power, vol. 129, pp. 13-20, January 2007.

[2] A. H. Lefebvre, "*Fuel effects on gas turbine combustion*," Combustion Laboratory, School of Mechanical Engineering, Purdue University, Indiana, USA, AFWAL-TR-83-2004, January 1983.

[3] United Kingdom. Ministry of Defence, Defence Standard 91-91, Turbine Fuel, Aviation Kerosene Type Jet A-1, NATO Code: F-35, Joint Service Designation: AVTUR, Issue 9, 3 October 2016.

[4] A. H. Lefebvre, *Gas Turbine Combustion, 2nd ed*. New York: Taylor and Francis, 1999, pp. 50-57.

[5] A. H. Lefebvre, *Gas Turbine Combustion, 2nd ed*. New York: Taylor and Francis, 1999, p. 35.

[6] C.A. Moses, and P.N. Roets, "Properties, Characteristics and Combustion Performance of SASOL Fully Synthetic Jet Fuel," in *Journal of Engineering for Gas Turbines and Power, 131(4)*, 2009.

[7] V. Burger, A. Yates, and C. Viljoen, "Influence of Fuel Physical Properties and Reaction Rate on Threshold Heterogeneous Gas Turbine Combustion," GT2012-68153, in *Proceedings of ASME Turbo Expo 2012*, Copenhagen, Denmark, 2012.

[8] D. Fyffe, J. Moran, K. Kannaiyan, R. Sadr, and A. Al-Sharshani, "Effect of GTL-like jet fuel composition on GT engine altitude ignition performance – Part I: Combustor operability," GT2011-45487, in *Proceedings of ASME Turbo Expo 2011*, Vancouver, Canada, 2011.

[9] V. Burger, A. Yates, T. Mosbach, and B. Gunasekaran, "Fuel influence on targeted gas turbine combustion properties Part II: Detailed results," GT2014-25105, in *Proceedings of ASME Turbo Expo 2014,* Düsseldorf, Germany, 2014.

[10] N. Rock, I. Chterev, T. Smith, H. Ek, B. Emerson, D. Noble, J Seitzman, and T. Lieuwen, "Reacting pressurized spray combustor dynamics, Part 1. Fuel sensitivities and blowoff characterization," GT2016-56346, in *Proceedings of ASME Turbo Expo 2016*, Seoul, South Korea, 2016.

[11] J. Grohmann, B. Rauch, T. Kathrotia, W. Meier, and M. Aigner, "Investigation of differences in lean blowout of liquid single-component fuels in a gas turbine model combustor," in *Proceedings of 52nd AIAA/SAE/ASEE Joint Propulsion Conference*, Salt Lake City, USA, 2016.

[12] C.A. Moses and G. Wilson, "Evaluation of Sasol synthetic kerosene for suitability as jet fuel," Southwest Research Institute, San Antonio, USA, Report 08-04438, 2003.

[13] C.A. Moses, "Evaluation of Sasol synthetic kerosene for suitability as jet fuel Phase II: Engine and combustor tests," Southwest Research Institute, San Antonio, USA, Report 08-04438-2, 2007.

[14] F. Hermann, "Cold day ignition and altitude relight testing of Sasol fully synthetic aviation kerosene-External report," Rolls-Royce, Derby, UK, DNS 126274-2, 2007.

[15] P. Yankowich, "Evaluation of Sasol fully synthetic jet fuel for approval for use as Jet A-1 fuel," Honeywell Aerospace, Phoenix, USA, 21-13781, 2007.

[16] A. H. Lefebvre, *Gas Turbine Combustion*, 2nd ed. New York: Taylor and Francis, 1999, pp. 135, 139.

[17] G. A. E. Godsave, "Studies of the combustion of drops in a fuel spray – The burning of single drops of fuel," in *Fourth Symposium (International) on Combustion*, The Combustion Institute, 1953, pp. 818-830.

[18] A. H. Lefebvre, *Atomization and Sprays*. United States of America: Hemisphere Publishing Corporation, 1989, p. 331.

[19] B. J. Wood, H. Wise, and S. H. Inami, "Heterogeneous combustion of multicomponent fuels," NASA TN D-206, 1959.

[20] J.S. Chin and A. H. Lefebvre, "Effective values of evaporation constant for hydrocarbon fuel drops," in *Proceedings of the 20th Automotive Technology Development Contractor Coordination Meeting*, 1982, pp. 325-331.

[21] A. H. Lefebvre, *Gas Turbine Combustion*, 2nd ed. New York: Taylor and Francis, 1999, pp. 142-145.

[22] A. H. Lefebvre, *Gas Turbine Combustion*, 2nd ed. New York: Taylor and Francis, 1999, p. 141.

[23] V. W. Greenhough, and A. H. Lefebvre, "Some applications of combustion theory to gas turbine development," in *Sixth Symposium (International) on Combustion*, The Combustion Institute, 1957, pp. 858-869.

[24] A. H. Lefebvre, *Gas Turbine Combustion*, 2nd ed. New York: Taylor and Francis, 1999, pp. 137-141.

[25] A. H. Lefebvre, and G. A. Halls, "Some experiences in combustion scaling," in *AGARD Advanced Aero Engine Testing, AGARD-ograph 37*, 1959, pp 177-204.

[26] A. H. Lefebvre, *Gas Turbine Combustion*, 2nd ed. New York: Taylor and Francis, 1999, p 36-38

[27] J. P. Longwell, E. E. Frost, and M. A. Weiss, "Flame stability in bluff body recirculation zones," in *Journal of Industrial and Engineering Chemistry,* Vol. 45, No. 8, 1953, pp. 1629-1633.

[28] R. A. Strehlow, *Fundamentals of Combustion*, Scranton Pennsylvania, International Textbook Company, 1968, pp. 181-184.

[29] J. E. Penner, D. H. Lister, D. J. Griggs, D. J. Dokken, and M. McFarland, *Aviation and the Global Atmosphere*. Cambridge, United Kingdom: Cambridge University Press, 1999.

[30] "Standard Atmosphere," International Organization for Standardization, ISO 2533:1975, 1975.

[31] N. Cumpsty, *Jet Propulsion*, 2nd ed. Cambridge: Cambridge University Press, 2003, p. 34.

[32] A. Rizkalla and A. H. Lefebvre, "The influence of air and liquid properties on airblast atomization," in *ASME Journal of Fluids Engineering*, Vol. 97, No. 3, 1975, pp. 316-320.

[33] A.H. Lefebvre, "Airblast Atomization," in *Progress in Energy and Combustion Science,* Volume 6, Number 3, 1980, pp. 233-261.

[34] A. H. Lefebvre, "Fuel effects on gas turbine combustion," Combustion Laboratory, School of Mechanical Engineering, Purdue University, Indiana, USA, AFWAL-TR-83-2004, 1983.

[35] K. S. Venkataramani, "Aviation fuel property effects on altitude relight," NASA Lewis Research Centre, Rep. AD-A183 088, 1987.

[36] H. N. Rao and A. H. Lefebvre, “Minimum ignition energies in flowing kerosine-air mixtures,” in *Combustion and Flame, vol. 27, no.1*, 1976, pp. 1-20.

[37] D. R. Ballal and A. H. Lefebvre, “Ignition and flame quenching of quiescent fuel mists,” in *Proceedings of the Royal Society London Ser. A, vol. 364, no 1717*, 1987, pp. 277-294.

[38] D. R. Ballal and A. H. Lefebvre, “General model of spark ignition for gaseous and liquid fuel/air mixtures,” in *Eighteenth Symposium (International) on Combustion*, 1981, pp. 1737-1746.

[39] A. H. Lefebvre, "Fuel effects on gas turbine combustion-ignition, stability, and combustion efficiency," in *ASME Journal of Engineering for Gas Turbines and Power 107: 24-37*, 1985.

[40] B. C. Heulskamp, B. V. Kiel, P. Gokulakrishnan, “Influence of fuel characteristics in correlation to predict lean blowout of bluff-body stabilized flames,”GT2015-43433, in *Proceedings of ASME Turbo Expo 2015*, Montreal, 2015.

[41] S. J. Shanbhogue, S. Husain, and T. Lieuwen, “Lean blowoff of bluff body stabilized flames: Scaling and dynamics,” in *Progress in Energy and Combustion Science 35*, 2009, pp. 98-120.

[42] K. Radhakrishnan, J.B. Heywood, and R.J. Tabaczynski, “Premixed turbulent flame blowoff velocity correlation based on coherent structures in turbulent flows,” in *Combustion and Flame 42*, 1981, pp. 19-33

[43] J. Kariuki, D.E. Cavaliere, C. Letty, and E. Mastorakos, “A comparison of the blow-off behaviour of swirl stabilized premixed and spray flames,” 50th AIAA Aerospace Science Meeting, Nashville, USA, 2012.

[44] M. Colket, S. Zeppieri, Z. Dai, and D. Hauptman, “Fuel research at UTRC,” Multi-Agency Coordinating Council for Combustion Research 5th Annual Research Meeting, Livermore, USA, 2012.

[45] S.H. Won, P.S. Veloo, S. Dooley, J. Santner, F.M. Haas, Y. Ju, F.L. Dryer, “Predicting the global combustion behaviours of petroleum-derived and alternative jet fuels by simple fuel property measurements,” in *Fuel 168*, 2016.

[46] V. W. Greenhough, and A. H. Lefebvre, “Some applications of combustion theory to gas turbine development,” in *Sixth Symposium (International) on Combustion*, The Combustion Institute, 1957, pp. 858-869.

[47] A. H. Lefebvre, *Gas Turbine Combustion*, 2nd ed. New York: Taylor and Francis, 1999, pp. 137-141.

[48] A. H. Lefebvre, and G. A. Halls, “Some experiences in combustion scaling,” in *AGARD Advanced Aero Engine Testing, AGARD-ograph 37*, 1959, pp 177-204.

[49] G. Damkoehler, Z. Elektrochem, 46, 601, 1940.

[50] K.J. Laidler, The development of the Arrhenius equation, in *Journal of Chemical Education*, 61 (6), 1984, pp.494-498.

[51] A. H. Lefebvre, *Gas Turbine Combustion*, 2nd ed. New York: Taylor and Francis, 1999, p 36-38

[52] R. A. Strehlow, *Fundamentals of Combustion*, Scranton Pennsylvania, International Textbook Company, 1968, pp. 181-184.

[53] N. Bester, “A test-cell installation of a gas turbine engine to investigate the performance advantages of low aromatic fuel,” MSc. dissertation, University of Cape Town, Cape Town, South Africa, 2008, p45.

[54] M. A. Weiss, J. C. Roherer, and J. P. Longwell, *Sixth Symposium (International) on Combustion*, The Combustion Institute, 1957.

[55] R. A. Strehlow, *Fundamentals of Combustion*, Scranton Pennsylvania, International Textbook Company, 1968, pp. 266-269.

[56] A. H. Lefebvre, Gas Turbine Combustion, 2nd ed. New York: Taylor and Francis, 1999, pp. 48-49

[57] J.B. Heywood, *Internal Combustion Engine Fundame*ntals, McGraw-Hill Book Company, 1988, p. 468.

[58] V. Burger, A. Yates, N. Savage, and O. Metcalf, “Assessment of the Role of Fuel Autoignition Delay at the Limits of Gas Turbine Combustion and Ignition,” GT2009-60332, Proceedings of ASME Turbo Expo 2009: Power for Land, Sea and Air, Orlando, USA. 2009.

[59] United Kingdom. Ministry of Defence, Defence Standard 91-91, Turbine Fuel, Aviation Kerosene Type Jet A-1, NATO Code: F-35, Joint Service Designation: AVTUR, Issue 6, 8 April 2008.

[60] ASTM Standard D1655–11b, Standard Specification for Aviation Turbine Fuels, ASTM International, 2011.

[61] ASTM Standard D2887–08, Standard Test Method for Boiling Range Distribution of Petroleum Fractions by Gas Chromatograph, ASTM International, 2008.

[62] R. van der Westhuizen, M. Ajam, P. de Coning, J. Beens, A. de Villiers, and P. Sandra, “Comprehensive Two-dimensional Gas Chromatography for the Analysis of Synthetic and Crude-derived Jet Fuels,” in *Journal of Chromatography A, 1218(28)*, 2011, pp. 4478-4486.

[63] ASTM Standard D68090 – 13a, Standard Test Method for Determination of Ignition Delay and Derived Cetane Number (DCN) of Diesel Fuel Oils by Combustion in a Constant Volume Chamber, ASTM International, 2013.

[64] A. Yates, V. Burger and C. Viljoen, “A method for determining the laminar flame speed of jet fuels using combustion bomb pressure,” in *Proceedings of ASME Turbo Expo 2012: Power for Land, Sea and Air, GT2012*, Copenhagen, Denmark, June 11-15, 2012.

[65] J. Grohmann, W. O’Loughlin, W. Meier, and M. Aigner, “Comparison of the Combustion Characteristics of Liquid Single-component Fuels in a Gas Turbine Model Combustor,” GT2016-56177, in *Proceedings of ASME Turbo Expo 2016: Turbomachinery Technical Conference and* Exposition, Seoul, South Korea, 2016.

[66] A. H. Lefebvre, and D. R. Ballal, *Gas turbine combustion: alternative fuels and emissions*, CRC Press, Taylor and Francis Group, 2010.

[67] D. Galley, S. Ducruix, F. Lacas, and D. Veynante, “Mixing and stabilization study of a partially premixed swirling flame using laser induced fluorescence” in *Combustion and Flame, 158(1)*, 2011 pp. 155–171.

[68] A. H. Lefebvre, *Gas Turbine Combustion, 2nd ed.* New York: Taylor and Francis, 1999, p 127.

[69] ASTM Standard D68090 – 13a, Standard Test Method for Determination of Ignition Delay and Derived Cetane Number (DCN) of Diesel Fuel Oils by Combustion in a Constant Volume Chamber, ASTM International, 2013.

[70] A. D. B. Yates, C. L. Viljoen, A. Swarts, “Understanding the relation between cetane number and combustion bomb ignition delay measurements”, SAE 2004-01-2017, 2004.

[71] W. Zeng, H. Ma, Y. Liang, E. Hu, “Experimental and modelling study on effects of N2 and CO2 on ignition characteristics of methane/air mixture,” in *Journal of Advanced Research 6*, Cairo University, 1998, p.371-378.

[72] A. H. Lefebvre, *Gas Turbine Combustion*, 2nd ed. New York: Taylor and Francis, 1999, p. 45.